Stellingen

Behorende bij het proefschrift

"Micro-Mechanical Structures as Optical Sensor Elements"

Shaodong Wu

Delft, Nederland

december, 1992

1. Fig. 7 in the article written by H. Bezzaoui and E. Voges†, showing a photograph of a waveguiding situation between two cantilevers, needs further explanation. The photograph shows unusual bright areas (brighter than the waveguiding areas) on the etched silicon surface, which suggests that there light scattering is stronger than that from the guided wave.

† H. Bezzaoui and E. Voges, "Integrated optics combined with micromechanics on silicon," Sensors and Actuators A, vol. 29, no. 3, pp. 219–223, Dec. 1991.

2. Radiation loss is neither the only factor to be considered nor the best parameter to determine the minimum allowable bending radius for a curved waveguide.

3. In the near future, the *mechanical* properties of silicon will be exploited even more intensively than presently for application both in micro-electronics and in integrated optics.

4. The scaling-down of the bridge- and cantilever-dimensions to the order of microns does not alter the principle governing the structures' mechanical behavior, but changes the structures' sensitivity and potential applications.

5. Considerable errors will occur when intuitive assumptions are introduced to model a problem before serious theoretical analysis has been carried out.

6. Journals would contribute more to the development of science and technology if they should publish more ideas than just facts.

7. Technically speaking, a human being functions excellently as a smart sensor, but in many circumstances it is immoral to use a human being as such. Technology, however, can greatly benefit from

imitating the human sensing capabilities as examples for new developments.

8. *Science*

The barrier for the public to understand science is still too high to be easily overcome. For today's scientists, explaining Einstein's theory of relativity into popular songs is a great challenge.

Technology

The increasing complexity of technology may be a joy to the technocrats, but it is growing into an intimidating nightmare to the public. The technocrats and the public are now standing at a road-crossing, with the risk that they will run in opposite directions.

9. Allowing a government in an economic recession to cut the expenditure for education is a recipe for a country to sink further into bankruptcy.

10. Taoist "*Wuwei*‡" philosophy is the best solution for the environment conservation since nature itself has the power to keep the environment in balance.

‡ Wuwei: the Chinese word literally means "doing nothing".

11. People waste a lot of time learning computer software that often becomes outdated before being mastered.

12. The wording "No part of this publication may be reproduced, stored in a retrieval system or transmitted in any form or by any means..." in a usual copyright claim implies that no part of the publication may be stored in our brain. This is an unreasonable statement.

Micro-Mechanical Structures as Optical Sensor Elements

Micro-Mechanical Structures as Optical Sensor Elements

PROEFSCHRIFT

ter verkrijging van de graad van doctor
aan de Technische Universiteit Delft,
op gezag van de Rector Magnificus,
prof. drs. P. A. Schenck,
in het openbaar te verdedigen
ten overstaan van een commissie aangewezen
door het College van Dekanen
op 1 december 1992 te 14:00 uur

door

Shaodong Wu,
geboren te Zhejiang, China,
natuurkundig ingenieur

Delft University Press
Delft

Dit proefschrift is goedgekeurd door de promotor:

Prof. dr. ir. H. J. Frankena

Royal Library Cataloging in Publication Data, The Hague

Wu, Shaodong

Micro-mechanical structures as optical sensor elements.

Includes index and bibliography.

1. Optical sensors 2. Integrated optics
I. Title

ISBN 90-6275-799-5
NUGI 841

First published in 1992 by Delft University Press
Stevinweg 1, 2628 CN Delft, The Netherlands

PRINTED IN THE NETHERLANDS

Dedicated to

my parents

Preface

This thesis is written to fulfill the requirements for the Ph.D. degree at Delft University of Technology, and conveys most of the results obtained during the four-year Ph.D. research period. It reports an investigation on micro-mechanical structures (bridges and cantilevers) and on their applications as integrated optical sensor elements.

Sensors are widely applied as tools for the mankind to strengthen and to extend the human sensing system. With the aid of various sensors, human beings are able to see the invisible, to hear the inaudible, and to understand the incomprehensible. For machines, sensors provide certain intelligence to the machines, and make the machines be able to sense their surroundings.

Sensors are very often based on more than one discipline. New sensors are often discovered and developed when one scientific or technological branch encounters another. The presently investigated sensor elements are the result of an interaction between integrated optics and micro-mechanics. Integrated optics lays down the operational principles for the sensor elements and uses guided waves as the information carrier of sensor signals. Micro-mechanics provides micro-structures as transducing interfaces to external influences and governs the mechanical behavior of the structures.

The idea to develop this kind of optical sensor elements came from a parallel way of thinking by considering micro-mechanical structures used as sensor elements in integrated electronics. If the micro-mechanical structures, especially bridges and cantilevers, can be constructed in such a way that they eventually become optical waveguides, the structures can then be applied as integrated optical sensor elements.

The application of optical sensors using micro-mechanical structures meets the trend of developing a broad range of inexpensive, batch-fabricated, high performance sensors, which can be easily interfaced with the highly developed micro-processors and communication systems. Micro-mechanical structures can be batch-fabricated using micro-fabrication (micro-machining) techniques that have already been highly developed for the electronic IC industry. At the same time, optical fiber communication systems have been developed with such a success that they have become the choice for communication in the future. This imposes high demands on optical information acquisition and processing for which optical integrated circuits, that fulfill similar roles as electronic IC's, have been introduced and developed. It is a logic extension of this tendency to investigate the sensors which use optical waveguides and guided waves to allow easy interfacing with optical communication. Besides, integrated optical sensors have a number of further advantages above existing devices.

The present thesis considers the fabrication as well as the application of micro-bridges and cantilevers. These bridges and cantilevers are fabricated upon silicon substrates and are used as optical waveguides. The waveguides have a sandwiched layer structure of an SiO_2 buffer, an Al_2O_3 waveguide and an SiO_2 cover. Such bridges and cantilevers can be applied as optical sensor elements for force-related quantities. In this thesis, both the theoretical and the technological aspects of these two structures will be investigated.

The thesis consists of six chapters. Chapter 1 first gives an introduction to the concept and history of integrated optical sensors, and then introduces micro-mechanics and the micro-structures of bridges and cantilevers. The operational principles of such micro-bridges and cantilevers as optical sensor

elements are also briefly described. In Chapter 2, some theoretical backgrounds concerning the operational principles of bridges and cantilevers are described. In the first section, both the static and the dynamic mechanical behavior of bridges and cantilevers are presented. A theoretical method dealing with curved waveguides has been developed in the second section in order to understand the optical loss induced by the deflection of the waveguide-bridges and cantilevers. The optical coupling process in a cantilever structure is analyzed in Section 2.3. In Chapter 3, micro-fabrication technology for producing three-dimensional micro-structures is briefly summarized. Chapter 4 gives details of the fabrication processes of the micro-bridges and cantilevers for integrated optical sensors. Etching techniques like isotropic, anisotropic and reactive ion etching (RIE) have been applied for the fabrication of the bridges and cantilevers. The application of such structures as optical sensor elements is evaluated and confirmed by the experiment results of acoustic signal detection, which is presented in Chapter 5. Some other possible applications are also proposed and discussed briefly. Chapter 6 provides some discussion and conclusions regarding the present investigation.

One part of research during the four-year Ph.D. period is not covered in this thesis. In the first year, research work was also carried out on integrated optical interferometers with stacked multilayers and coupled waveguide structures and their application as sensor elements, which led to three publications.

I wish to acknowledge my gratitude to all those who contributed to the success of my research and to the completion of this dissertation. First of all, I'd like to thank Prof. dr. H. J. Frankena for his encouragement and guidance with which I have been able to push the research to proceed and yet to keep on the right track. With numerous fruitful discussions, sometimes arguments, new ideas became plans and plans have been turned into results, finally leading to this dissertation. I am also grateful to many of my colleagues: Dr. H. van Brug, F. H. Groen, J. de Jong, C. J. van der Laan and many others whose names could not be mentioned here for space reasons, for numerous pleasant and useful

discussions. They, in many ways, helped me a lot during my Ph.D. period. I am greatly indebted to A. J. van der Lingen for his constant help and assistance in arranging much of the equipment needed for experiments, to R. C. Horsten for the arrangement of equipment needed for acoustic signal measurement, and to A. Looijen and A. Kuntze for their excellent high-quality thin films, which enabled me to fabricate micro-bridges and cantilevers. Thanks to the Acoustic Research Laboratory of this university for providing advanced acoustic equipment and to J. L. Joppe from FEL (Physical and Electronic Laboratory) of TNO (the Netherlands Organization for Applied Physics Research) for carrying out the reactive ion etching process, the result of their effort enriched both the research and this thesis enormously. The research has also been benefited a great deal from the facilities of DIMES (Delft Institute of Micro-Electronics and Submicrotechnology).

It is a pleasure to thank the Chinese Education Ministry for sending me to the Netherlands for further study in the first place and providing financial support in the beginning. I also appreciate the financial support from Shell Nederland B.V. and NWO (Netherlands Organization for Scientific Research) for my participation at international conferences.

Finally, my gratefulness goes to my parents whose encouragement and support are the constant source of motivation of my study. Special words should also go to all my friends both in China and in the Netherlands who have made my life here enjoyable and my study successful.

It is also an exceptional occasion to finish my Ph.D. work in a year when this excellent university celebrates her 150-th anniversary.

Shaodong Wu

Delft, The Netherlands

December 1992

Contents

Preface vii

1 Introduction 1

1.1 Introduction to Integrated Optical Sensors 2

1.1.1 Sensors 2
1.1.2 Principles of Integrated Optical Sensors 3
1.1.3 Features of Integrated Optical Sensors 5
1.1.4 History of Integrated Optical Sensors 7

1.2 Micro-Mechanical Structures for Optical Sensors 9

1.2.1 Micro-Structures 9
1.2.2 Micro-Mechanical Structures for Optical Sensors 10

2 Theoretical Background 17

2.1 Mechanical Behavior of Bridges and Cantilevers 17

2.1.1 Dynamic Behavior 18
2.1.2 Static Behavior 24

2.2 Optical Loss in Bridges and Cantilevers 26

2.2.1 Introduction to Curved Waveguides 26
2.2.2 Theory of Curved Waveguides 28
2.2.3 Numerical Results and Discussion 33

2.3 Optical Coupling in Cantilevers 37
2.3.1 Introduction 37
2.3.2 Coupling Efficiency 37

3 Technological Background 45

3.1 Thin Film Deposition and Growth 46
3.2 Lithography 47
3.3 Micro-Processing Techniques 49

4 Fabrication of Micro-Mechanical Structures 55

4.1 Fabrication of Waveguide Bridges and Cantilevers 56
4.1.1 Waveguide Layer Structure and Exposure Mask Patterns 56
4.1.2 Fabrication Process Using Isotropic Etching 58
4.1.3 Fabrication Process Involving Reactive Ion Etching 65
4.2 Waveguiding in Bridge and Cantilever Structures 71
4.3 Discussion 73

5 Applications 77

5.1 Acoustic Signal Detection 77
5.1.1 Experimental Setup 78
5.1.2 Experimental Results 81
5.1.3 Discussion 87
5.2 Other Applications 87
5.2.1 Measurement of Vibrations and Acceleration 87
5.2.2 Scanning Force Microscope and Surface Profiler 89
5.2.3 Sensitivity Evaluation 91

6 Discussion and Conclusions 95

6.1 Discussion 95
6.2 Conclusions 98

Appendix A Formulation for the Radiation Loss Using Coupled Mode Theory 101

Bibliography 105

Summary 113

Index 119

Biography 123

1

Introduction

About ten years have passed since the first application of integrated optical sensors was reported. Numerous sensors, mostly involving interferometer structures, have been investigated. New sensor structures and sensor applications are still intensively searched and investigated. In this thesis, integrated optical sensors using micro-mechanical structures are proposed and studied. Such optical sensors are based both on integrated optics and on micro-mechanics and take advantages from both areas. They use guided waves as information carriers, and micro-mechanical structures as transducing elements, which makes the structures very sensitive and favorable for sensor applications. Using the guided waves for the sensors allows an easy interface with the advancing optical communication, and applying the micro-structures makes it possible to batch-fabricate the sensors. There is actually a growing trend in such merging between integrated optics and micro-mechanics. Quite recently, the first international conference devoted especially to micro-structures in integrated optics has been organized [1].

In this first chapter, an introduction to the concept and history of integrated optical sensors will be presented. Then, micro-mechanical structures

(bridges and cantilevers) and the operational principles of these structures used as optical sensor elements will be described.

1.1 Introduction to Integrated Optical Sensors

1.1.1 Sensors

A sensor is a device that senses either the value or a change in value of a physical quantity (such as temperature, flow rate, or pH, ...) and converts that into a useful input signal for an information processing system [2].

Classification of sensors is generally based upon the physical quantities to be measured and on the nature of sensing elements. Thus, an optical sensor can be defined as a sensor in which the effects on optical properties are used for sensing other physical quantities, including other optical ones.

The basic operation of a sensor is illustrated in Fig. 1.1. If a sensor is exposed to its environment, an unknown quantity X in that environment will influence a certain variable V in the sensor. Through a specially designed sensing structure, this variable is converted into another output variable O which can be more easily detected. The detected signal S can then be connected to an information processor or a display unit.

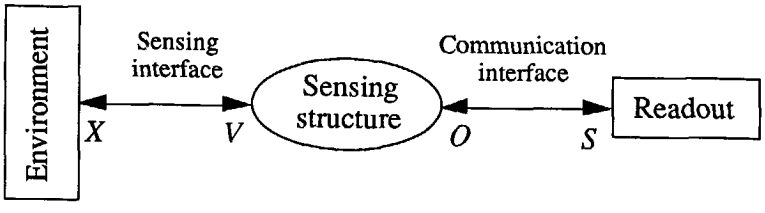

Fig. 1.1 Diagram of a sensor setup.

1.1.2 Principles of Integrated Optical Sensors

An integrated optical sensor is based upon the changes which take place in the characteristics of guided waves traveling through an optical waveguide when part of this guide is exposed to the environment. It usually comprises a light source, photo-detectors, optical waveguides with sensing structures, signal processors and other optical or opto-electronic components such as couplers, connectors and modulators. In many aspects, an optical fiber sensor has the same operation principles as an integrated optical sensor. Integrated optical sensors and optical fiber sensors are two major branches of the optical sensor family.

For integrated optical sensors, several types of modulation (sensing) principles, using guided waves acting as information carriers, can be used. The quantity to be measured modulates these waves and the resulting modulation can be later determined to evaluate the quantity.

A guided wave, represented by its electric field strength $\vec{E}(\vec{r},t)$, can be expanded as [3]

$$\vec{E}(\vec{r},t) = \sum_m A_m \vec{E}_m(\vec{r},t), \tag{1.1}$$

where $\vec{E}_m(\vec{r},t)$ denotes the $m\text{-}th$ order guided mode of the pertinent waveguide and A_m the amplitude of that mode. There are four possible ways to modulate the guided wave, viz., by changing

1. the mode amplitudes;
2. the mode polarizations;
3. the mode phases;
4. the wavelength or the power distribution among modes.

Each modulation type leads to a certain characteristic of the sensors. These sensors can be broadly categorized into intensity, polarization, phase or spectral sensors.

Optical intensity sensors. An optical sensor using a sensing technique which directly produces a change in optical intensity proportional to the applied signal can be classified as an intensity sensor. Here, the light intensity is affected by an attenuator in the light path, which is controlled by the quantity to be measured. As an example, the intensity loss in a fiber micro-bend sensor [4] depends on an induced coupling from propagating modes to radiation modes. The fluctuation in intensity will be directly related to the quantity to be measured and can be easily detected. In the case of an intensity instability in the light source, a reference channel and electronic circuitry can be employed to compensate for the resulting intensity change.

Optical polarization sensors. If polarized light is launched into a waveguide, the polarization plane will be rotated by induced birefringence [5]. With respect to this, the Faraday effect is well-known. If an external magnetic field is applied to a suitable medium with a field component parallel to the propagation direction of linearly polarized light, the polarization plane will be rotated. The rotation angle can be determined to evaluate the applied magnetic field.

Optical phase (interferometric) sensors. These are sophisticated optical sensors which encode the sensed information into the phase of a guided wave propagating through a sensing waveguide [6]. To detect the resulting phase changes, another coherent light wave serves as a reference. Using optical couplers, the sensing and reference paths can be combined to form an optical interferometer.

Optical phase sensors are very effective because they offer an extremely high sensitivity and wide dynamic ranges, using digital processing systems for

the interference fringes. A phase modulation scheme requires a coherent light source and mono-mode operation of the guides. To satisfy these conditions, semiconductor lasers are the most promising candidates for use as coherent light sources in this type of sensors because they can be integrated into optical circuits to ensure the reliability of devices and to allow compact structures.

Optical spectral sensors. Utilizing more complex modulators and filters in a sensor, a sensed signal can be encoded into the optical spectrum or into the power distribution among different guided modes to reduce the influence of various losses in transmission lines [7]. One form of spectral modulation is simply a Doppler shift which may be induced by, e.g., back scattering from moving particles beyond the end of a fiber or an integrated waveguide. Laser Doppler Anemometry (LDA) is a well-known example.

Since optical waveguide materials have optical, mechanical, electro-magnetic and thermo-dynamic properties which are significant for the wave propagation, integrated optical sensors up to date have covered many aspects of conventional sensors, such as for detecting electro-magnetic field, current, sound, pressure, acceleration, displacement, temperature and gases etc., which will be briefly reviewed in Section 1.1.4. Table 1.1 lists some physical quantities which can be sensed by optical waveguides along with their optical transducing mechanisms.

1.1.3 Features of Integrated Optical Sensors

An extremely high sensitivity is possible for an integrated optical sensor, typically increasing linearly with the length of the waveguide section which forms the sensing part. Theoretically, optical phase (interferometric) sensors have orders of magnitude higher sensitivity over their electronic counterparts.

The sensing part of an integrated optical sensor can be entirely optical, that is, devoid of electric phenomena. Thus, the sensor is immune to electric or magnetic interference which is a problem restricting the use of conventional

electronic devices in some cases. This permits their use in environments such as high voltage, electrically noisy, or explosive atmospheres. Also, there is almost no interference among neighboring optical sensor probes. The reason behind this is that, unlike conventional electric wires or cables, the optical field is well confined within the waveguides.

Table 1.1 Quantities and their optical sensing methods

Physical Quantities	Transducing Mechanisms
Displacement	Optical phase interference, Induced losses, Attenuators
Vibration Acceleration Sound	Induced losses, Attenuators
Force Pressure	Photo-elastic effect
Flow	Doppler effect, LDA
Rotation	Sagnac interferometry
Temperature	Thermal expansion
Magnetic field	Faraday effect
Electrical field	Electro-optical effect

The most intriguing applications of an optical fiber sensor result from its geometric versatility which is related to the fact that the sensing takes place in a thin, long and bendable fiber. An integrated optical sensor, although less flexible, provides the possibility to be integrated with other optical or even the necessary electronic components onto a single chip and therefore possesses a superior degree of compactness, stability and reliability.

Integrated optical sensors have an intrinsic compatibility with optical fiber communication and optical telemetric techniques. The sensors can realize remote

sensing and remote control if connected to optical fibers of low transmission loss.

Several measurements may be carried out simultaneously with a single optical waveguide using passive multiplexing techniques. For instance, the polarization of a wave propagating through a mono-mode optical waveguide can be modulated by a magnetic field (Faraday effect) while an intensity sensor is fabricated from the same guide to sense another quantity [8]. The two modulations are independent and the detection of the polarization and intensity can be separated.

1.1.4 History of Integrated Optical Sensors

The earliest sensor application using integrated optical waveguides was reported by Johnson et al. in 1981 [6]. The basic element of the integrated optical sensor is a waveguide version of a Mach-Zehnder interferometer with unequal arms as shown in Fig. 1.2. It was used for temperature sensing. The interferometer was made from Ti-doped channel waveguides in an $LiNbO_3$ substrate with dimensions of 10 mm in length and 0.7 mm in width. The device had a projected range and a sensitivity of larger than 700 °C and 2×10^{-3} °C, respectively.

An early integrated optical sensor for displacement sensing has been demonstrated using a Michelson interferometer composed of an optical waveguide hybrid coupler, as illustrated in Fig. 1.3 [9]. The reference arm is terminated by a mirror attached directly onto the end surface of the waveguide substrate. To detect an object displacement, a reflecting mirror is mounted on the object and placed closely behind the sensing port. Light from the input port is divided by the hybrid coupler into two beams which are reflected at the two mirrors and then return to the coupler. The resulting change of the optical phase

difference is converted to an intensity signal by the hybrid coupler. With this method, a displacement in the submicron range could be easily measured.

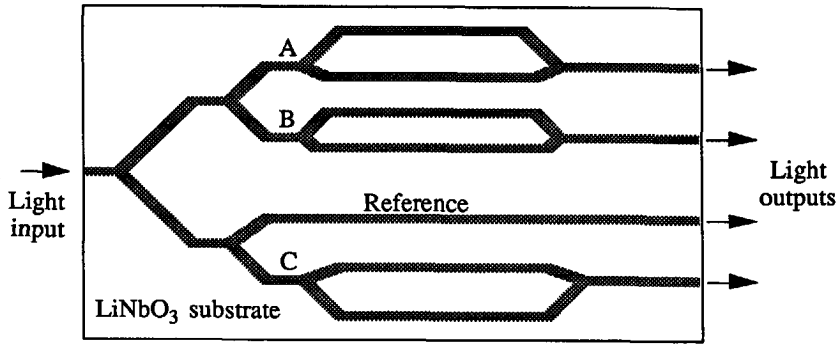

Fig. 1.2 Optical waveguide temperature sensor.

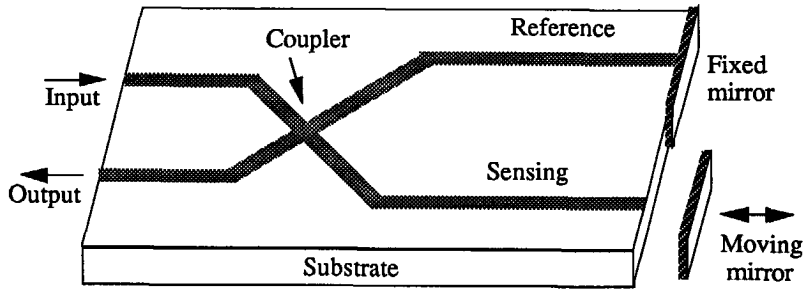

Fig. 1.3 Optical waveguide displacement sensor.

The Michelson interferometer used for displacement sensing was also applied to sense pressure and force [10]. The coupler's two branches forming the sensing and reference arms are both terminated by a fixed mirror. Mechanical pressure is applied onto the surface of the sensing arm and induces a refractive index change which affects the phase of the light propagating through it due to the elasto-optic effect. The phase change can be detected to evaluate the applied pressure or force. The measured half-wave force which results in a phase change of π had a value of 0.31 N.

Since the advent of integrated optical sensors, intensive research has been carried out at different institutions and numerous sensors have been developed. According to their applications, these are sensors for the measurement of temperature [6][11], pressure [12], displacement [9][13], flows [14], wavefront shapes [15], voltage [16], electro-magnetic fields [17], pH values [18], gases [19], humidity [20], biochemical quantities [21], etc. The sensor structures include interferometers, couplers, gratings, diode lasers, resonant cavity structures etc. Doubtlessly, the most widely used structures as sensor elements are the interferometer type ones.

1.2 Micro-Mechanical Structures for Optical Sensors

1.2.1 Micro-Structures

While the effort on the exploitation of new integrated optical sensor structures and on the development of new optical sensor applications continues, there has been impressive progress in another technological aspect e.g. micro-fabrication (or micro-machining) techniques. A research area called micro-mechanics has been developed and numerous micro-structures have been fabricated [22]. Silicon and its related materials like SiO_2 become undisputedly the most suitable and most widely used materials for making micro-structures because of their excellent mechanical properties.

Micro-mechanics as a silicon-based device technology was initiated by H. C. Nathanson et al [23][24] at Westinghouse Research Laboratories in 1965, when the resonant gate transistors (RGT) were introduced. The RGT consists of a plated-metal cantilever beam with typical dimensions of length 240 μm, thickness 4.0 μm, beam-to-substrate separation 10 μm. It lasted, however, till the mid 1970s that the potentials of micro-mechanics were widely recognized [25]. Since then, the concept of micro-mechanics has evolved with the development of the highly sophisticated IC technology. Nowadays, micro-mechanics is

referred to the application of silicon as a mechanical material and to the fabrication of mechanical structures with very small dimensions. Along with the role of silicon as a semiconducting material for its electronic properties, the application of silicon has obtained a new dimension by allowing the fabrication of mechanical devices. All the well known advantages of silicon technology, such as high reliability, small geometric dimensions, and cost effectiveness due to batch fabrication apply to the mechanical elements as well. The fabrication of most micro-mechanical components relies on a three-dimensional structuring of the silicon substrate or of deposited layers. A detailed overview of various applications involving micro-mechanical structures can be found in the literature [26].

Recently, micro-mechanics has also found its way into micro-optics and integrated optics. The progress made in these two areas has been summarized by P. P. Deimel in a review article [27], and has also been reported quite recently at the first international conference devoted especially to micro-structures in integrated optics [1].

1.2.2 Micro-Mechanical Structures for Optical Sensors

Although micro-mechanical structures have already been widely applied in electronic devices, they are quite new for integrated optics. The work presented in this thesis is one of the early researches on micro-mechanical structures for integrated optics and for optical sensor applications. Only very recently, related work has been carried out by others [28][29].

In this thesis, we propose two micro-mechanical structures for integrated optical sensor applications. One is a bridge structure suspended over a gap between two planar waveguide areas, the other a cantilever structure over a similar gap, but not completely bridging the open space.

The micro-bridge structure is illustrated in Fig. 1.4. For the simplicity, only the substrate and waveguide are shown in the picture. In an actual situation the waveguide can consist of a multilayer structure. The waveguiding situation in the bridge structure can be described as follows. A guided wave can be coupled into the waveguide through the input section. It will propagate through the waveguide bridge and reaches the output section where it can be coupled out and measured. The wave propagation through the bridge, and so the output signal, is changed by a small bending or vibration of the bridge section. Consequently, this bridge structure can be applied for the detection of force-related physical quantities, such as sound, vibration and acceleration.

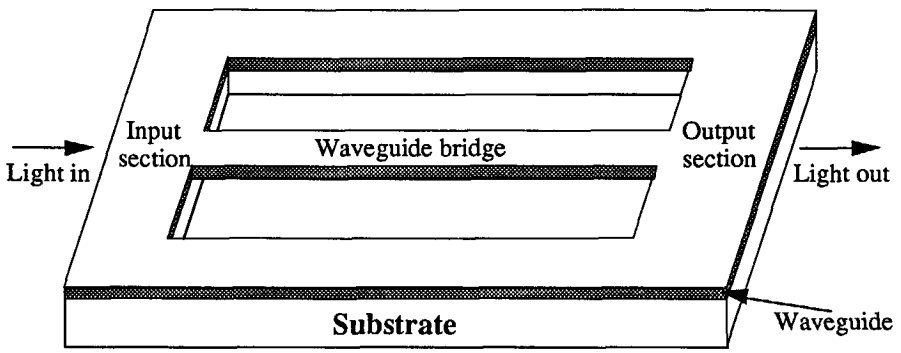

Fig. 1.4 Micro-mechanical bridge for integrated optical sensor applications.

The micro-cantilever structure is presented in Fig. 1.5. The difference in the waveguiding situation as compared with the bridge structure is the occurrence of an additional coupling process when a guided wave reaches the cantilever's free end. The guided wave will diffract from that end and only part of the diffracted wave will be coupled into the output section.

The operational principles of both the waveguide bridge and the cantilever proposed here can be described as follows. A bridge- or cantilever-shaped

waveguide will be at rest when external influences are absent. If, however, an external force is applied, it will undergo a forced deflection or vibration. The deflecting amplitude is related to the applied force. The deflection will increase the propagation loss for a guided wave within the waveguide. In a cantilever structure, apart from the loss due to bending, also the optical coupling between the free end of the cantilever and the output section will introduce loss. A shift of the cantilever's free end causes a change in coupling efficiency and consequently a change in the intensity of the outgoing wave. Thus, external forces cause a change in the intensity of a guided wave propagating through such a bridge- or cantilever-shaped waveguide. For vibrations, the output signal can yield information about the source's amplitude and frequency.

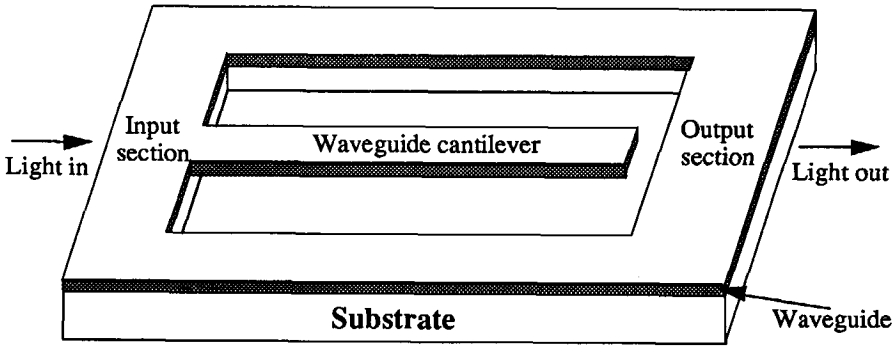

Fig. 1.5 Micro-mechanical cantilever for integrated optical sensor applications.

The proposed micro-bridges and cantilevers are fabricated upon silicon substrates. The waveguides have a sandwiched layer structure of an SiO_2 buffer, an Al_2O_3 waveguide and an SiO_2 cover. The use of silicon permits application of the highly developed batch-fabrication IC technology to the sensor field. It also makes it feasible to combine sensors and integrated circuits on a single chip, thereby creating so-called "smart sensors". Furthermore, a silicon substrate provide an excellent surface for depositing optical layers.

Our research has been oriented to the analysis of the possibility for sensor applications of micro-mechanical bridge and cantilever waveguides using guided waves as information carrier. The work may serve as the first step toward developing actual sensor devices that can be readily used for sensor applications. Much work and time are still needed to construct practical optical sensors based on these structures.

References

1. SPIE Conference 1793 – Integrated Optics and Microstructures, *SPIE's International Symposium OE/FIBERS'92*, Boston, USA, 8 – 11 Sept., 1992.
2. McGraw-Hill, *Dictionary of Scientific and Technical Terms*. McGraw-Hill, 1984.
3. T. Tamir (Editor), *Integrated Optics*. New York: Springer-Verlag, 1979.
4. J. N. Fields and J. H. Cole, "Fiber microbend acoustic sensor," *Applied Optics*, vol. 19, pp. 3265–3267, 1980.
5. C. H. Bulmer, R. P. Moeller and W. K. Burns, "Linear Mach-Zehnder interferometers in $LiNbO_3$ for electromagnetic field sensing," in *Proc. IEE of Second European Conf. on Integrated Optics*, Florence, Italy, 1983, pp. 140–143.
6. L. M. Johnson, F. J. Leonberger and G. W. Pratt, Jr., "Integrated optical temperature sensor," *Appl. Phys. Lett.*, vol. 41, no. 2, pp. 134–136, July 1982.
7. M. Johnson, "Optical-actuator frequency-coded pressure sensor," *Optics Lett.*, vol. 11, no. 9, pp. 587–589, Sept. 1986.
8. B. Culshaw, "Optical sensor multiplexing systems," in *Proc. Sensors and Systems'82*, Pasadena, 1982, pp. 47–57.
9. M. Izutsu, A. Enokihara and T. Sueta, "Optical-waveguide micro-displacement sensor," *Electronic Lett.*, vol. 18, pp. 867–868, 1982.
10. M. Izutsu, A. Enokihara, N. Mekada and T. Sueta, "Optical-waveguide pressure sensor," in *Proc. IEE of Second European Conf. on Integrated Optics*, Florence, Italy, 1983, pp. 144–147.

11. S. Wu and H. J. Frankena, "Integrated optical interferometer with a stacked waveguide structure," *Applied Optics*, vol. 28, no. 20, pp. 4424–4428, Oct. 1989.
12. M. Ohkawa, M. Izutsu and T. Sueta, "Integrated optical pressure sensor on silicon substrate," *Applied Optics*, vol. 28, no. 23, pp. 5153–5157, Dec. 1989.
13. S. Ura, T. Suhara and H. Nishihara, "Integrated-optic interferometer position sensor," *J. Lightwave Techn.*, vol. 7, no. 2, pp. 270–273, Feb. 1989.
14. A. Enokihara, M. Izutsu and T. Sueta, "Integrated-optic fluid sensor using heat transfer," *Applied Optics*, vol. 27, no. 1, pp. 109–113, Jan. 1988.
15. R. H. Rediker, T. A. Lind and F. J. Leonberger, "Integrated optics wave front measurement sensor" *Appl. Phys. Lett.*, vol. 42, no. 8, pp. 647–649, April 1983.
16. N. A. F. Jaeger and L. Young, "High-voltage sensor employing an integrated optics Mach-Zehnder interferometer in conjunction with a capacitive divider," *J. Lightwave Techn.*, vol. 7, no. 2, pp. 229–235, Feb. 1989.
17. C. H. Bulmer, W. K. Burns and R. P. Moeller, "Linear interferometric waveguide modulator for electromagnetic-field detection," *Optics Lett.*, vol. 5, no. 5, pp. 176–178, 1980.
18. P. K. Spohn and M. Seifert, "Interaction of aqueous solutions with grating couplers used as integrated optical sensors and their pH behavior," *Sensors and Actuators*, vol. 15, pp. 309–324, 1988.
19. K. Tiefenthaler and W. Lukosz, "Integrated optical switches and gas sensors," *Optics Lett.*, vol. 9, pp. 137–139, 1984.
20. S. Wu and H. J. Frankena, "An integrated optical interferometer and a coupled-waveguide humidity sensor," in Sensors and Actuators, A. Driessen, Ed., Kluwer Technical Books, 1990, pp. 75–78.
21. Ph. M. Nellen, K. Tiefenthaler and W. Lukosz, "Input grating couplers as biochemical sensors," *Sensors and Actuators*, vol. 15, pp. 285–295, 1988.
22. L. Csepregi, "Micromechanics: a silicon microfabrication technology," *Microelectronic Engineering*, vol. 3, pp. 221–234, 1985.
23. H. C. Nathanson and R. A. Wickstrom, "A resonant-gate silicon surface transistor with high-Q bandpass properties," *Appl. Phys. Lett.*, vol. 7, p. 84, 1965.
24. H. C. Nathanson, W. E. Neweil, R. A. Wickstrom and J. R. Davis, Jr., "The resonant gate transistor," *IEEE Trans. Electron Devices*, vol. ED-14, p. 117, 1967.

25. K. E. Petersen, "Dynamic micromechanics on silicon: techniques and devices," *IEEE Trans. Electron Devices*, vol. ED-25, pp. 1241–1250, 1978.
26. K. E. Petersen, "Silicon as a mechanical material," *Proc. IEEE*, vol. 70, no. 5, pp. 420–457, May 1982.
27. P. P. Deimel, "Micromachining processes and structures in micro-optics and optoelectronics," *J. Micromech. Microeng.*, vol. 1, pp. 199–222, 1991.
28. H. Bezzaoui and E. Voges, "Integrated optics combined with micromechanics on silicon," *Sensors and Actuators A*, vol. 29, no. 3, pp. 219–223, Dec. 1991.
29. K. E. Burcham, G. N. De Brabander and J. T. Boyd, "Micromachined silicon cantilever beam accelerometer incorporating an integrated optical waveguide," presented at *SPIE's International Symposium OE/FIBERS'92*, Boston, USA, 8 – 11 Sept., 1992.

2

Theoretical Background

This chapter provides a concise theoretical background concerning micro-mechanical bridges and cantilevers used as optical sensor elements. Section 2.1 is devoted to the mechanical behavior of bridges and cantilevers in order to understand how these two mechanical structures respond to external forces. The other two sections are mainly for the analysis of optical loss. Section 2.2 presents a theory over optical loss induced by the waveguide's bending. The theory, which is introduced to understand the bending loss in a bridge or a cantilever structure, is essentially a general theory for a curved waveguide with an arbitrary cross-section. Effects caused by inhomogeneous stress in the bridge or the cantilever are difficult to be analyzed, especially for multilayer structured waveguides, and are not considered here. Section 2.3 deals with the optical coupling process when the wave crosses the separation gap in a cantilever structure (from the cantilever's free end to the output section), and describes an approximate approach for the evaluation of the coupling efficiency.

2.1 Mechanical Behavior of Bridges and Cantilevers

Since the dimension of a micro-bridge or a micro-cantilever is a few micrometers in thickness, several to a few tens of micrometers in width and tens

to hundreds of micrometers in length, the bridge and the cantilever can be treated as beams which are shown in Fig. 2.1. In the following analysis, the materials of bridges and cantilevers are assumed to be homogeneous and isotropic and to obey Hooke's law.

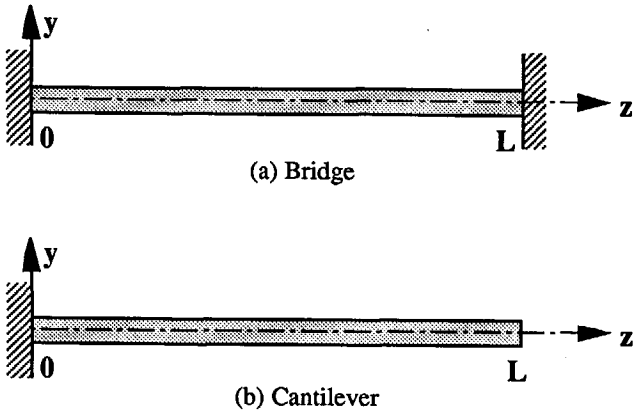

Fig. 2.1 Mechanical beams: (a) a bridge and (b) a cantilever.

2.1.1 Dynamic Behavior

Dynamic mechanical systems with distributed masses can be treated in terms of the vibration theory for continuous solid media [1]. They have an infinite number of natural frequencies and natural modes of vibration. In general, the vibrations of continuous solid media are termed as longitudinal, transverse or torsional and can be described through partial differential equations. Since we treat a bridge or cantilever as a beam, the problem to be solved regards the transverse vibration of the beams.

The differential equation of motion for a beam of length L is

$$\frac{\partial^2 y(z,t)}{\partial t^2} + a^2 \frac{\partial^4 y(z,t)}{\partial z^4} = 0 \qquad (0 \le z \le L), \tag{2.1}$$

where y represents the beam's deflection, z is the coordinate along the longitudinal beam axis. In Eq. (2.1), $a^2 = EI/m$ where m is the mass per unit length, E is Young's modulus of elasticity and I is the cross-sectional area moment of inertia. EI together represents the flexural rigidity of the beam.

A general solution from separation of the variables takes the form

$$y(z,t) = Q(t)Y(z), \tag{2.2}$$

where, for time-harmonic phenomena,

$$Q(t) = A_1 \cos(\omega t) + A_2 \sin(\omega t), \tag{2.3}$$

and for z-dependent deflection amplitude

$$Y(z) = B_1 \sin(kz) + B_2 \cos(kz) + B_3 \sinh(kz) + B_4 \cosh(kz). \tag{2.4}$$

Here, $\omega = ak^2$ is natural frequency; the relations between the constants A_1, A_2 are to be obtained from two initial conditions, and between B_1, B_2, B_3, B_4 from four boundary conditions of the vibration problem. From Eq. (2.3), we can see that $Q(t)$ is harmonic no matter what the factor $Y(z)$ is.

The boundary conditions can be stated as follows. At a fixed end (in $z=z_0$) of a beam, where the displacement and slope both vanish, the boundary conditions are

$$y\big|_{z_0} = 0, \qquad \left.\frac{\partial y}{\partial z}\right|_{z_0} = 0. \tag{2.5}$$

At a free end (in $z=z_1$), where the bending moment and the shearing force are both zero, we have

$$\left.\frac{\partial^2 y}{\partial^2 z}\right|_{z_1} = 0, \quad \left.\frac{\partial^3 y}{\partial^3 z}\right|_{z_1} = 0. \tag{2.6}$$

Free vibration of a bridge

Using the boundary conditions of Eq. (2.5) at both $z = 0$ and $z = L$, the solution for free vibration of a bridge can be obtained as

$$\begin{aligned} Y(z) = & \frac{B_1}{\sin(kL)+\sinh(kL)} \\ & \times\{[\sin(kL)+\sinh(kL)][\sin(kz)-\sinh(kz)] \\ & +[\cos(kL)-\cosh(kL)][\cos(kz)-\cosh(kz)]\}, \end{aligned} \tag{2.7}$$

where k is the eigenvalue of the characteristic equation

$$\cos(kL)\cosh(kL) = 1. \tag{2.8}$$

The solutions of Eq. (2.8) can be obtained numerically, yielding an infinite set of eigenvalues k_i ($i = 1, 2, \ldots$). Inserting each k_i for k into Eq. (2.7), we obtain the corresponding natural mode $Y_i(z)$. The first four modes of a bridge are shown in Fig. 2.2.

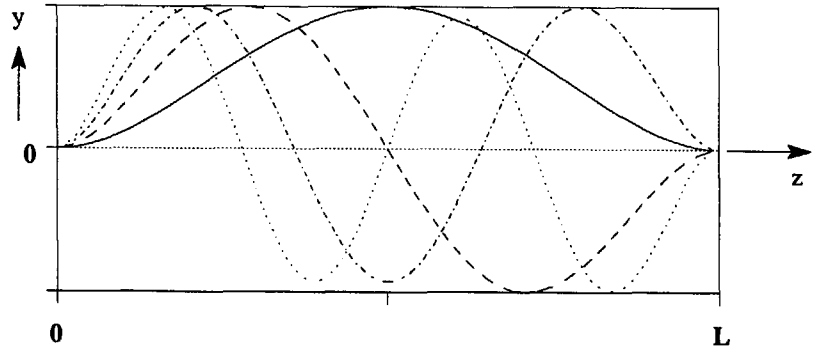

Fig. 2.2 Transverse vibration modes of a bridge.

Free vibration of a cantilever

Substituting the general solution to the boundary conditions of Eq. (2.5) at $z=0$ and of Eq. (2.6) at $z = L$ for a cantilever yields

$$Y_i(z) = \frac{B_1}{\sin(k_iL) - \sinh(k_iL)} \times\{[\sin(k_iL) - \sinh(k_iL)][\sin(k_iz) - \sinh(k_iz)] + [\cos(k_iL) + \cosh(k_iL)][\cos(k_iz) - \cosh(k_iz)]\}, \quad (2.9)$$

while k_i can be determined from the characteristic equation

$$\cos(kL)\cosh(kL) = -1. \quad (2.10)$$

The first four modes of a freely vibrating cantilever are presented in Fig. 2.3.

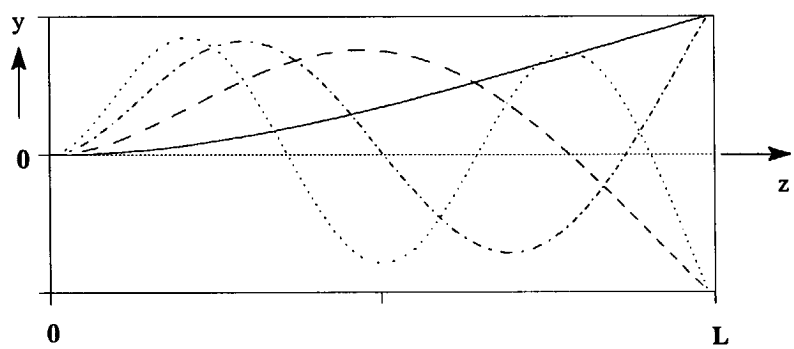

Fig. 2.3 Modes of transverse vibrations of a cantilever.

Forced Vibration

We consider the case that a uniformly distributed force of intensity $F\sin(\omega' t)$ is applied to a cantilever or to a bridge. The equation for transverse vibrations in the existence of an external force as $F\sin(\omega' t)$ is

$$\frac{\partial^2 y}{\partial t^2} + a^2 \frac{\partial^4 y}{\partial z^4} = \frac{1}{m} F \sin(\omega' t). \tag{2.11}$$

Since we are interested in the steady state vibration, we assume $y(z,t) = Y(z)\sin(\omega' t)$ to be the solution form. Substituting this expression for y in Eq. (2.11) and using the notation $p = \sqrt{\omega'/a}$, we obtain

$$\begin{aligned} Y(z) = {} & B_1 \sin(pz) + B_2 \cos(pz) \\ & + B_3 \sinh(pz) + B_4 \cosh(pz) - \frac{F}{m\omega'^2}. \end{aligned} \tag{2.12}$$

Using the boundary conditions for a bridge, the solution of the forced vibration takes the form

$$\begin{aligned} Y(z) = {} & B_1[\sin(pz) - \sinh(pz)] + B_2[\cos(pz) - \cosh(pz)] \\ & + \frac{F}{m\omega'^2}[\cosh(pz) - 1], \end{aligned} \tag{2.13}$$

where

$$B_1 = \frac{F}{2m\omega'^2} \frac{\sin(pL)[1 - \cosh(pL)] + \sinh(pL)[1 - \cos(pL)]}{1 - \cos(pL)\cosh(pL)}, \tag{2.14}$$

and

$$B_2 = \frac{F}{2m\omega'^2}\left[1 - \frac{\sin(pL)\sinh(pL) + \cos(pL) - \cosh(pL)}{1 - \cos(pL)\cosh(pL)}\right]. \tag{2.15}$$

Similarly, applying the boundary conditions of a cantilever, the solution becomes

$$\begin{aligned} Y(z) = {} & B_1[\sin(pz) - \sinh(pz)] + B_2[\cos(pz) - \cosh(pz)] \\ & + \frac{F}{m\omega'^2}[\cosh(pz) - 1], \end{aligned} \tag{2.16}$$

where

$$B_1 = \frac{F}{2m\omega'^2}\frac{\sin(pL)\cosh(pL)+\cos(pL)\sinh(pL)}{1+\cos(pL)\cosh(pL)}, \tag{2.17}$$

and

$$B_2 = \frac{F}{2m\omega'^2}\left[1-\frac{\sin(pL)\sinh(pL)}{1+\cos(pL)\cosh(pL)}\right]. \tag{2.18}$$

The deflection $y(z)$ of a bridge undergoing forced vibration is calculated and drawn in Fig. 2.4, while that of a cantilever is shown in Fig. 2.5. This kind of deflection will in its turn contribute to the optical bending loss in the waveguide bridges and cantilevers, which will be discussed in more detail in the next two sections.

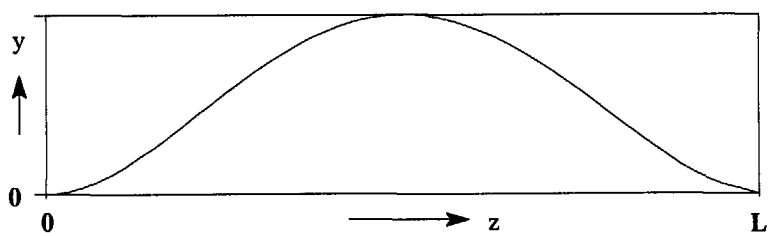

Fig. 2.4 Deflection of a bridge under forced vibration (uniformly distributed force).

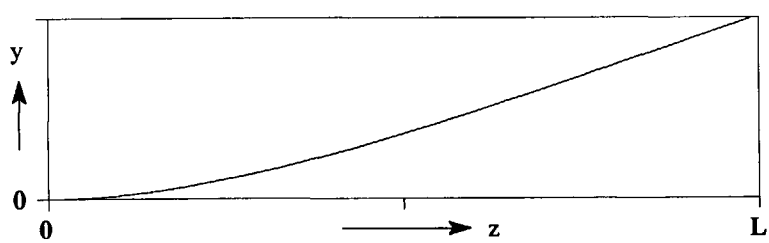

Fig. 2.5 Deflection of a cantilever under forced vibration (uniformly distributed force).

For both structures, we see that resonance will occur if the forcing frequency ω' equals the natural frequency ω_i. Then, the amplitude of the steady vibration will theoretically tend to infinity.

2.1.2 Static Behavior

In terms of static behavior, we are interested in the static deflection of a beam due to an applied force F. The beam is again assumed homogeneous and the deflection is small. The effect of a beam's own weight is ignored. Under these conditions, the beam's deflection curve is governed by [2]

$$\frac{d^2y(z)}{dz^2} = \frac{M(z)}{EI}, \tag{2.19}$$

where $M(z)$ is the bending moment at point z.

For a bridge beam with a force F applied at the center, the bending moment $M(z) = F(L-4z)/8$ when $0 \le z \le L/2$. The deflection curve $y(z)$ takes the form

$$y(z) = \frac{F}{8EI}\left(\frac{Lz^2}{2} - \frac{2z^3}{3}\right) \qquad (0 \le z \le L/2). \tag{2.20}$$

In the region when $L/2 \le z \le L$, $y(z)$ is symmetric with respect to the central line $z = L/2$. The deflection at the center is

$$y_b = \frac{L^3}{192EI}F. \tag{2.21}$$

Similarly, for a cantilever beam with a force F applied at the free end, the bending moment $M(z)=F(L-z)$ and

$$y(z) = \frac{FL^3}{6EI}\left[3\left(\frac{z}{L}\right)^2 - \left(\frac{z}{L}\right)^3\right]. \tag{2.22}$$

The deflection y_c at the free end can be written in the form

$$y_c = \frac{L^3}{3EI}F. \tag{2.23}$$

The deflection curves for these two cases are plotted in Fig. 2.6.

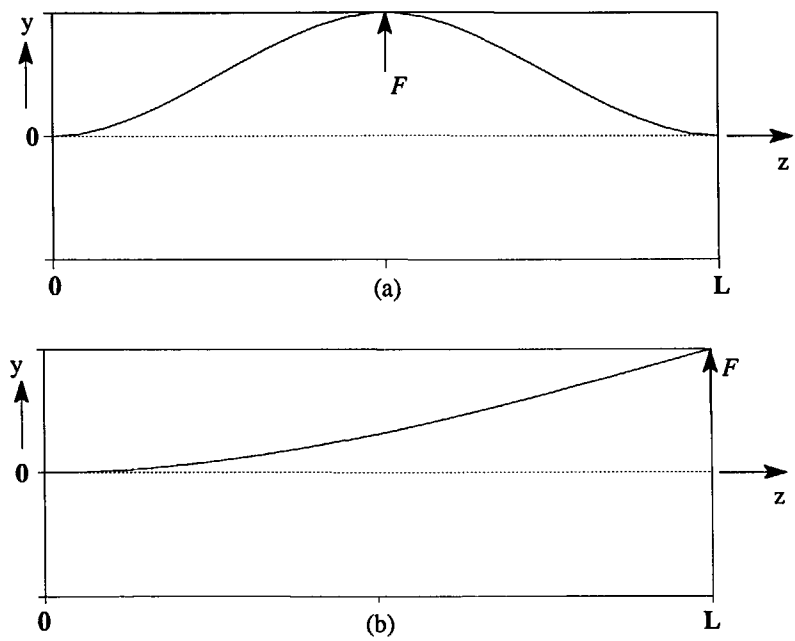

Fig. 2.6 Deflection curves for (a) a bridge under a point force at the center and (b) a cantilever under a point force at its free end.

The results obtained in this section will be helpful to understand the operational principles of micro-bridges and cantilevers used as optical sensor elements, and to evaluate the sensitivities of the sensor elements.

2.2 *Optical Loss in Bridges and Cantilevers*

It is essential in integrated optics to use curved waveguides in order to place a certain number of optical components on a single substrate. For various reasons, curved waveguides may be used to connect two waveguides with different directions or to introduce a lateral displacement without changing directions. In some circumstances, curved waveguides are basically required to achieve certain components for integrated optical circuits, such as mode filters, couplers or sensor elements.

In a waveguide bridge or cantilever, transverse vibrations or static deflections will create bends. It is necessary to know the change of the mode propagation properties and the additional loss in a curved waveguide in comparison to a straight one. This section describes a method for analyzing curved waveguides with arbitrary cross-sections.

2.2.1 Introduction to Curved Waveguides

It is well known that a dielectric waveguide loses power by radiation if its axis is curved. Because of its importance in determining the minimum allowable radius of waveguide curvature, many researchers have dedicated their efforts to calculate the radiation loss of a curved guide, and various methods for analyzing curved waveguides have been proposed. Marcatili and Miller [3] described an approach studying the group velocity distribution in a cross section, which is a simple method to understand bending radiation loss qualitatively. Another approximate method developed by Marcatili [4] solves eigenvalue equations with boundary conditions in order to calculate the loss in a curved waveguide. M. Heiblum and J. H. Harris [5] applied conformal transformations in their analysis of curved waveguides. Marcuse and Lewin [6][7] investigated the bend loss problem by representing the fields in the external region by Hankel functions and assuming the fields within the waveguiding layer undeformed as compared to those in a straight waveguide. The method was extended by M.

Miyagi and S. Nishida [8] from slab to rectangular waveguides. K. S. Kaufman [9] used the same method and developed a closed-form integral to calculate the losses of high-order modes. Recently, the beam propagation method (BPM) was employed by R. Baets and P. E. Lagasse [10] and a numerical solution was found for radiation loss in arbitrarily curved waveguides. D. C. Chang and E. F. Kuester [11] utilized an approach that resembles the perturbation theory of quantum mechanics. E. C. M. Pennings [12] spent much effort tackling the curved waveguide problem; several methods, such as the effective index approach, the WKB approximation and the transfer-matrix, were applied in his thesis.

The described methods differ in many ways since intuitive assumptions are quite often introduced before the serious theoretical derivation begins. There is also much confusion about the definitions of attenuation and radiation loss of a guided mode caused by waveguide curvature. The contribution to the attenuation should include not only the radiation loss, but also the power converted to other guided modes (both forward- and backward-propagating modes). Furthermore, the analysis of the mode conversion or the change in propagation constants have not yet been paid considerable attention. However, the mode conversion is the core in the analysis of a curved waveguide since radiation loss is actually caused by the conversion of a guided mode to radiation modes. As we will show, the change in propagation constants can also be used as a parameter to determine the minimum allowable bending radius.

In the theory to be described, Maxwell's equations in cylindrical coordinates are the starting point for the analysis of a curved waveguide with an arbitrary cross section. The electro-magnetic field in a curved guide is expanded in the modes of a straight waveguide with the same cross-section. Due to the curvature of the waveguide, those modes will be coupled. The attenuation of a guided mode comes from two sides: radiation loss and mode conversion to other guided modes; all those guided modes couple to radiation

modes and as such contribute to the radiation loss. The method described here is capable to obtain the solution to radiation loss, changes in propagation constants, and coupling coefficients, provided that the modes of the corresponding straight waveguide are known.

2.2.2 *Theory of Curved Waveguides*

A curved waveguide is schematically depicted in Fig. 2.7, along with a

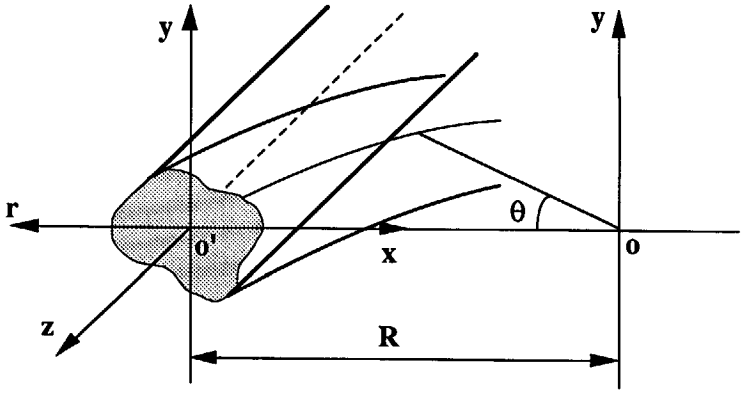

Fig. 2.7 Curved waveguide with cylindrical coordinates and a reference waveguide with local rectangular coordinates (r,θ in xz-plane).

reference straight waveguide with the same cross section. If a cylindrical coordinate system (r, θ, y) is defined for the curved waveguide and a rectangular coordinate system (x, y, z) for the reference straight waveguide, as shown in the figure, the relations between the two coordinates are apparently

$$\begin{cases} x = R - r, \\ y = y, \\ dz = rd\theta, \end{cases} \tag{2.24}$$

where R is the radius of the curved waveguide. The actual field in the curved waveguide satisfies Maxwell's equations in cylindrical coordinates:

$$\begin{cases} j\omega\varepsilon r E_r = \dfrac{\partial H_y}{\partial \theta} - r\dfrac{\partial H_\theta}{\partial y}, \\ j\omega\varepsilon r E_y = \dfrac{\partial (r H_\theta)}{\partial r} - \dfrac{\partial H_r}{\partial \theta}, \\ j\omega\varepsilon E_\theta = \dfrac{\partial H_r}{\partial y} - \dfrac{\partial H_y}{\partial r}, \\ -j\omega\mu r H_r = \dfrac{\partial E_y}{\partial \theta} - r\dfrac{\partial E_\theta}{\partial y}, \\ -j\omega\mu r H_y = \dfrac{\partial (r E_\theta)}{\partial r} - \dfrac{\partial E_r}{\partial \theta}, \\ -j\omega\mu E_\theta = \dfrac{\partial E_r}{\partial y} - \dfrac{\partial E_y}{\partial r}. \end{cases} \tag{2.25}$$

Similarly, Maxwell's equations for the *m-th* order mode (m= 1,2,3,...) of the straight waveguide can be expressed in the rectangular coordinates *(x,y,z)* as:

$$\begin{cases} j\omega\varepsilon E_x^m = \dfrac{\partial H_z^m}{\partial y} + j\beta_m H_y^m, \\ -j\omega\varepsilon E_y^m = \dfrac{\partial H_z^m}{\partial x} + j\beta_m H_x^m, \\ j\omega\varepsilon E_z^m = \dfrac{\partial H_y^m}{\partial x} - \dfrac{\partial H_x^m}{\partial y}, \\ -j\omega\mu H_x^m = \dfrac{\partial E_z^m}{\partial y} + j\beta_m E_y^m, \\ j\omega\mu H_y^m = \dfrac{\partial E_z^m}{\partial x} + j\beta_m E_x^m, \\ -j\omega\mu H_z^m = \dfrac{\partial E_y^m}{\partial x} - \dfrac{\partial E_x^m}{\partial y}. \end{cases} \tag{2.26}$$

Since the modes of a straight waveguide form a complete set, the field in a curved waveguide can be expanded in terms of the modes in a straight waveguide. Supposing that the fields perpendicular to the z-direction, (for the moment indicated as "transverse") in the (r,θ,y) system are described by $\mathbf{E}_t(r,\theta,y)$ and $\mathbf{H}_t(r,\theta,y)$, then

$$\begin{aligned}\mathbf{E}_t(r,y,\theta) &= \sum_m a_m(\theta)\mathbf{E}_t^m(x,y)\,,\\ \mathbf{H}_t(r,y,\theta) &= \sum_m b_m(\theta)\mathbf{H}_t^m(x,y)\,.\end{aligned} \tag{2.27}$$

Dividing $\mathbf{E}_t^m$ and $\mathbf{H}_t^m$ into forward fields (propagating in the positive z direction) $\mathbf{E}_t^{m+}$, $\mathbf{H}_t^{m+}$ and backward fields $\mathbf{E}_t^{m-}$, $\mathbf{H}_t^{m-}$, we have [13]

$$\begin{aligned}a_m(\theta)\mathbf{E}_t^m(x,y) &= c_m^+(\theta)e^{-j\beta_m^+ z}\mathbf{E}_t^{m+} + c_m^-(\theta)e^{j\beta_m^- z}\mathbf{E}_t^{m-}\,,\\ b_m(\theta)\mathbf{H}_t^m(x,y) &= c_m^+(\theta)e^{-j\beta_m^+ z}\mathbf{H}_t^{m+} - c_m^-(\theta)e^{j\beta_m^- z}\mathbf{H}_t^{m-}\,.\end{aligned} \tag{2.28}$$

We extend m from the interval $(1,+\infty)$ to $(-\infty,+\infty)$ by putting that backward-propagating fields have negative m's and use the following transformations

$$\begin{aligned}\beta_m^+ &= -\beta_m^-\,,\\ \mathbf{E}_t^{m+} &= \mathbf{E}_t^{m-}\,,\\ \mathbf{H}_t^{m+} &= -\mathbf{H}_t^{m-}\,.\end{aligned} \tag{2.29}$$

Omitting the propagation signs, Eq. (2.27) can be re-written subsequently as

$$\begin{aligned}\mathbf{E}_t(r,\theta,y) &= \sum_{m=-\infty}^{+\infty} A_m(\theta)\mathbf{E}_t^m(x,y)\,,\\ \mathbf{H}_t(r,\theta,y) &= \sum_{m=-\infty}^{+\infty} A_m(\theta)\mathbf{H}_t^m(x,y)\,.\end{aligned} \tag{2.30}$$

Here, $A_m(\theta) = c_m(\theta)\exp(-j\beta_m z)$. From Eq. (2.30), we obtain

$$
\begin{aligned}
E_r(r,\theta,y) &= -\sum_{m=-\infty}^{+\infty} A_m(\theta) E_x^m(x,y)\,, \\
E_y(r,\theta,y) &= \sum_{m=-\infty}^{+\infty} A_m(\theta) E_y^m(x,y)\,, \\
H_r(r,\theta,y) &= -\sum_{m=-\infty}^{+\infty} A_m(\theta) H_x^m(x,y)\,, \\
H_y(r,\theta,y) &= \sum_{m=-\infty}^{+\infty} A_m(\theta) H_y^m(x,y)\,.
\end{aligned}
\tag{2.31}
$$

Inserting Eq. (2.31) into Eq. (2.25) leads, with the aid of Eq. (2.26), to

$$
\begin{aligned}
E_\theta(r,\theta,y) &= \sum_{m=-\infty}^{+\infty} A_m(\theta) E_z^m(x,y)\,, \\
H_\theta(r,\theta,y) &= \sum_{m=-\infty}^{+\infty} A_m(\theta) H_z^m(x,y)\,.
\end{aligned}
\tag{2.32}
$$

From now on, we will omit the range indication of m $(-\infty,+\infty)$ in the summations. Substituting E_r, E_y, E_θ, H_r, H_y, and H_θ into Maxwell's equations (2.25), we obtain

$$
\begin{aligned}
\sum_m \frac{dA_m(\theta)}{d\theta} E_x^m &= -\sum_m \left[A_m(\theta) E_z^m + jr\beta_m A_m(\theta) E_x^m \right], \\
\sum_m \frac{dA_m(\theta)}{d\theta} E_y^m &= -\sum_m jr\beta_m A_m(\theta) E_y^m\,, \\
\sum_m \frac{dA_m(\theta)}{d\theta} H_x^m &= -\sum_m \left[A_m(\theta) H_z^m + jr\beta_m A_m(\theta) H_x^m \right], \\
\sum_m \frac{dA_m(\theta)}{d\theta} H_y^m &= -\sum_m jr\beta_m A_m(\theta) H_y^m\,.
\end{aligned}
\tag{2.33}
$$

If we express $A_m(\theta)$ in the rectangular coordinates (x,y,z) and use the relations between z and θ, as well as between x and r, as described in Eq. (2.24), then

$$\frac{dA_m}{d\theta} = (R-x)\frac{dA_m}{dz}. \tag{2.34}$$

Multiplying the proper equations from Eq. (2.33) with the complex conjugates of the field components $-H_y^{l*}$, H_x^{l*}, E_y^{l*} and $-E_x^{l*}$, and adding them properly, we obtain [14]

$$\begin{aligned}\sum_m \left(E_y^m H_x^{l*} + H_x^m E_y^{l*} - E_x^{l*} H_y^m - H_y^{l*} E_x^m\right)\frac{dA_m}{dz} \\ = -\sum_m j\beta_m \left(E_y^m H_x^{l*} + H_x^m E_y^{l*} - E_x^{l*} H_y^m - H_y^{l*} E_x^m\right)A_m \\ + \sum_m \frac{1}{R-x}\left(E_y^{l*} H_z^m - E_z^m H_y^{l*}\right)A_m .\end{aligned} \tag{2.35}$$

Integrating Eq. (2.35) across the entire transverse plane and utilizing the orthogonality and normalization conditions, we arrive at

$$\frac{dA_l}{dz} = -j\beta_l A_l + \sum_m \frac{1}{4}\left[\iint \frac{1}{R-x}\left(E_y^{l*} H_z^m - E_z^m H_y^{l*}\right)dxdy\right]A_m . \tag{2.36}$$

If we introduce the abbreviation

$$k_{lm} = \frac{1}{4}\iint \frac{1}{R-x}\left(E_y^{l*} H_z^m - E_z^m H_y^{l*}\right)dxdy, \tag{2.37}$$

the equation (2.36) can be rewritten as

$$\frac{dA_l}{dz} = -j\beta_l A_l + \sum_m k_{lm} A_m \,. \tag{2.38}$$

This is a coupled mode equation, and k_{lm} represents the coupling coefficient between the *m-th* order and *l-th* order modes. With Eq. (2.37), k_{lm} can be determined from the fields of modes in the *(x,y,z)* rectangular coordinates.

2.2.3 Numerical Results and Discussion

In this analysis of a curved waveguide, strategies have to be followed to treat the curved waveguide problem as a whole, not only the radiation loss. A general case of curved guides has been considered instead of particular types. The waveguiding properties due to waveguide bending is believed to be governed by the same theory regardless its type (open or closed guide) or its cross-sectional shape (planar, rectangular or circular). Following such an approach, the solutions concerning the radiation loss, the changes in the propagation constant and the coupling coefficients are obtained altogether. In the following, some useful results will be derived.

Propagation constant. Bending of a waveguide causes a change in the propagation constant of a guided mode in comparison to that of a straight waveguide. The change in the propagation constant for *m-th* order mode equals

$$\Delta\beta_m = \frac{j}{4}\iint \frac{1}{R-x}\left(E_y^{m*} H_z^m - E_z^m H_y^{m*}\right) dxdy. \tag{2.39}$$

Computing examples for the propagation constant changes are presented in Fig. 2.8 for the symmetric and asymmetric configurations. In the calculation, the wavelength of a TE_0 mode is taken as 632.8 nm. The bent planar waveguides have a thickness of 0.3 μm and a refractive index of N_f. The

refractive index outside the bent waveguides is denoted as N_o and inside as N_i. The results can be utilized to determine the minimum allowable radius of a curved waveguide which is usually determined by evaluating the radiation loss in other methods. When $\Delta\beta$ of a guided mode begins to alter rapidly corresponding to a change of the bending radius, the guided mode is likely to undertake a transit from a stable, low-loss propagation to a lossy one, and the radius is regarded as the minimum allowable radius. In the examples presented in the Fig. 2.8, the minimum allowable radius for the second curve can be judged as 12 μm. Asymmetric distribution of the refractive indices alongside a curved waveguide plays an additional role in the propagation constant change, as shown in the figure. $\Delta\beta$, which is positive in the symmetric case, can become negative if $N_o > N_i$. This phenomenon may be utilized in the practical design of waveguide bends to minimize $\Delta\beta$ for a given radius by properly balancing the refractive indices of N_o and N_i.

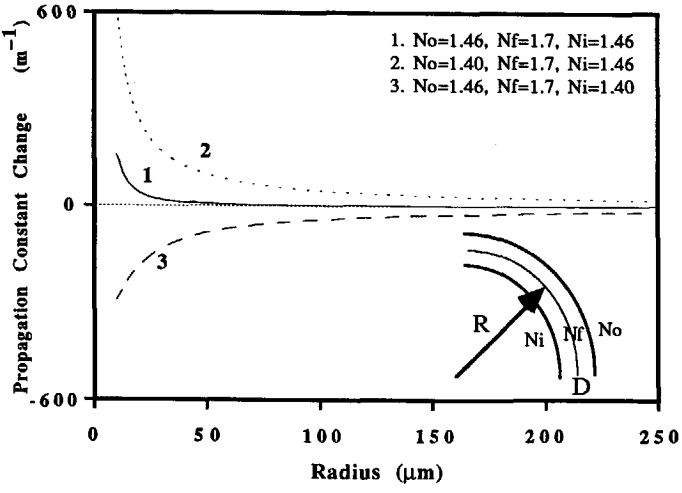

Fig. 2.8 Propagation constant changes due to bending, subscript *o* denotes outside the bending guide while *i* inside.

Coupling coefficients. The coupling between two different modes is expressed by the coefficient k_{lm}. Because of the bending, a single mode can not propagate in a curved waveguide alone, and mode conversion to other guided modes and to radiation modes must occur. Coupling to the radiation modes contributes to radiation loss. It is also possible that the power of a guided mode will be coupled to backward modes ($k_{lm} \neq 0$), even to the same but backward-propagating mode; the coupling coefficient for TE modes is $k_{-m,m} = -j\Delta\beta_m$, while for TM modes $k_{-m,m} = j\Delta\beta_m$. From Eq. (2.37), we can easily prove that coupling between an TE and an TM mode will not occur in a curved guide.

Radiation loss. Assuming that the power coupled into radiation modes will not be coupled back and therefore becomes radiation loss, the total radiation loss of a guided mode should include power coupled to all radiation modes. The radiation loss is different from the power loss (attenuation) of the guided mode which should include power coupled both to radiation modes and to other guided modes. The radiation loss can be calculated by a method discussed by Marcuse [13]. Numerical analysis of the radiation loss, however, is a quite complicated process. We simply present the resulting formula for calculating the radiation loss 2α as

$$2\alpha = \sum \int_{-n_o k}^{n_o k} \left| k_{rg} \right|^2 \frac{2\sin(\beta_g - \beta_r)z}{\rho_r (\beta_g - \beta_r)} |\beta_r| d\beta_r , \qquad (2.40)$$

where the subscript r indicates a quantity for radiation modes and the g for a guided mode, and $\rho_r = \sqrt{k_0^2 n_0^2 - \beta_r^2}$. k_{rg} is the coupling coefficient and is determined from Eq. (2.37). Detailed derivation of Eq. (2.40) can be found in Appendix A. As indicated in the equation, the radiation loss is z-dependent which is confirmed by the experiments performed by Neumann and Rudolph [15]. The relation between the radiation loss 2α and the bending radius R is determined by the quantity $\left| k_{rg} \right|$ which can be numerically

calculated. Taking the same symmetric case as in Fig. 2.8 and $\beta_r = \frac{1}{2}\beta_g$, the solution for $|k_{rg}|$ and $|k_{rg}|^2$ is presented in Fig. 2.9. The figure shows the influence of the bending radius on the radiation loss.

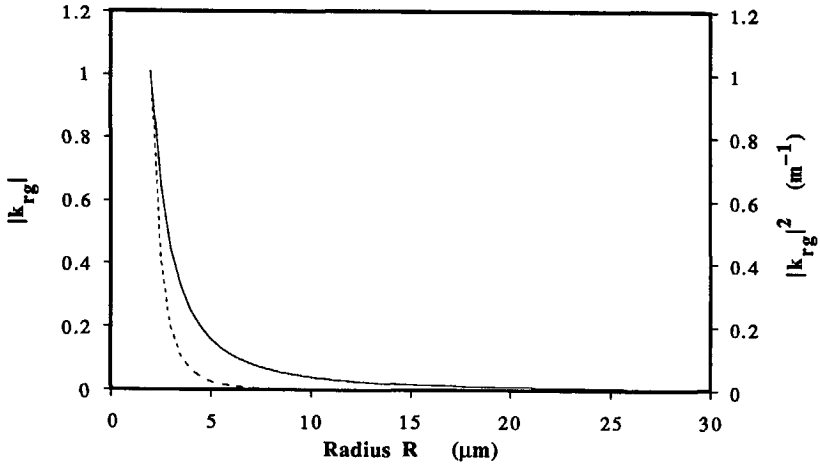

Fig. 2.9 Coupling coefficient between a guided mode and a radiation mode due to waveguide bending, solid line: $|k_{rg}|$ and dashed line: $|k_{rg}|^2$.

From Eq. (2.37), it is obvious that there is a singular point at $x=R$ (the curvature center) in the integral function. This may imply that the excitation of other modes due to waveguide bending seems to be caused by a fictitious point source at the curvature center. The existence of this singularity provokes difficulties in the numerical calculation. In most cases, however, the electromagnetic field of a guided mode is well confined within the waveguide, and the part of the field tailing into the region near $x=R$ is negligible. Thus, numerical analysis can proceed quite easily. When the waveguide dimension (denoted as D in the bending direction) approaches the bending radius R and the tailing field at $x=R$ is no longer negligible, the waveguide gets more lossy, and the numerical analysis becomes more difficult, and results in more serious calculation

errors. Practically, such a situation is avoided in the waveguide design. In an extreme case, when $D \geq 2R$ (a bending guide turns into a disk), the coupling coefficient shows an infinite value.

2.3 Optical Coupling in Cantilevers

An exact theoretical evaluation of the sensitivities of the micro-mechanical structures to external forces is very complicated, especially for a bridge structure, since the radiation loss due to bending and inhomogeneous stress induced by the external forces is hard to be calculated. For a cantilever structure, the optical loss induced by external forces is mainly determined by the optical coupling between the cantilever's free end and the output section. In this section, an approximate method is introduced to deal with the optical coupling in the cantilever structure.

2.3.1 Introduction

When a guided wave is launched into the input section in a cantilever structure, the wave will first propagate through the waveguide cantilever. Then it will meet the free end of the cantilever and is converted into radiated waves in free space. Part of the radiated waves will be coupled into the waveguide in the output section and the rest becomes optical loss. It is important to analyze this coupling process in order to understand the sensing principles of cantilever structures. The cantilever which is under deflection or without deflection can be illustrated in Fig. 2.10.

2.3.2 Coupling Efficiency

An exact analysis for coupling efficiency in a cantilever structure should involve: (1) the conversion of the guided waves in the waveguide to radiated waves in free space; (2) the wave propagation from the cantilever's free end

toward the output section; (3) coupling of the radiated waves back to guided waves in the output section and (4) reflections at both interface surfaces. Besides, the tilt angle of the surface of the cantilever's free end and the direction change in the waveguide axis of the deflected cantilever will also influence the coupling efficiency. All these aspects make an exact theoretical analysis an impossible task. Using proper approximations, however, it is possible to estimate the coupling coefficient.

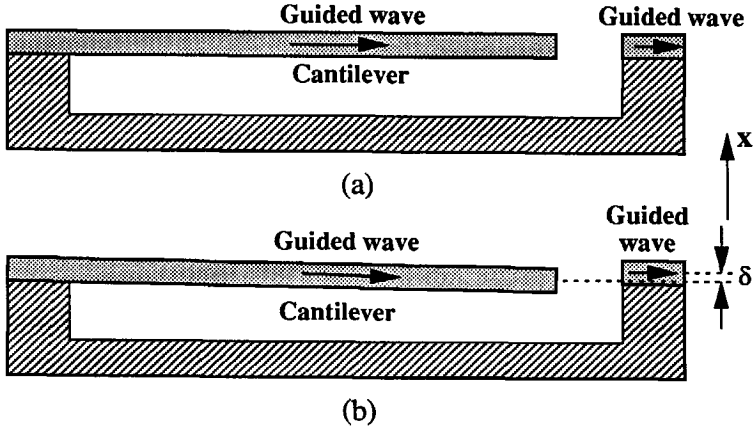

Fig. 2.10 Optical coupling in a cantilever structure, (a) cantilever without deflection, (b) cantilever under deflection.

We will ignore the reflections and the tilt angle of the cantilever's end surface. The cantilever-shaped waveguide is assumed to be a planar guide, restricting the theory to cantilever widths of more than a few wavelengths. The fundamental modes are also assumed symmetric in the x-direction. Thus, a fundamental mode within the waveguide can be described by a wave function with an x-dependence of the form

$$\psi_w(x,z) = A_w(z)\cos(k_x x), \tag{2.41}$$

where A_w is the mode amplitude. Outside the waveguide, the wave has an exponentially decay function. Now we introduce a Gaussian beam

$$\psi_g(x,z) = A_g(z)e^{-\frac{x^2}{w^2}}, \tag{2.42}$$

to approximate the guided mode [16]. Here A_g is the amplitude of the Gaussian beam. Detailed discussions on the Gaussian approximation of the fundamental modes have been provided by D. Marcuse [16]. Here w represents the beam half-width and is chosen to satisfy $\cos(k_x w)=1/e$. Choosing also $\psi_g=\psi_w$ at the point $x=0$, then ψ_g equals ψ_w at the points $x=\pm w$ and is a good approximation to the mode in the waveguide. However, it is a poor approximation for the evanescent field away from the waveguide. Let's consider a symmetric configuration of a waveguide with a thickness of 0.3 μm, and a refractive index of 1.70. The refractive index outside of the waveguide is taken as 1.46. Fig. 2.11 exhibits the profiles of an actual TE mode and a Gaussian approximation.

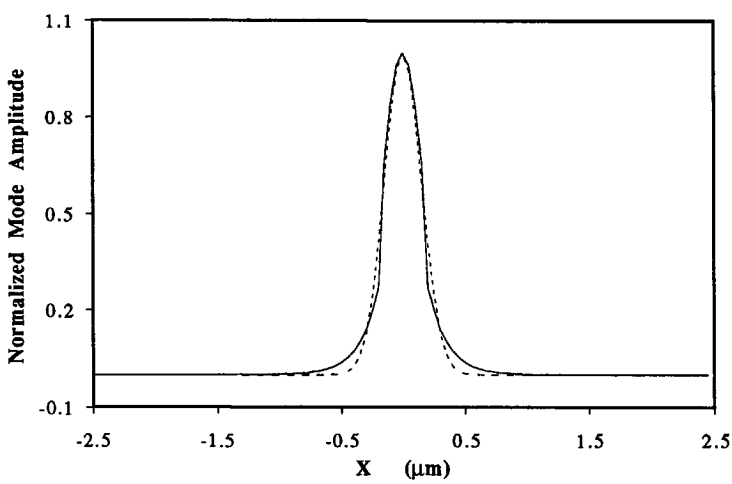

Fig. 2.11 Gaussian approximation to a fundamental TE mode, solid line: actual wave profile in a planar waveguide; dashed line: Gaussian approximation profile.

The coupling process now becomes simple to describe and is depicted in Fig. 2.12. A guided wave ψ_0 with a Gaussian profile emerges from the cantilever's free end, propagates through a distance d (the separation gap) and has a wave function ψ when reaching the output section. The coupling coefficient η is then the overlap integral [17] between ψ and the field ψ' in the output section which has also a Gaussian profile. Thus,

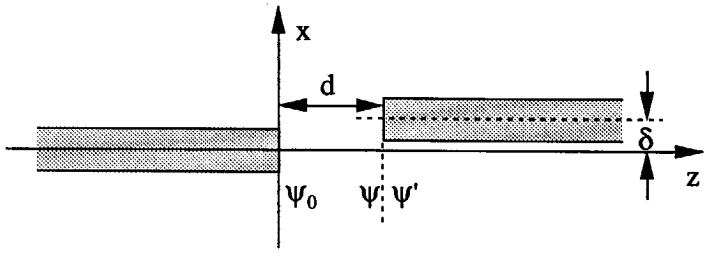

Fig. 2.12 Coupling process in a cantilever structure for the calculation of coupling coefficient.

$$\eta = \frac{\left|\iint \psi\psi'^{*}\, dxdy\right|^2}{\iint \psi\psi^{*} dxdy \iint \psi'\,\psi'^{*}\, dxdy}. \tag{2.43}$$

According to the Gaussian approximation, ψ_0 with a beam half-width w_0 has the form

$$\psi_0(x) = A_0 e^{-\frac{x^2}{w_0^2}}, \tag{2.44}$$

where A_0 is the amplitude of ψ_0. w_0 can be determined by making $\cos(k_x w_0)=1/e$. After propagating over a distance d, the wave ψ_0 reaches the output section and has a new Gaussian profile

$$\psi(x) = A e^{-\frac{x^2}{w^2}}, \tag{2.45}$$

where A is the amplitude of ψ; w is the new half-width and satisfies

$$w^2 = w_0^2\left[1+\left(\frac{\lambda d}{\pi w_0^2}\right)^2\right]. \tag{2.46}$$

Again according to the Gaussian approximation, the guided wave in the output section has the same profile as ψ_0 but with a shift along the x-direction equal to δ, and its field ψ' with an amplitude of A' can be expressed as

$$\psi'(x) = A' e^{-\frac{(x-\delta)^2}{w'^2}}. \tag{2.47}$$

Inserting Eqs. (2.45) and (2.47) into (2.43), yields the coupling coefficient

$$\eta = \frac{2ww'}{w^2+w'^2} e^{-\frac{2\delta^2}{w^2+w'^2}} = \eta_0 e^{-\frac{2\delta^2}{w^2+w'^2}}. \tag{2.48}$$

Here, η_0 is the coupling coefficient when there is no shift of the cantilever's free end, i.e., δ=0. The dependence of η_0 on the separation distance is presented in Fig. 2.13. Here, the same waveguide configuration as in Fig. 2.11

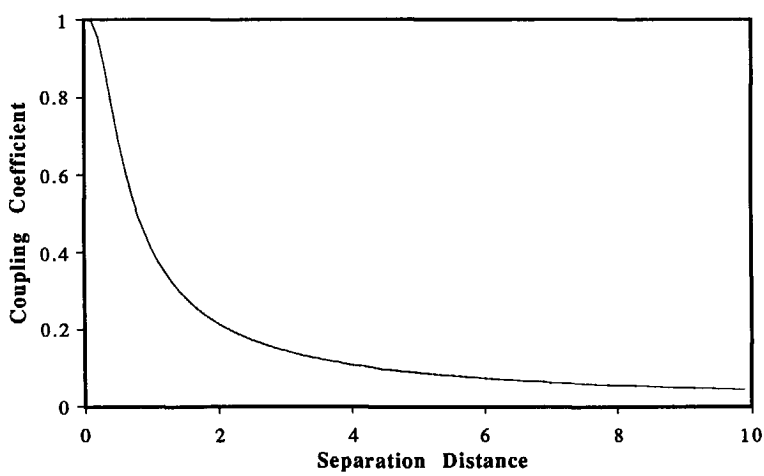

Fig. 2.13 Coupling efficiency in relation with the separation distance at zero shift.

is taken for the computation.

As we can see, the coupling coefficient is dependent on the shift of the cantilever's free end. This is the theoretical basis for using a cantilever structure as an optical sensor element.

References

1. W. T. Thomson, *Theory of Vibration with Applications*. Prentice-Hall, Inc., Englewood Cliffs, New Jersey, USA, 1972.
2. R. Kronig (Editor), *Textbook of Physics*. Pergamon Press, London, UK, 1959.
3. E. A. J. Marcatili, and S. E. Miller, "Improved Relations Describing Directional Control in Electromagnetic Wave Guidance," *The Bell System Technical J.*, vol. 48, no. 7, pp. 2161–2188, September 1969.
4. E. A. J. Marcatili, "Bends in Optical Dielectric Guides," *The Bell System Technical J.*, vol. 48, no. 7, pp. 2103–2132, September 1969.
5. M. Heiblum and J. H. Harris, "Analysis of Curved Optical Waveguides by Conformal Transformation," *IEEE J. Quantum Electronics*, vol. QE–11, no. 2, pp. 75–83, Feb. 1975.
6. D. Marcuse, "Bending Losses of the Asymmetric Slab Waveguide," *The Bell System Technical J.*, vol. 50, no. 8, pp. 2551–2563, Oct. 1971.
7. L. Lewin, "Radiation from Curved Dielectric Slabs and Fibers," *IEEE Trans. Microwave Theory and Techn.*, vol. MTT–22, no. 7, pp. 718–727, July 1974.
8. M. Miyagi and S. Nishida, "Bending losses of dielectric rectangular waveguides for integrated optics," *J. Opt. Soc. Am.*, vol. 68, no. 3, pp. 316–319, March 1978.
9. K. S. Kaufman, R. Terras and R. F. Mathis, "Curvature loss in multimode optical fibers," *J. Opt. Soc. Am.*, vol. 71, no. 12, pp. 1513–1518, Dec. 1978.
10. R. Baets and P. E. Lagasse, "Loss Calculation and Design of Arbitrarily Curved Integrated Optical Waveguide," *J. Opt. Soc. Am.*, vol. 73, no. 2, pp. 177–182, Feb. 1983.

11. D. C. Chang and E. F. Kuester, "Radiation and Propagation of a Surface-wave Mode on a Curved Open Waveguide of Arbitrary Cross Section," *Radio Science*, vol. 11, no. 5, pp. 449–457, May 1976.
12. E. C. M. Pennings, *Bends in Optical Ridge Waveguides*. Ph.D. Thesis of Delft University of Technology, 1990, ISBN 90-9003413-7.
13. D. Marcuse, *Theory of Dielectric Optical Waveguides*. New York: Academic Press, 1974.
14. T. Tamir (Editor), *Integrated Optics*. New York: Springer-Verlag, 1979.
15. E. Neumann and H. Rudolph, "Radiation from Bends in Dielectric Rod Transmission Lines," *IEEE Trans. Microwave Theory and Techn.*, vol. MTT–23, no. 1, pp. 142–149, Jan. 1975.
16. D. Marcuse, *Light Transmission Optics*. New York: Van Nostrand Reinhold Company, 1982.
17. W. K. Burns and G. B. Hocker, "End fire coupling between optical fibers and diffused channel waveguides," *Applied Optics*, vol. 16, pp. 2048–2050, 1977.
18. Hung-chia Huang, *Coupled Mode Theory*. Utrecht: VNU Science Press, The Netherlands, 1984.
19. Hung-chia Huang, *Principles of Microwaves*. Beijing: Science Press, 1963.

3

Technological Background

The operational principles of the micro-mechanical bridges and cantilevers have been described in the previous chapters. In this chapter, the micro-fabrication techniques underlying the fabrication of these bridges and cantilevers will be summarized. The emphasis is laid on the logical scheme for the fabrication of three-dimensional structures rather than on details of each technique since almost all of these techniques are common in electronic and optical IC's. Detailed documentation concerning these techniques can be found in numerous papers and books and a few of them are listed in the references of this chapter.

This chapter is divided into three sections. The first section discusses thin film deposition and growth techniques which are the tools for depositing certain materials upon a substrate or for changing preferentially the substance at certain locations. Patterning techniques (lithography) which determine the shapes of various components and their locations upon a substrate will be briefly considered in Section 3.2. Micro-processing (or micro-machining) techniques responsible for fine-shaping three-dimensional structures are going to be discussed in Section 3.3. These three technical aspects (deposition, patterning

and micro-processing) provide powerful tools for fabricating complicated three-dimensional structures.

3.1 Thin Film Deposition and Growth

A deposition or growth process creates a thin layer in or upon a substrate, as illustrated in Fig. 3.1. Available techniques are abundant, including spin

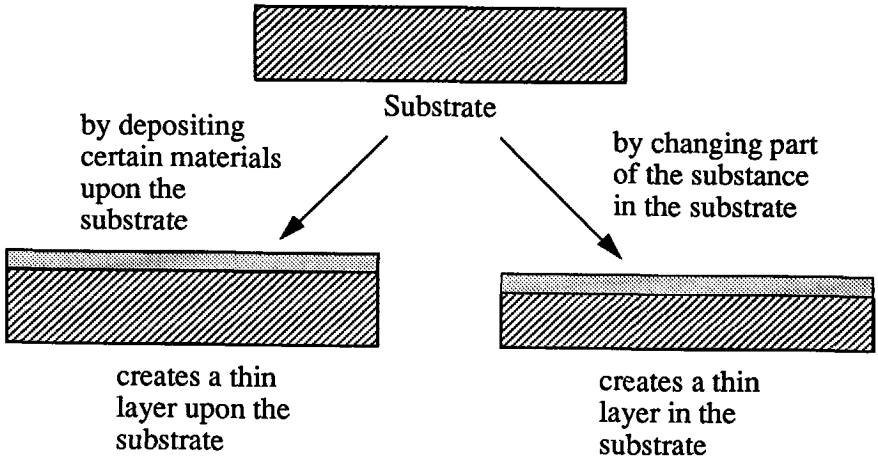

Fig. 3.1 Two ways to obtain a thin layer in or upon a substrate.

coating, dip coating, vacuum evaporation, sputtering, chemical vapor deposition (CVD), epitaxial growth, polymerization, ion exchange, ion implantation, thermal diffusion and others like thermal oxidation. Each of these techniques can be executed in various forms. For instance, epitaxial growth can have forms like liquid phase epitaxy (LPE), vapor phase epitaxy (VPE) or molecular beam epitaxy (MBE). Techniques such as ion exchange, ion implantation, thermal diffusion and thermal oxidation usually produce a thin layer in a substrate and

the new layer will have optical, electronic or mechanical properties different from those of the substrate. Other techniques usually deposit a thin layer of different material upon a substrate causing a step-wise change of those properties. Epitaxial growth requires a substrate in a crystal form and results in a crystalline layer of a similar material.

From those numerous ways to deposit or to form a very thin layer of certain material on a substrate, it is generally difficult to state which technique is the best. Choosing the right technique depends on various aspects such as the materials to be deposited, the required quality and the desired optical or mechanical properties of the thin layers. Among the thin film quality requirements, stability, adhesiveness, uniformity and reproducibility of fabrication are important factors. If used as a building material for optical components, a thin layer needs to be deposited according to a specified thickness, optical propagation loss, refractive index change or distribution. In the case of making three-dimensional structures like bridges and cantilevers, the mechanical properties of a thin film should also be considered seriously.

3.2 Lithography

The process of lithography is widely applied to produce high-resolution patterns on a substrate. There are three different patterning methods, i.e. patterning with a mask, through which the resist layer is exposed, direct resist patterning in which the resist is exposed by a moving laser, electron, X-ray or ion-beam following a pattern, and direct processing in which patterns are written directly in a substrate by a laser or an electron beam. The lithographic techniques can be classified, according to their exposure source, as photolithography, electron-, ion- or laser-beam lithography, X-ray lithography, etc.

Before any lithographic process begins, data concerning desired patterns need to be prepared either digitally by a computer or analogically by drawing the enlarged patterns. Nowadays, special computer programs are widely available to design high resolution micro-patterns, and mask making or direct processing has become an automatic or semi-automatic process.

Once a substrate is properly prepared, the lithographic process can begin. There are several major steps which are common to all lithographic process. The basic sequence of a lithographic process, as shown in Fig. 3.2, involves resist coating, softbaking, exposure, development, and postbaking.

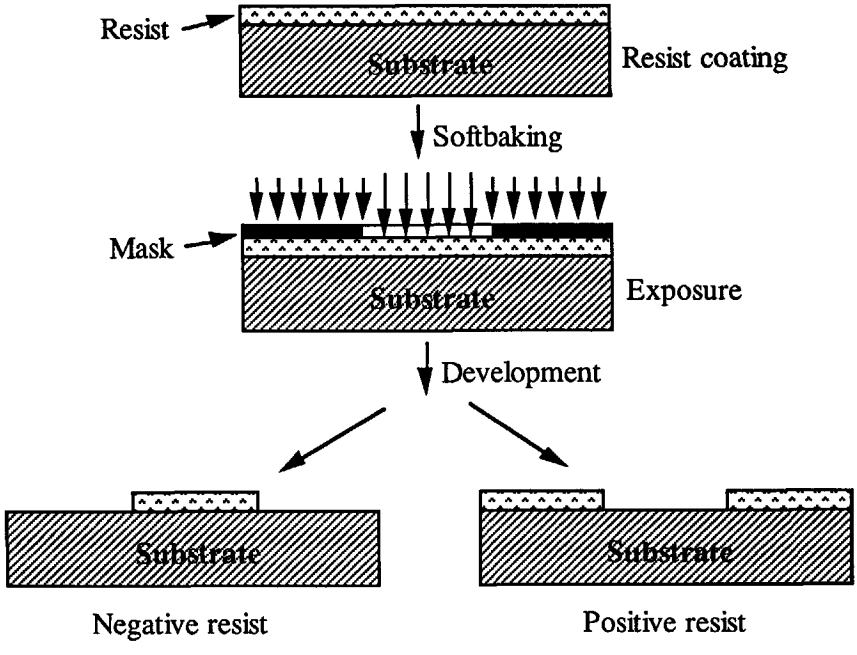

Fig. 3.2 Lithographic process to transmit designed patterns onto a substrate.

Spin coating is the most widely used technique for applying resist film onto a substrate. The resist film is then baked (softbaking) to remove the solvents present in the spin-coated resist film. This softbaking step is usually performed immediately after the spin coating. After the softbaking, exposure of the resist takes place through a mask or through patterned beams in the case of direct patterning. The goal of this exposure is to transmit a latent image of the designed pattern into the resist film. This latent image is fixed in the subsequent development process in which the developer selectively attacks and removes either the exposed regions (positive resist) or the unexposed regions (negative resist), leaving behind a resist coating in the required pattern to serve as a mask for further processes like etching. Postbaking is not always carried out but may be preferred in order to remove any residual moisture from the developing operation. Further, it bonds the resist to the substrate, and additionally hardens the resist by making it chemically inert to etchant solutions or gases. Direct processing is an exception to these process steps since no resist is involved.

3.3 Micro-Processing Techniques

Micro-processing (also often called micro-machining) techniques are introduced to transfer the pattern, formed in a resist layer or in a layer of other materials, to the substrate. They are especially important in the fabrication of three-dimensional micro-structures.

Although lift-off is classified as one of the processing techniques and is widely used for the patterning of relatively thin layers, it may be indicated as a masked deposition process. The patterned resist layer works as a mask layer. The most powerful and versatile processing tool continues to be etching even though new techniques are continuously being developed for use in micro-structures. The goal of etching is to precisely remove materials left exposed by holes in the mask layer. The basic etching process is illustrated in Fig. 3.3. As a

result, the same pattern as formed in the mask layer is transferred into the material below.

Photoresist can be used as a mask layer material. In cases when resist can not withstand the etching process, however, hard materials like metals, SiO_2, Si_3N_4 etc. can be applied as etching masks. Etching processes can be divided into wet etching (which occurs in liquid solutions), and dry etching (which uses gaseous etchants). Wet chemical etchants are numerous and usually different for etching different materials. They can be isotropic or anisotropic, dopant dependent or not, and have varying degrees of selectivity to different materials, which determines the appropriate masking materials. In an isotropic etching process, the etchants remove material in all directions at the same etch rate, while an anisotropic etching exhibits a strong dependence of the etch rate on the crystallographic orientation. Dry etching includes plasma, reactive ion, or sputter etching and is generally considered as anisotropic etching.

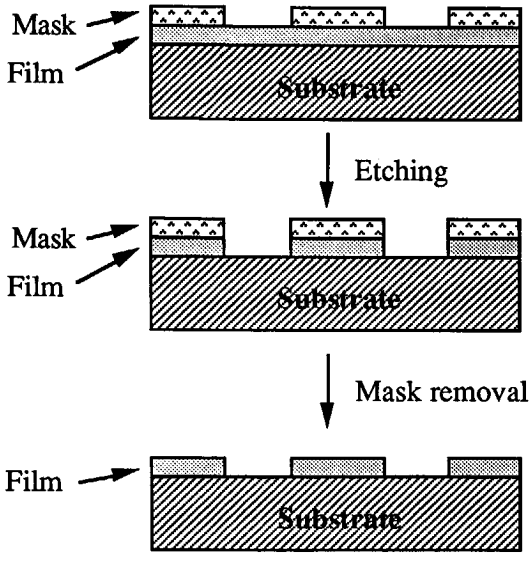

Fig. 3.3 Pattern transfer by etching technique.

To better understand the etching mechanism for both isotropic and anisotropic etching, and eventually leading to the concept of making three-dimensional micro-structures, Fig. 3.4 presents some structures which can be expected as a result from different etching techniques. These are the basic shapes underlying the formation of more complicated micro-structures such as micro-mechanical bridges and cantilevers.

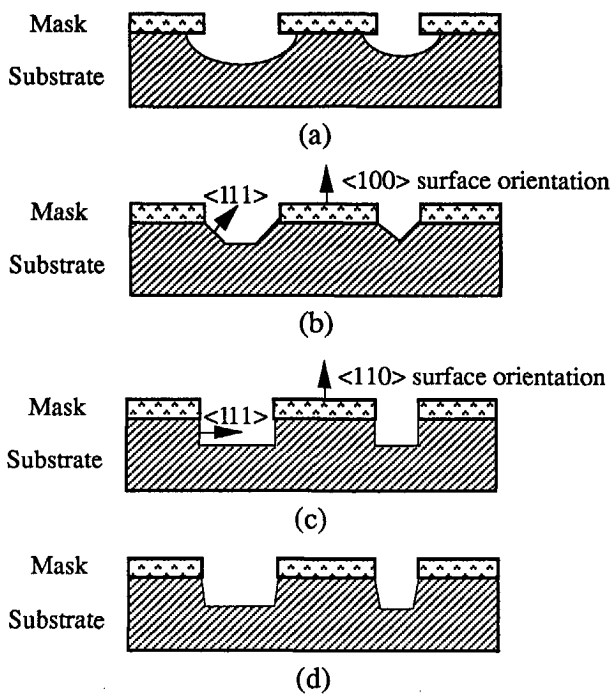

Fig. 3.4 Etched geometries which are common in micro-structure fabrication: (a) isotropic etching, (b) anisotropic etching on <100> surface, (c) anisotropic etching on <110> surface, (d) dry etching.

While, in general, the processing techniques for electronic or optical IC's consist of a sequence of planar processes, the fabrication of most micro-

mechanical structures relies on a three-dimensional structuring of the substrate or of deposited layers. Taking a silicon substrate for an example, micro-mechanical bridges or cantilevers can be realized by isotropic or anisotropic wet etching. Fig. 3.5 gives some illustrations of the formation of micro-mechanical structures.

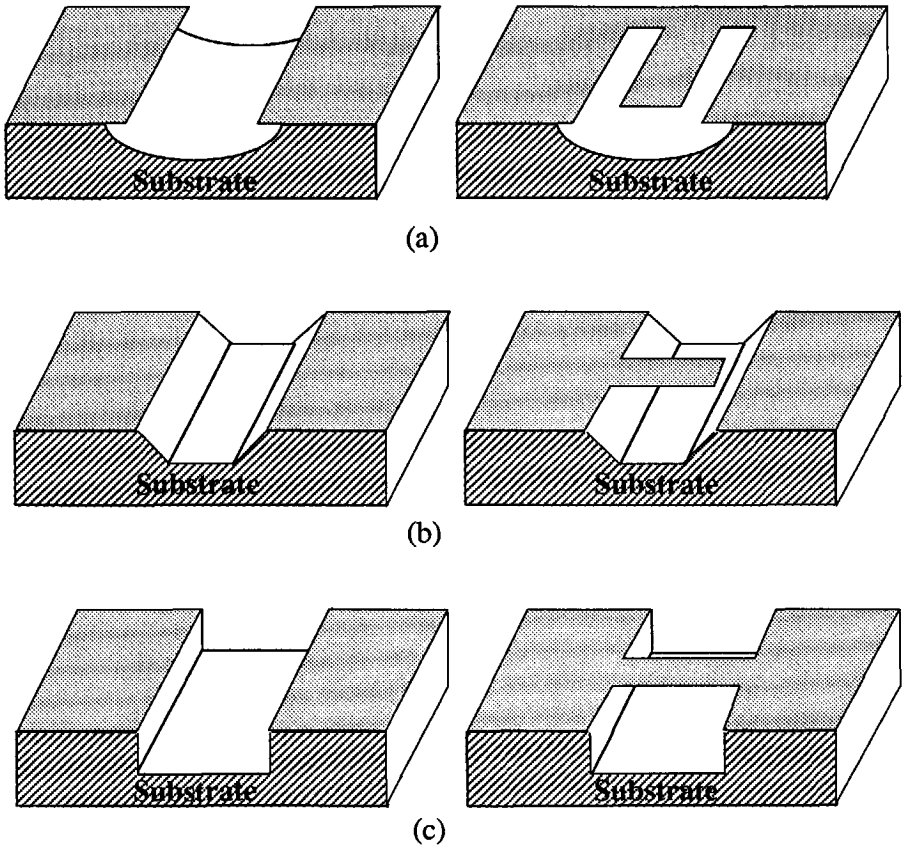

Fig. 3.5 Formation of micro-mechanical structures in different situations: (a) isotropic etching, (b) anisotropic etching for <100> surface orientation, (c) anisotropic etching for <110> surface orientation.

With the combination of above techniques, more complicated microstructures can be produced. In this research, it is desirable to fabricate microbridge and cantilever structures which can be used as optical waveguides and as optical sensor elements. Therefore, the structures should demonstrate not only excellent mechanical properties but also good optical ones, which adds extra complications for the fabrication.

References

1. D. J. Elliott, *Integrated Circuit Fabrication Technology*. McGraw-Hill Book Company, 1982.
2. H. Nishihara, M. Haruna and T. Suhara, *Optical Integrated Circuits*. McGraw-Hill Book Company, 1989.
3. K. E. Petersen, "Silicon as a mechanical material," *Proc. IEEE*, vol. 70, no. 5, pp. 420–457, May 1982.
4. L. Csepregi, "Micromechanics: a silicon microfabrication technology," *Microelectronic Engineering*, vol. 3, pp. 221–234, 1985.
5. E. Bassous, "Fabrication of novel three-dimensional microstructures by the anisotropic etching of (100) and (110) silicon," *IEEE Trans. Electron Devices*, vol. ED-25, no. 10, pp. 1178–1185, October 1978.
6. K. E. Bean, "Anisotropic etching of silicon," *IEEE Trans. Electron Devices*, vol. ED-25, no. 10, pp. 1185–1193, October 1978.
7. G. Kaminsky, "Micromachining of silicon mechanical structures," *J. Vac. Sci. Techn.*, vol. B3, no. 4, pp. 1015–1024, 1985.
8. H. Seidel and L. Csepregi, "Three-dimensional structuring of silicon for sensor applications," *Sensors and Actuators*, vol. 4, pp. 455–463, 1983.
9. W. Kern, "Chemical etching of silicon, germanium, gallium arsenide and gallium phosphide," *RCA Review*, vol. 39, pp. 278–308, 1978.

4

Fabrication of Micro-Mechanical Structures

The combination of micro-machining technology and the excellent mechanical properties of silicon and its related materials like SiO_2 provides possibilities to produce high precision, miniaturized three-dimensional structures on Si-substrates. Furthermore, an advanced micro-fabrication technology has already been developed for silicon material processing as stated in Chapter 3. A substrate made from silicon also offers an excellent surface for further optical thin-film deposition. These facts lay down a solid base to develop new integrated optical structures and components upon silicon substrates for specific application purposes.

The production of the proposed micro-waveguide bridges and cantilevers upon silicon substrates requires specific micro-fabrication procedures and techniques. Fabrication process steps can differ very much when different techniques are used. In the present chapter the fabrication process, comprising sputter deposition, photo-lithography and isotropic wet etching techniques, will be described in detail. Another fabrication process involving reactive ion

etching (RIE) will also be presented. Waveguiding through such a bridge or a cantilever will be demonstrated by coupling a laser beam into the structure.

4.1 Fabrication of Waveguide Bridges and Cantilevers

4.1.1 Waveguide Layer Structure and Exposure Mask Patterns

The waveguide structure consists of sandwiched layers of an SiO_2 buffer, an Al_2O_3 waveguide and an SiO_2 cover, as shown in an SEM photograph in Fig. 4.1. The SiO_2 buffer layer between the Al_2O_3-layer and the Si-substrate is relatively thick (about 1.7 μm) in order to prevent guided waves from tunneling into the lossy Si-substrate. It also provides a firm support for the construction of bridges and cantilevers. The SiO_2 cover layer (about 0.6 μm thick in this case) on top of the structure is used for prism coupling and for better confinement of guided waves within the waveguide. Planar waveguides of such sandwiched layer structures show excellent optical waveguiding properties and have already been investigated extensively [1]. The optical loss of such a planar waveguide can be as low as 1.0 dB/cm at a wavelength of 632.8 nm.

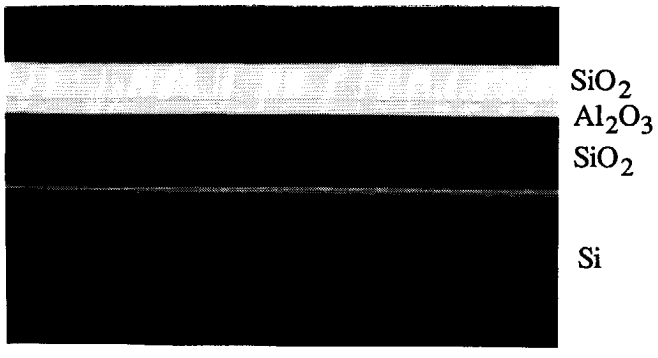

Fig. 4.1 Sandwiched waveguide structure consisting of an SiO_2 buffer, an Al_2O_3 waveguide and an SiO_2 cover.

The bridge and cantilever patterns on the exposure mask are designed using the Computer Aided Transcript System (CATS) developed by Transcript Enterprises and are written by an electron beam pattern generator (EBPG) on chromium-coated glass. Typical bridge and cantilever patterns are drawn in Fig. 4.2. Numerous bridge or cantilever patterns of different dimensions have been designed on the mask. The sets include bridges/cantilevers with lengths of 500 μm, 200 μm, 100 μm, 50 μm and 25 μm, while for each length four different widths of 30 μm, 20 μm, 10 μm and 5 μm occur. For cantilever-shaped waveguides, the separation distances between a cantilever's free end and the output section have been chosen as 2.5 μm, 10 μm or 25 μm.

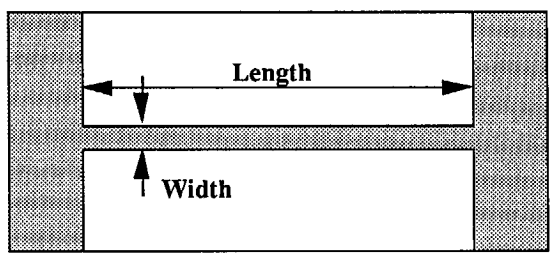

A bridge pattern

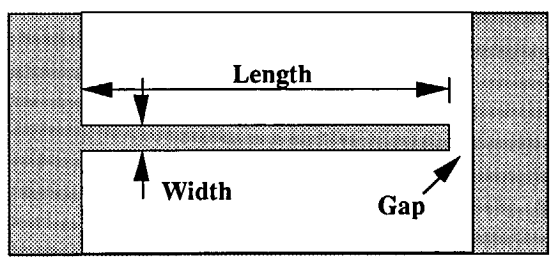

A cantilever pattern

Fig. 4.2 Designed patterns of a bridge and a cantilever.

4.1.2 Fabrication Process Using Isotropic Etching

The fabrication process of the waveguide bridges or cantilevers using isotropic wet etching, illustrated in Fig. 4.3, starts with a polished Si-substrate. To obtain a high quality optical buffer layer and an excellent surface for further film deposition, an SiO_2-layer is produced on top of the Si-substrate by thermal oxidation, which takes place in an oxide furnace at 1200 °C under an atmosphere of steam during 210 minutes. The thickness of the resulting SiO_2-layer is about 1.7 μm and its refractive index is 1.455±0.005.

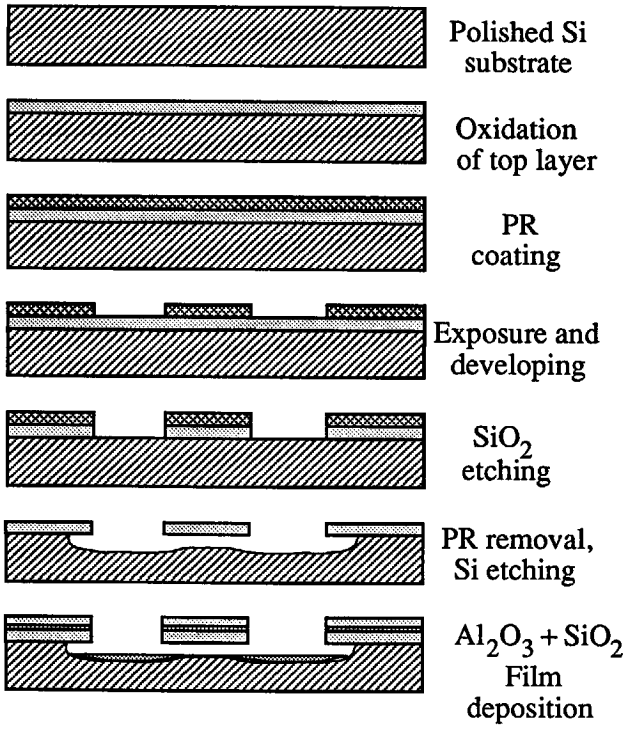

Fig. 4.3 Fabrication process of bridge- or cantilever-shaped waveguides using isotropic wet etching.

After cleaning the oxidized SiO_2 surface thoroughly, spin coating is employed for applying photoresist (denoted as PR in Fig. 4.3) to the substrate. The coating process starts at a rotational speed of 2400 rpm for 10 seconds, immediately followed by a rotation of 4000 rpm for 40 seconds. The positive photoresist used is Microposit 1470 from Shipley. Before the exposure process, soft-baking at a temperature of 90 °C is applied for 15 minutes. The photoresist-coated substrate is then exposed through a mask using an optical mask aligner to transmit a latent image of the designed patterns into the resist film. Then, the photoresist coating is developed using the Microposit 351 developer and is baked afterwards at a temperature of 120 °C during 30 minutes.

The patterns on the developed resist coating are transmitted to the SiO_2-layer by HF buffered etching. The etchant is prepared by mixing one part of 49% HF (by weight) with six parts of 40% NH_4F (by weight), yielding an etch rate of 91 nm/min. The etching process continues until the SiO_2-layer is etched through completely. Then, the photoresist is removed.

Another etching process follows to remove silicon underneath the SiO_2-layer. For isotropic etching of Si, a solution has been prepared of one part of 49% HF (by weight) and two parts of 65% HNO_3 (by weight) and one part of CH_3COOH, yielding an etch rate about 9 μm/min. If the complete undercut of Si underneath the areas where bridges and cantilevers are to be formed occurs, suspended bridges or cantilevers are obtained, this occurs in the silicon etching (sixth) step in Fig. 4.3.

A cantilever made from the oxidized SiO_2-layer is shown in Fig. 4.4. It is 100 μm long, 20 μm wide and 1.7 μm thick. The gap between the cantilever's free end and the output section is 2.5 μm. The cantilever itself already forms an SiO_2 waveguide, but unfortunately guided waves can not propagate through the in- and output sections because the (lossy) Si-substrate has a higher refractive index (of 3.42).

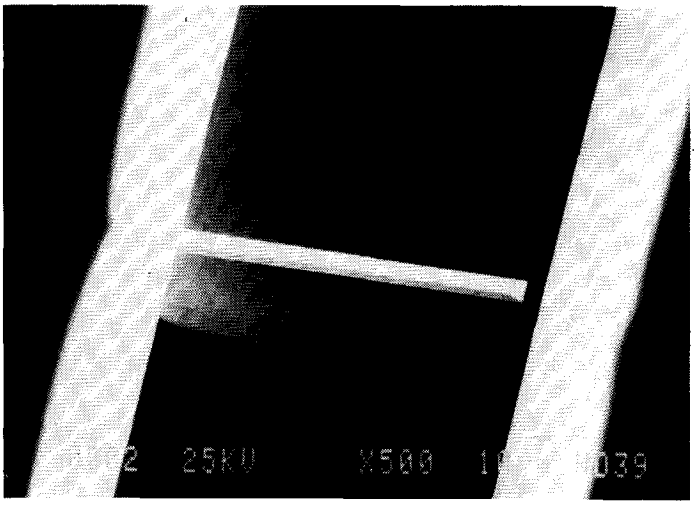

Fig. 4.4 A micro-cantilever made from an SiO_2 layer upon an Si-substrate.

Our experiments have indicated that a cantilever made from the oxidized SiO_2-layer can not survive in the subsequent sputtering process (to produce Al_2O_3 and SiO_2 layers) which involves a strong ion bombardment. The free end of the cantilever will be bent down permanently toward the surface of the Si-substrate as shown in Fig. 4.5. Therefore, the silicon etching process has been modified to remove the Si underneath the designed cantilever patterns only partially by controlling the etch duration, leaving an Si-ridge supporting the yet to be formed cantilevers. The resulting cross-sections are mushroom-shaped, as shown in Fig. 4.6. The top layer of the mushroom-shaped structure consists of SiO_2 material. The remaining support part in the center is from Si and will be removed after the Al_2O_3-guide and the SiO_2-cover are deposited. On the other hand, the bridge structures can survive the ion bombardment in the sputtering process reasonably well, for them the process modification is not necessary.

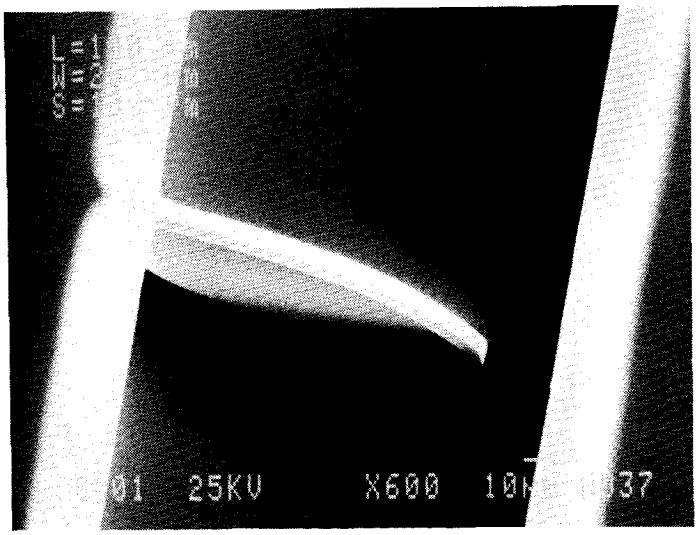

Fig. 4.5 A cantilever bent down to the silicon surface.

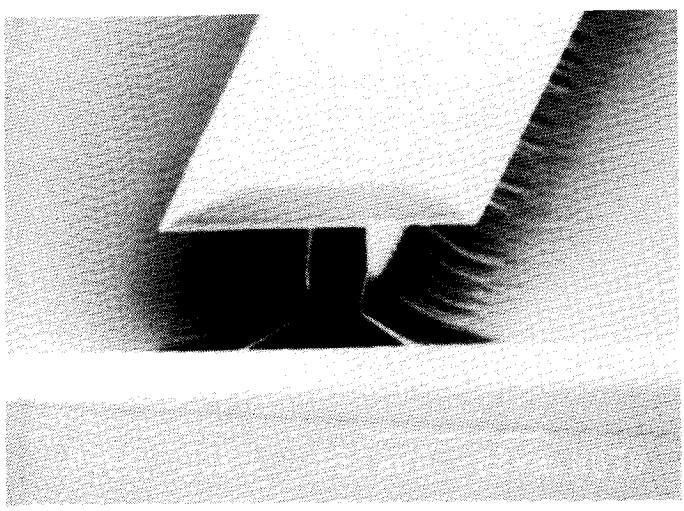

Fig. 4.6 Etched mushroom-shaped structure showing an SiO_2 cap (the future cantilever), below that the Si stem (support ridge) and at the bottom the Si substrate.

Since sputtered Al_2O_3 material is hard to be etched, the formation of bridges and cantilevers is accomplished by the Si and SiO_2 etching just described. In the next step, an Al_2O_3 waveguiding layer and another SiO_2 cover layer are sputtered using an Alcatel SCM-600 system. In this way, an $SiO_2/Al_2O_3/SiO_2$ sandwiched waveguide structure is obtained. The sputtering process is performed in a gas mixture of 90% Ar and 10% O_2 under a pressure of 0.8 Pa. The resulting refractive indices are 1.455 ± 0.005 for SiO_2 and 1.693 ± 0.002 for Al_2O_3.

Finally, the entire micro-mechanical structures on the Si-substrate are annealed to reduce the optical waveguide loss. It was thought in the first place that such structures would have difficulties to endure a high temperature process because of stress in the layers and the difference in thermal expansion coefficients between different layers. Experimental results, however, have shown that the bridges and cantilevers are able to withstand large temperature changes. Annealing tests of such structures have been carried out at 800 °C without any evidence of damage or changes in their mechanical structures. Since the lowest optical loss of such $SiO_2/Al_2O_3/SiO_2$ waveguide structures occurs after annealing at a temperature between 700 °C and 800 °C, the high temperature annealing process obviously presents no problems.

Sets of optical waveguides, shaped as micro-mechanical bridges or cantilevers with in- and output sections, have been produced. Fig. 4.7 shows an SEM photograph of a waveguide bridge with the $SiO_2/Al_2O_3/SiO_2$ sandwiched layer structure. The bridge's dimensions are 100 μm in length, 10 μm in width and about 2.5 μm in thickness. The waveguide is slightly bent toward the substrate surface, which is caused by a combination of the difference in thermal expansion coefficients among the various layers and the effects of ion bombardment during the sputtering process.

The bright regions bordering the in- and output sections are caused by etching undercut underneath those regions. The undercut can also be seen in

Fig. 4.6. This undercut is essential in the case of cantilever fabrication to form the mushroom-shaped structures which prevent sputtered SiO_2 and Al_2O_3 particles from reaching the undercut areas, leaving silicon material under the designed cantilever patterns bare such that the remaining support ridge of silicon material can be removed in the later etching process.

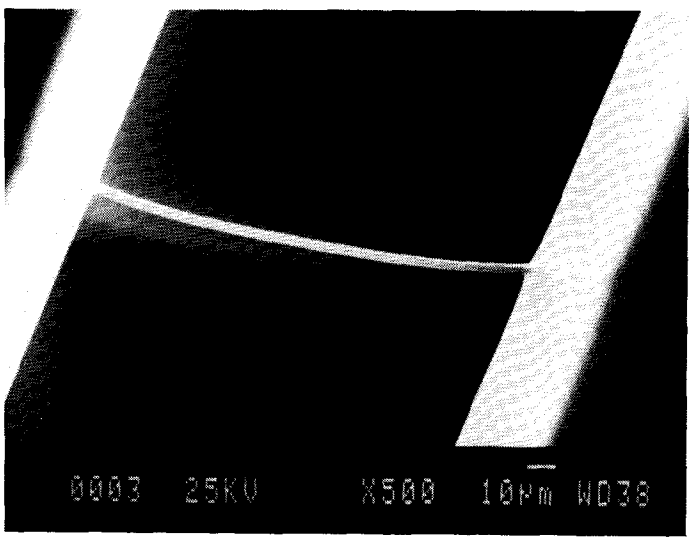

Fig. 4.7 SEM photograph of a bridge-shaped waveguide.

A SEM photograph of a waveguide cantilever is shown in Fig. 4.8. It has the same layer structure as that of the bridge-shaped waveguide of Fig. 4.7. Its dimensions are 100 µm in length, 30 µm in width and about 2.5 µm in thickness. The separation distance between the cantilever's free end and the output section is 25 µm.

The rippled patterns at the sides occur during the second silicon etching process when the remaining support part of silicon material is etched away. They actually indicate that silicon etching happens also under the sputtered Al_2O_3-layer in the exposed areas which are located in the undercuts under the

cantilever patterns and along the regions bordering the in- and output-sections. This can be understood better from the SEM photograph of Fig. 4.9, showing both the rippled patterns and the etching undercut.

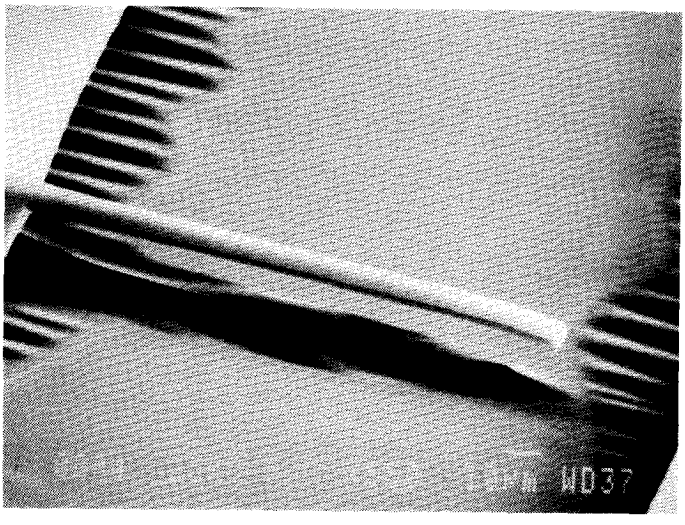

Fig. 4.8 SEM photograph of a cantilever-shaped waveguide.

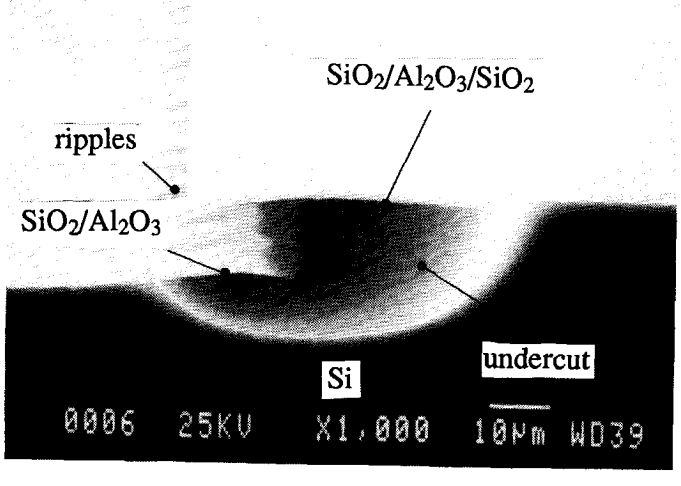

Fig. 4.9 SEM photograph of an etched structure showing the undercut and the rippled patterns.

4.1.3 Fabrication Process Involving Reactive Ion Etching

Although waveguide bridges and cantilevers can successfully be fabricated using isotropic wet etching only, major optimization of the fabrication process in order to achieve better quality elements is possible. Technological improvements including plasma dry etching of SiO_2 to obtain steep etching walls and anisotropic etching of the silicon material to achieve better process control and etching quality can be utilized. There is, however, one disadvantage for the fabrication of micro-mechanical structures in using the sputtered Al_2O_3 as the waveguide material. The sputtered Al_2O_3 has a micro-crystalline structure containing crystallites of the order of 10 nm [1] and exhibits high resistance to wet chemical etching. This is the reason that complicated silicon etching steps need to be applied to avoid Al_2O_3 etching.

The sputtered Al_2O_3 can be etched by using other techniques such as reactive ion etching (RIE), and an etching process for subsequently etching $SiO_2/Al_2O_3/SiO_2$ sandwiched layers has been developed [2]. RIE utilizes both chemical and physical sputtering and the material is etched away by the combined effects of chemical reactions and physical sputtering. The etching is performed in a plasma reactor and occurs essentially anisotropic. The application of such a process becomes ideal for the fabrication of the proposed mechanical structures and further results in a much simpler fabrication process.

Many process steps, such as thermal oxidation, patterning, Al_2O_3 and SiO_2 sputtering, are the same as in the fabrication process using isotropic etching. The fabrication process steps involving RIE are the following. A silicon substrate is thermally oxidized to obtain an SiO_2 buffer. An Al_2O_3 waveguide and an SiO_2 cover are sputtered subsequently. An additional chromium layer is sputtered to be used as a mask during the RIE process. After patterning the Cr layer, which is performed by photolithography, and a Cr etching process, the substrate is ready for the RIE process. The Cr etching is carried out in a solution of ceric

ammonium nitrate ($Ce(NH_4)_2(NO_3)_6$) and perchloric acid ($HClO_4$). The further fabrication process is straightforward and is illustrated in Fig. 4.10.

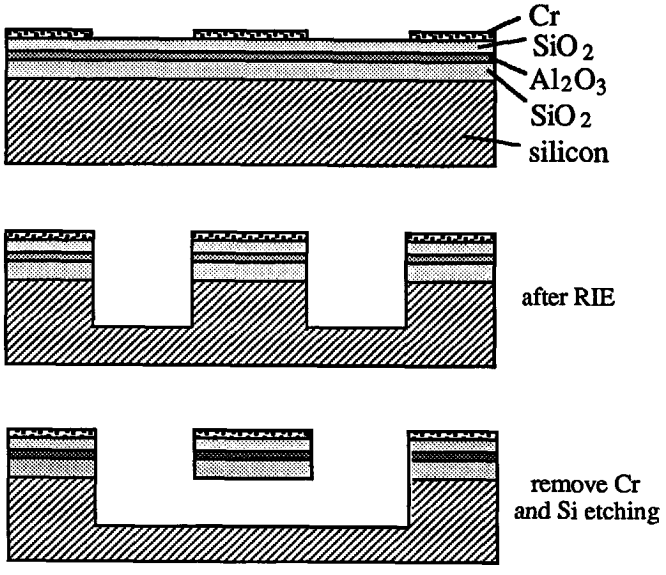

Fig. 4.10 Fabrication of micro-mechanical bridges and cantilevers involving RIE.

The RIE process is performed in a RIE reactor using a mixture of four different gases e.g. C_2F_6, SF_6, CHF_3 and O_2. Some etching results are presented in Fig. 4.11, showing the etched walls and the silicon surface. From this figure one can see that the etched walls of the Al_2O_3 and SiO_2 layers are quite vertical, but this is not the case for Si substrate. Etching undercut in silicon can clearly be seen. For an etching depth of 9 μm in Si, an undercut of 2.5 μm has been observed (see Fig. 4.11 (a)). The peaks and valleys on the etched Si surface seem to be a result of remaining unetched Al_2O_3 particles which serve as micro-masks for the underlying layers. Although a smooth and flat Si surface is preferred, the rough Si surface does not hinder the fabrication of the micro-mechanical bridges

and cantilevers very much, and will become smoother after further Si etching in a later process step.

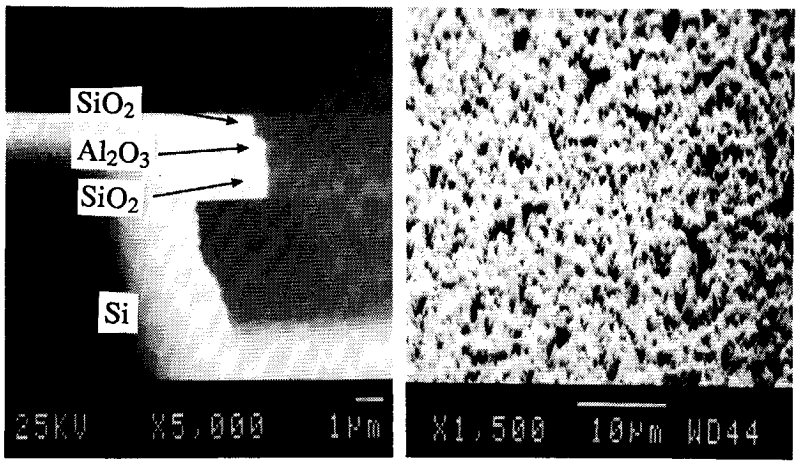

(a) (b)

Fig. 4.11 Results obtained from the RIE process, (a) showing the etched walls of different layers, and (b) the etched Si surface.

To obtain suspended bridges and cantilevers, Si etching is carried out to remove the Si underneath the bridge and cantilever structures. Either isotropic wet etching using an $HF + HNO_3 + CH_3COOH$ solution or anisotropic wet etching using diluted potassium hydroxide (KOH) have been applied for that purpose. The KOH etchant is prepared by diluting 100 gram KOH in 200 ml water, and etching is performed at a temperature of 70 °C.

Fig. 4.12 shows a waveguide cantilever which is 200 μm long, 20 μm wide and is obtained by the isotropic etching process after RIE. As it can be seen, the sharp peaks and valleys on the silicon surface have been eased and flattened. With this same process, long structures have be produced successfully. Fig. 4.13 presents another suspended cantilever with a length of 500 μm and a width of 20 μm.

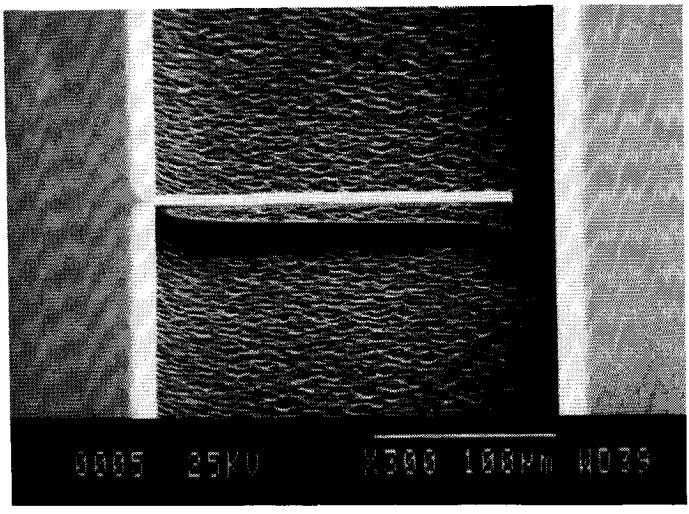

Fig. 4.12 A waveguide cantilever fabricated using RIE and isotropic wet etching.

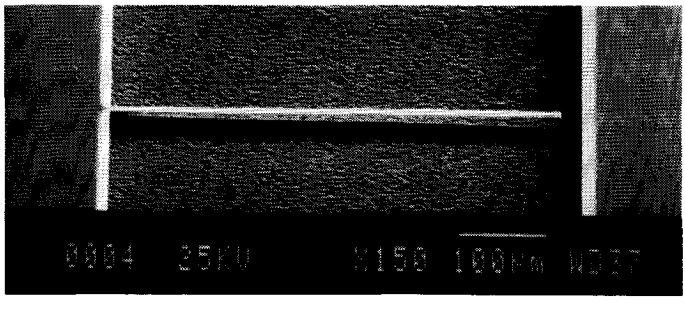

Fig. 4.13 A long waveguide cantilever of a length of 500 μm and a width of 20 μm.

With anisotropic wet Si etching, the structure can obtain a shape as shown in Fig. 4.14. The etching occurs in the direction parallel to the structure's axis. Little etching in the direction perpendicular to the axis occurs. There exists still a section of the cantilever supported by a silicon ridge, which would disappear by a longer etching duration. The rough Si surface now becomes more or less flat. The cantilever in the figure is 100 μm long, 20μm wide. Completely

suspended cantilevers of 50 μm in length have been obtained for the same etching duration, which is shown in Fig. 4.15.

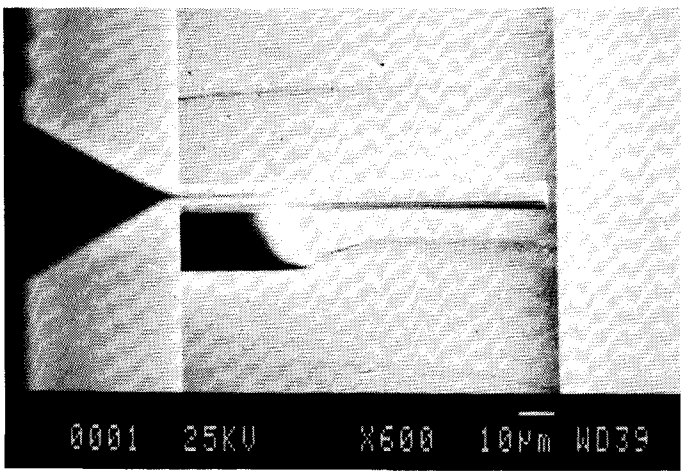

Fig. 4.14 A partially suspended waveguide cantilever fabricated using RIE and anisotropic wet etching.

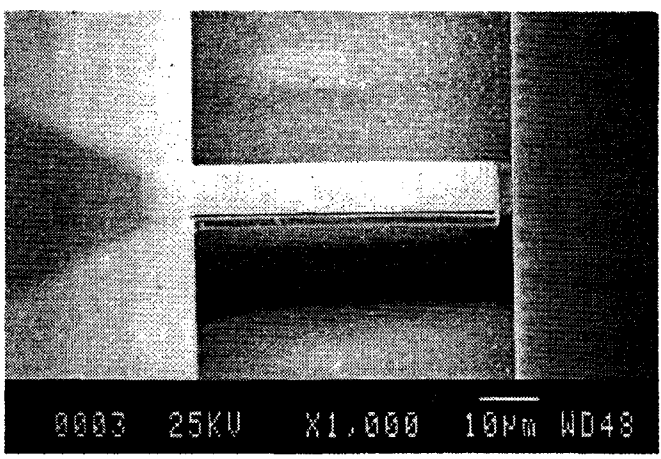

Fig. 4.15 A completely suspended waveguide cantilever fabricated using RIE and anisotropic wet etching.

The cantilever's free end and part of the output section are shown in the SEM photograph of Fig. 4.16, from which the quality of the micro-structures

produced by RIE can be inspected. The etched walls and the structure's multilayers can also be observed from that figure. There, the width of the cantilever's free end is 20 μm and the separation gap is 2.5 μm.

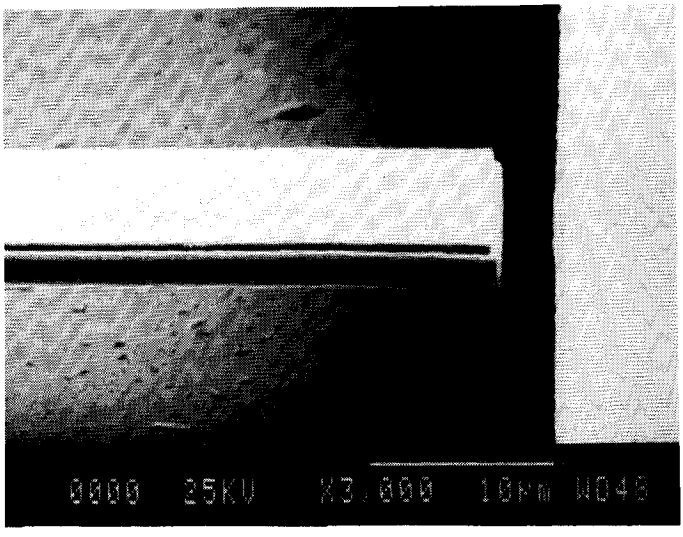

Fig. 4.16 SEM photograph showing a cantilever's free end and part of the output section, produced by RIE and anisotropic wet etching.

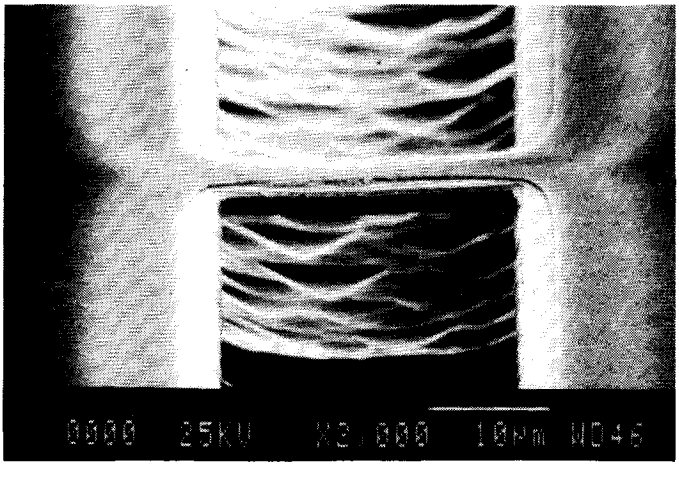

Fig. 4.17 A waveguide bridge fabricated using RIE and isotropic wet etching.

Waveguide bridges have also been produced with these processes. Fig. 4.17 shows a bridge with a length of 25 μm and a width of 10 μm, fabricated using RIE and isotropic wet etching.

4.2 Waveguiding in Bridge and Cantilever Structures

Waveguiding through the bridges and cantilevers has successfully been demonstrated by coupling a He-Ne laser beam with a wavelength of 632.8 nm into the input sections. Fig. 4.18 shows a photograph of a laser beam propagating through a bridge-shaped waveguide, together with a schematic drawing to illustrate the waveguiding situation in the photograph. The bridge's dimensions are 50 μm in length, 10 μm in width and 2.5 μm in thickness.

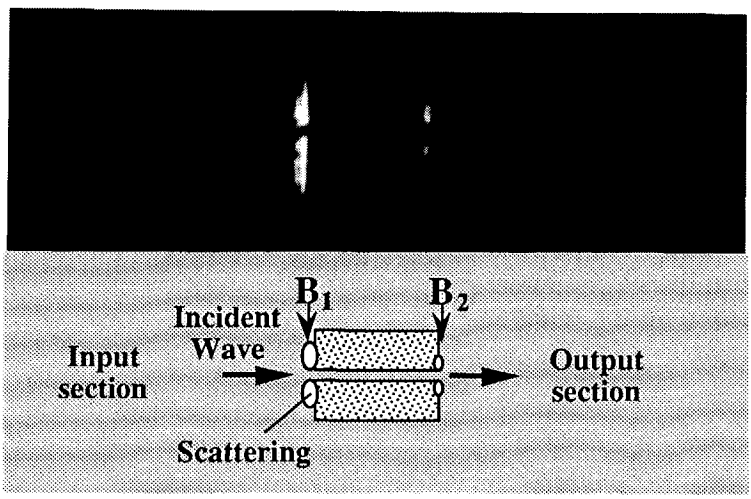

Fig. 4.18 Observation of a wave guided through a bridge-shaped waveguide.

Fig. 4.19 illustrates how a guided wave, propagating through a cantilever-shaped waveguide, exits at the free end of the cantilever and, after crossing the

gap, part of the wave is coupled into the output section. The cantilever's dimensions are 100 μm in length, 30 μm in width and 2.5 μm in thickness. The gap between its free end and the output section has a length of 10 μm. Those pictures have been taken by a commercial camera attached to an optical microscope.

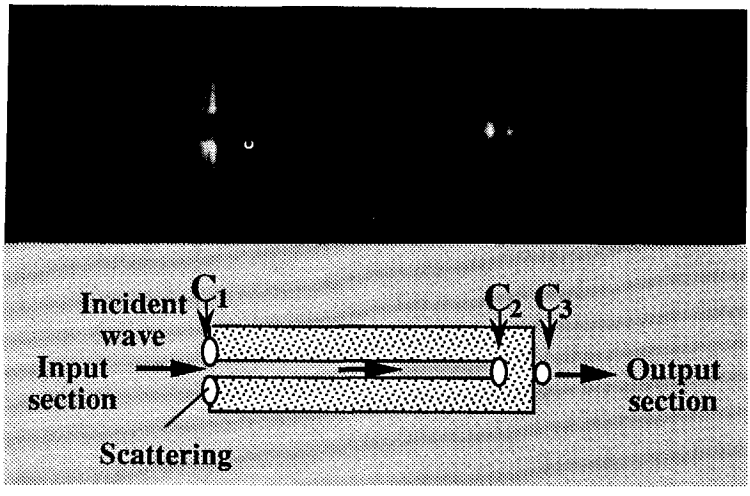

Fig. 4.19 Observation of a wave guiding through a cantilever-shaped waveguide.

The bright spots in both Figs. 4.18 and 4.19 indicate scattered waves occurring when the light meets discontinuities. Within the waveguide regions, too little scattering occurs to be recorded; thus, the waveguides can not be seen from the figures. The bright spots can be understood better from the schematic drawings in Figs. 4.18 and 4.19. The laser beam in the input section has a transverse dimension exceeding the bridge's or cantilever's widths, causing the scattering at places indicated by B_1 and C_1, respectively. The main portion of the wave propagates through the waveguide. When reaching the other side of the bridge, it scattered only slightly (see the spots in Fig. 4.18 indicated by B_2) since the guided wave is well confined within the waveguide. In the cantilever-

shaped guide of Fig. 4.19, the beam radiates into air at the cantilever's free end (spot C_2), and part of radiation is picked up further on by the planar output section (spot C_3).

4.3 Discussion

The distance over which a bridge or a cantilever lies above the substrate is actually the maximal distance over which the bridge or the cantilever can be deflected. A suitable value of this distance is important in order to limit the structure's operational range and to protect it from breaking in the case of excessive external influences. This distance can be controlled by the etching duration, in our case the structures occur about 10 μm above the Si-substrate surface with an air gap in between.

Extremely long or narrow structures are vulnerable. They are likely to be broken in the fabrication process. But still, some of those vulnerable structures have been produced successfully, including those with a length of 500 μm and those with a width of 2.5 μm.

The waveguides are mono-mode waveguides if the thickness of the sputtered Al_2O_3-layer is less than 0.35 μm. Normally, a value between 0.2 μm and 0.3 μm is used. In all examples shown in this chapter, the thickness of the Al_2O_3-waveguides equals 0.3 μm.

As long as isotropic etching is applied in the fabrication process, crystal orientations in the substrate are irrelevant. For anisotropic etching, the orientations of an Si-substrate will be a major factor to be considered. A detailed investigation on anisotropic etching in this thesis has been obstructed by the lack of supply of silicon substrates with <110> and <100> orientations. All substrates that have been processed had a <111> orientation.

Due to their small sizes, arrays of the waveguide bridges or cantilevers with different dimensions can be produced on the same chip to obtain different sensitivities and operational ranges. Since for those Si-based structures the usual fabrication techniques for electronic IC's are applied, it is possible to integrate necessary electronic circuits and detectors on the same chip to control the structures or to process the output signals.

References

1. M. K. Smit, A. Acket and C. J. van der Laan, "Al_2O_3 Films for Integrated Optics," Thin Solid Films, vol. 138, pp. 171–181, 1986.
2. J. L. Joppe, "Het reacief ionen etsen van een $SiO_2/Al_2O_3/SiO_2$ optisch golfgeleiderpakket op silicium," Fysisch en Elektronisch Laboratorium TNO, TNO-rapport FEL-90-B339, December, 1990.
3. K. E. Petersen, "Silicon as a Mechanical Material," Proc. IEEE, vol. 70, no. 5, pp. 420–457, May 1982.
4. L. Csepregi, "Micromechanics: a silicon microfabrication technology," *Microelectronic Engineering*, vol. 3, pp. 221–234, 1985.
5. E. Bassous, "Fabrication of Novel Three-Dimensional Microstructures by the Anisotropic Etching of (100) and (110) Silicon," IEEE Trans. Electron. Devices, vol. ED-25, no. 10, pp. 1178–1185, October 1978.
6. K. E. Bean, "Anisotropic Etching of Silicon," IEEE Trans. Electron. Devices, vol. ED-25, no. 10, pp. 1185–1193, October 1978.
7. G. Kaminsky, "Micromachining of silicon mechanical structures," *J. Vac. Sci. Techn.*, vol. B3, no. 4, pp. 1015–1024, 1985.
8. H. Seidel and L. Csepregi, "Three-dimensional structuring of silicon for sensor applications," *Sensors and Actuators*, vol. 4, pp. 455–463, 1983.
9. W. Kern, "Chemical etching of silicon, germanium, gallium arsenide and gallium phosphide," *RCA Review*, vol. 39, pp. 278–308, 1978.
10. H. Bezzaoui and E. Voges, "Integrated optics combined with micromechanics on silicon," Sensors and Actuators A, vol. 29, No. 3, pp.219 – 223, Dec. 1991.

11. K. E. Burcham, G. N. De Brabander and J. T. Boyd, "Micromachined silicon cantilever beam accelerometer incorporating an integrated optical waveguide," presented at *SPIE's International Symposium OE/FIBERS'92*, Boston, USA, 8 – 11 Sept., 1992.
12. A. Sugita, et al., "Bridge-suspended silica-waveguide thermo-optic phase shifter and its application to Mach-Zehnder type optical switch," *Transactions of IEICE*, vol. E 73, no. 1, pp. 105–109, Jan. 1990.

5

Applications

In the previous chapters, we have introduced micro-mechanical bridges and cantilevers and discussed the principles and the fabrication of such structures. These bridges and cantilevers are mechanically unstable structures and undergo vibrations or deflections due to external influences, especially force-related disturbances. Thus, they can be utilized as sensor elements. This chapter presents the experimental results of such structures used as sensors for the detection of acoustic signals. Further possible applications to the measurement of vibrations and acceleration will be discussed briefly. The purpose of this experimental work is to verify the predicted behavior of micro-bridges and cantilevers when used as optical sensor elements.

5.1 Acoustic Signal Detection

The presence of an acoustic wave will create a pressure variation in the medium surrounding a mechanical element. The acoustic wave interacts with the mechanical structure and induces vibration there. This is the basic principle underlying the operation of most acoustic detection devices such as microphones. The micro-bridges and cantilevers described in this thesis can be

applied as sensor elements for measuring acoustic waves based on the same principle. The experiments have been performed within the audio-frequency spectrum from 20 – 20000 Hz due to the limitations imposed by some of the employed acoustic and electronic units in the measuring setup. The use of these sensors, however, is not limited to this frequency range; they can be applied for acoustic signals of higher frequencies as well.

5.1.1 Experimental Setup

The setup performing our measurement of acoustic signals is illustrated in Fig. 5.1. The acoustic signal is generated by a signal generator and then after amplification directed onto the sensor device through a loudspeaker. The acoustic wave is propagating normally to the sensor surface; this is important

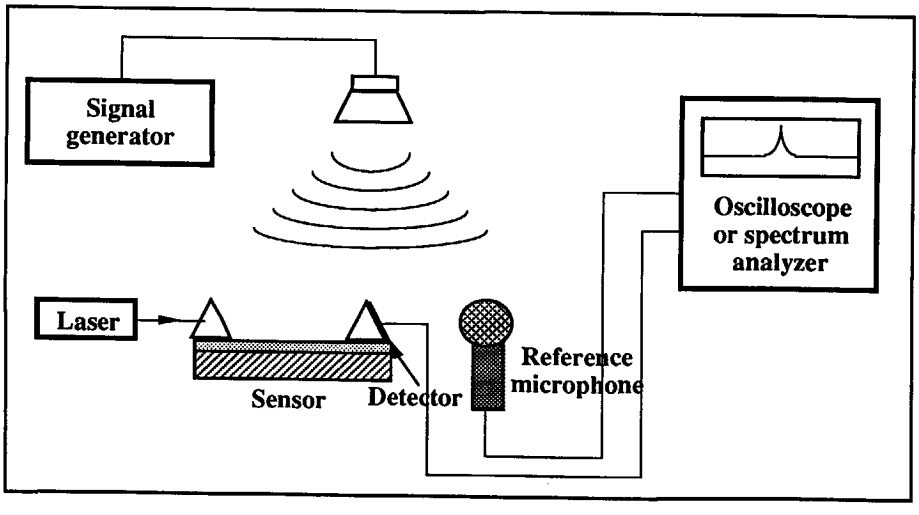

Fig. 5.1 Experimental setup for the measurement of acoustic signals using the micro-mechanical structures as sensor elements.

since the sensor is orientation sensitive. A laser beam at the wavelength of 632.8 nm is coupled into the sensor structure through a prism to excite a guided mode in the sensor's waveguide. The guided wave propagates through the sensor structure (either a waveguide bridge or a cantilever). The emerging wave is out-coupled by another prism and detected by a photodiode mounted directly on the out-coupling prism. The detected signal is then analyzed or displayed by a spectrum analyzer or an oscilloscope.

A Hewlett Parkard 8904A Multifunction Synthesizer has been used to generate acoustic signals. It can produce accurate sine waves from 0 Hz (DC signals) to 600 kHz with 0.1 Hz resolution. It also has some other standard functions like square waves, triangular waves, as well as noise. All waveform values in the synthesizer are calculated digitally in real time, yielding a 12 bit digital accuracy.

The generated signals are amplified by a Sony 1120 Integrated Amplifier and then converted into acoustic waves by a custom-made loudspeaker. The loudspeaker is designed by the Acoustic Research Laboratory of Delft University of Technology using a Vifa type M-110 speaker unit from Audio Design GmbH. A reference microphone is placed near the sensor device for comparison of the signal. The microphone is a BK 4165 type, flat response device from Bruel & Kjear.

For the detection of the outgoing guided wave in the sensor structure, a silicon planar PIN photodiode, BPW 34 from Siemens, is incorporated into the sensor and is directly mounted on the out-coupling prism. The photodiode is favorable for its short response time and high signal-to-noise ratio. The noise equivalent power (NEP) of the diode is equal to 4.2×10^{-14} W/$\sqrt{\text{Hz}}$.

An ADVANTEST TR 9402 Digital Spectrum Analyzer has been used to analyze the detected signals either from the reference microphone or from the sensor device. This spectrum analyzer covers a frequency range from 0 Hz (DC

signals) up to 100 kHz with an input sensitivity from +30 dBV (31.6 Vrms) to -120 dBV (1 μVrms). During the measurements, the AC coupling mode was used to eliminate the DC bias (or offset) voltage from the input signals. The spectrum analyzer is also fully equipped as a time-domain oscilloscope and was used for observing the wave forms of the detected signals.

The positioning of the loudspeaker, the sensor device and the reference microphone is shown in the photograph of Fig. 5.2. The distance between the speaker and the sensor is the same as that between the speaker and the microphone and is approximately 15 cm, while the microphone is positioned about 5 cm away from the sensor. The loudspeaker is placed in a face-to-face position with the sensor surface during the actual measurement, ensuring the acoustic wave to propagate normally to the sensor surface. The position of the loudspeaker in the picture, however, is somewhat rotated for photographic purposes.

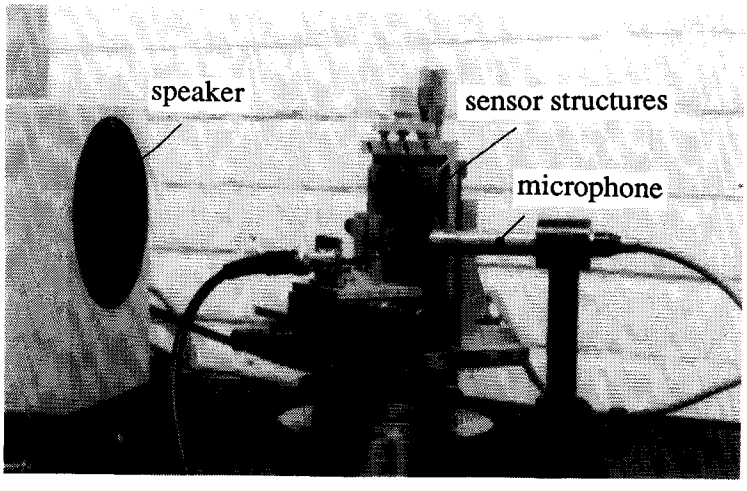

Fig. 5.2 Photograph showing the arrangement of the speaker, the sensor and the reference microphone.

The characteristics of the amplifier and the loudspeaker together are not exactly known and have been measured with the aid of the reference microphone. The transfer function, represented as the frequency response, is shown in Fig. 5.3, which represents the characteristics of the system consisting of the amplifier and the speaker.

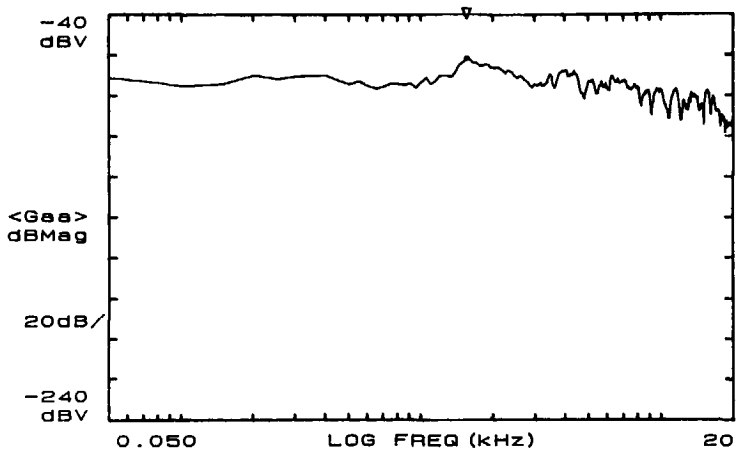

Fig. 5.3 Frequency response representing the characteristics of the amplifier and the speaker together.

5.1.2 Experimental Results

The experiments on acoustic signal detection were performed in an ordinary laboratory room with the presence of noise from the operating equipment. The obtained results, however, are encouraging and concluding. They demonstrate and prove the working principles of the sensor elements.

Fig. 5.4 presents the response of a bridge structure with a length of 100 μm and a width of 10 μm to an acoustic signal at a frequency of 2000 Hz. The figure shows a sharp response and the peak of the detected signal is exactly

at 2000 Hz. Other small peaks arise from the noise existing in the experimental environment.

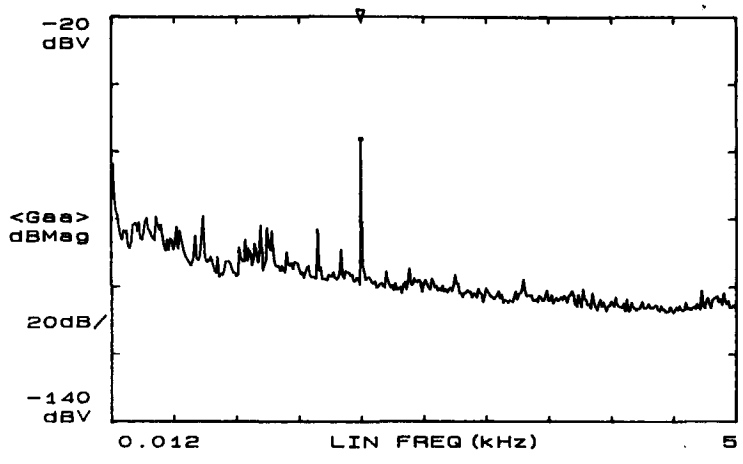

Fig. 5.4 Response of a bridge structure to an acoustic signal at 2000 Hz.

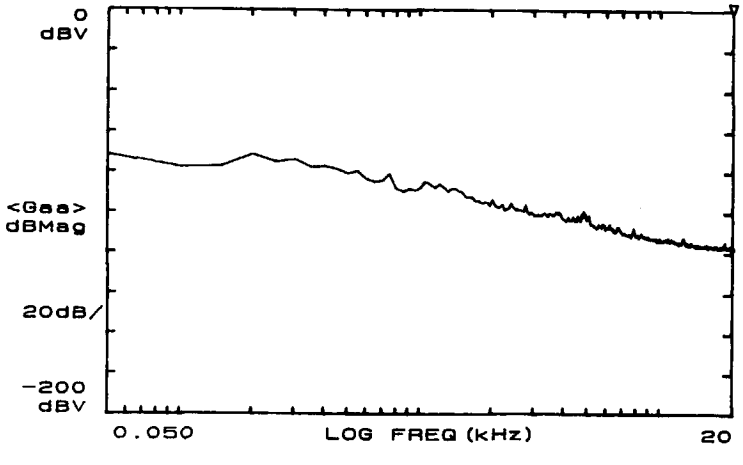

Fig. 5.5 Frequency response of a bridge structure in the audio range.

The frequency response of the bridge structure is plotted in Fig. 5.5. The bridge's resonant frequency is as high as approximately 1.39 MHz. Theoretically, the response curve should be almost flat since the measured acoustic signal has a frequency spectrum from 0.50 Hz to 20 kHz, which is far low from the resonant frequency. The possible cause of the bridge's decreasing response for higher frequencies is the existence of stress in the bridge structure. The influence of this stress becomes more pronounced when the bridge vibrates more quickly.

The response of the sensor element with a cantilever structure, to an acoustic signal at 2000 Hz is presented in Fig. 5.6. The cantilever is 100 μm long and 30 μm wide and has a separation gap of 2.5 μm. The figure also shows a sharp peak response at 2000 Hz. The cantilever seems to be more sensitive to the acoustic signal but also shows a higher noise level.

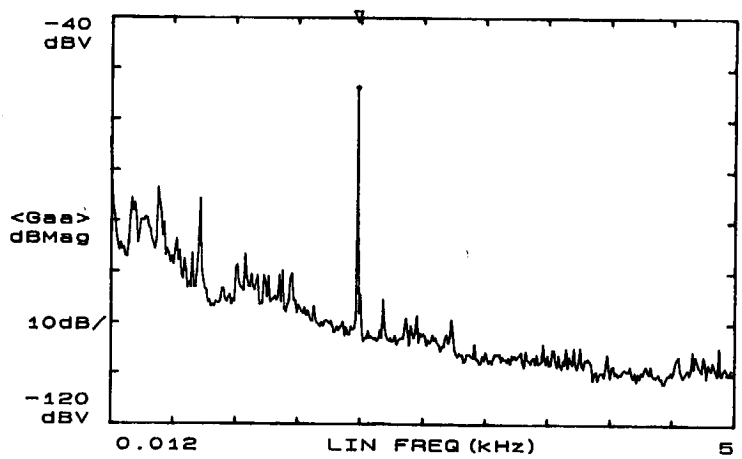

Fig. 5.6 Response of a cantilever structure to an acoustic signal at 2000 Hz.

The frequency response of the cantilever structure is plotted in Fig. 5.7, which shows a fairly flat line. The reason behind this excellent performance is

probably that the cantilever has a free end such that potential stress is released. Another reason is that the cantilever also has a resonant frequency of approximately 218 kHz, which is high as compared to the measured acoustic waves with a frequency spectrum in the audio range.

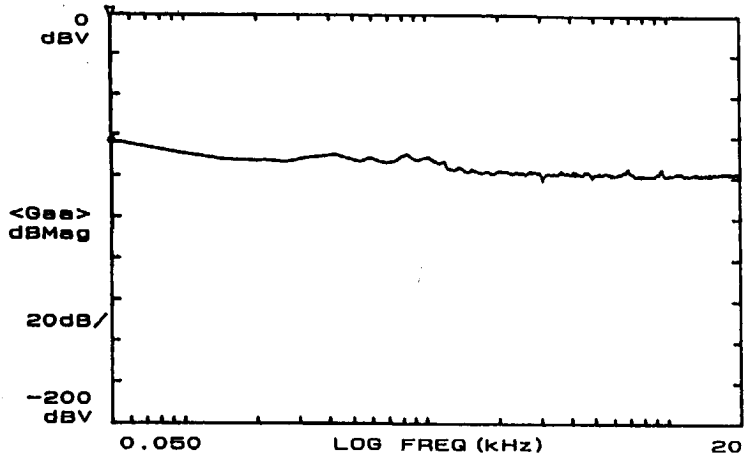

Fig. 5.7 Frequency response of a cantilever structure.

The sensor response in the time domain to an acoustic signal can also be observed by the spectrum analyzer. Fig. 5.8 shows the response of the bridge structure to an acoustic signal at 2000 Hz, with the signal directly coming from the signal generator as a reference. As shown in the figure, the sensor's response curve demonstrates some irregularities and a phase shift. Similar phenomena can be observed for the cantilever structure, as presented in Fig. 5.9.

To measure the intensity dependence of the sensor structures, an acoustic signal at 1000 Hz was used and its magnitude was measured and compared with that measured by the reference microphone. This is important to see the performance of the sensor structures.

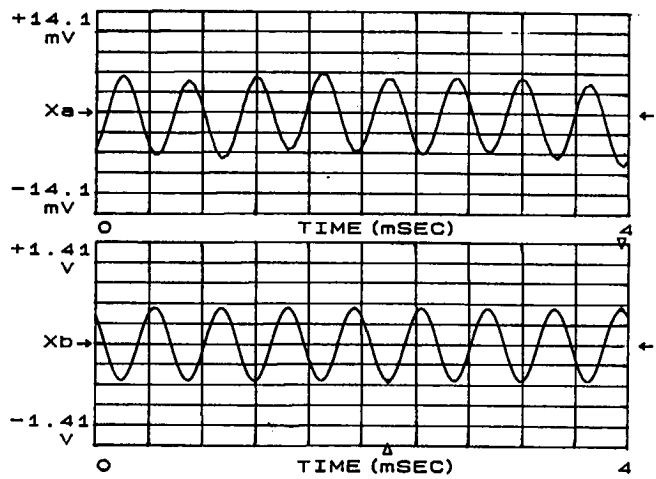

Fig. 5.8 Response of a bridge structure to an acoustic signal at 2000 Hz in time domain, Xa represents the sensor's response while Xb is the reference signal.

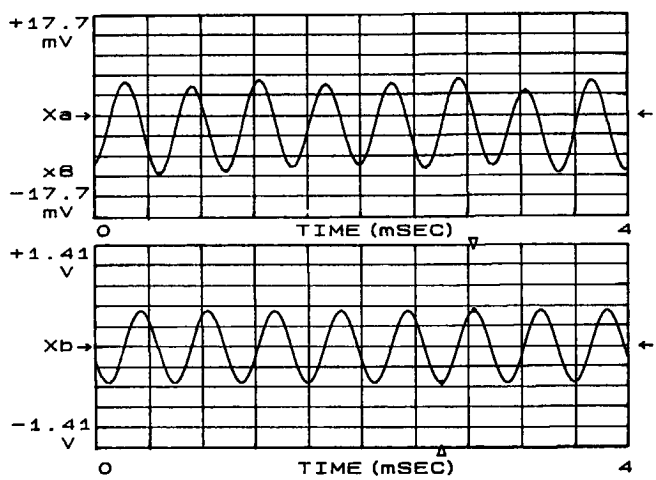

Fig. 5.9 Response of a cantilever structure to an acoustic signal at 2000 Hz in time domain, Xa represents the sensor's response while Xb is the reference signal.

By adjustment of the signal power and monitoring the sensor response we obtained the results as presented in Fig. 5.10, for a bridge (100 μm long and 10 μm wide) and for a cantilever (100 μm long and 30 μm wide) structure. Perfect sensors with a perfect reference microphone would display linear curves. However, for the cantilever structure undergoing a strong vibration, the deflection can exceed a certain limit (which is in the order of the waveguide thickness) beyond which the coupling between the cantilever's free end and the output section vanishes rapidly. That is why the cantilever's response curve tends to flatten in the higher signal range. The results shown in Fig. 5.10 demonstrate a relatively good linearity for the bridge structure for all signal intensities and for the cantilever structure in the lower signal range.

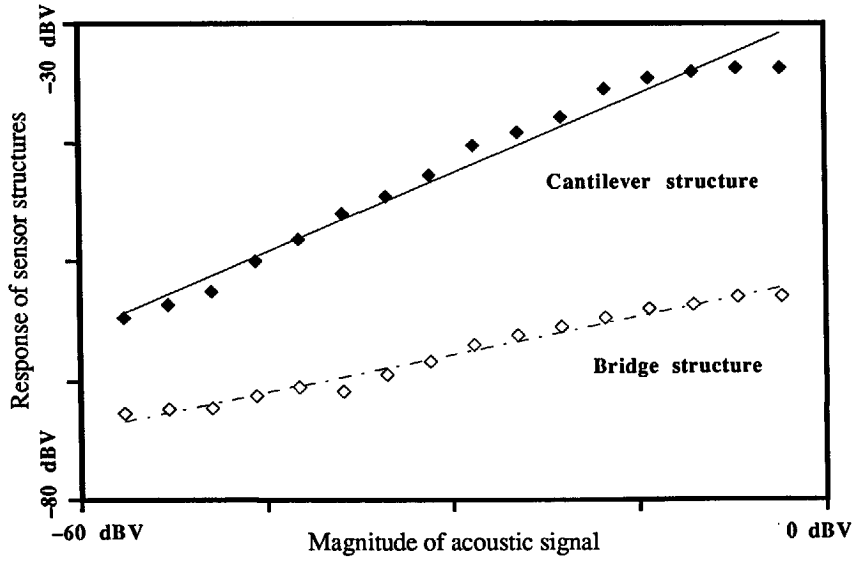

Fig. 5.10 Measured intensity responses to an acoustic signal at 1000 Hz.

5.1.3 Discussion

For the accurate measurement of an acoustic signal, it is essential that the acoustic wave is not disturbed by undesired reflections or by external noise. These conditions may be satisfied in open air, far from noise sources, or in a well-designed sound-proof anechoic chamber which is completely isolated from external sources of acoustic waves and which has boundaries made of highly absorbing materials. For the measurement of the absolute intensity of an acoustic wave as a reference, one needs a calibrated microphone.

All these conditions pose difficulties on the experiments for accurate acoustic signal measurement. Since the adoption of the experimental setup to an open air satisfying the above requirements is impractical and to a sound-proof anechoic chamber is difficult and requires quite much effort, all the experiments have been performed in an ordinary laboratory room.

No attempts have been made to measure the absolute intensity of the acoustic signals; the results presented here are relative values. This is hardly a limitation to the value of our experiments since the absolute intensities are dependent on the amplification used in the measurement and we are concerned with the performance of the sensor structures without amplification. It will become important, however, when such integrated sensors are developed for the end users.

5.2 Other Applications

5.2.1 Measurement of Vibrations and Acceleration

The micro-mechanical structures are not only favorable for the detection of acoustic waves, but are also applicable for the measurement of vibrations and acceleration. The mechanism of vibration is essentially similar to that of acceleration. The differences between them are that the accelerating direction of

vibration varies rather rapidly while that of acceleration changes much more slowly. The sensing principles for vibration and acceleration are the same as those for acoustic signal detection. Both vibration and acceleration will induce vibrations or deflections of bridges or cantilevers in the sensor structures.

The force acting on a micro-mechanical structure due to a vibration or a accelerating action satisfies the Newton's law

$$F = ma. \tag{5.1}$$

Here a is the acceleration magnitude which is experienced by the mechanical structure. For a vibration, a undergoes a rapid, periodic change, while for acceleration, a is regarded as relatively slow varying, non-periodic quantity. The deflection of the mechanical structure is determined by both the magnitude and the distribution along the structure of the force F which is proportional to the mass m for a given acceleration a.

To increase sensitivity in vibration or acceleration measurements, one needs to increase the deflection, which can be achieved by distributing the force effectively over the structure. As an example, loading an additional concentrated mass block at the center of a bridge or at a cantilever's free end, as shown in Fig. 5.11, is an effective way to increase the deflection for a given a. This can be accomplished by some modifications in the fabrication process.

Practical measurement of vibration and acceleration has not been carried out since a solid construction for the in- and out-coupling was not available. Prism coupling, which has only a loose mechanical contact with the substrate, is not suitable for such a measurement. For this purpose, an optical fiber in-coupling and out-coupling construction can be considered since the silicon substrate provides the possibility of precise alignment of a fiber by etching suitable grooves in the substrate.

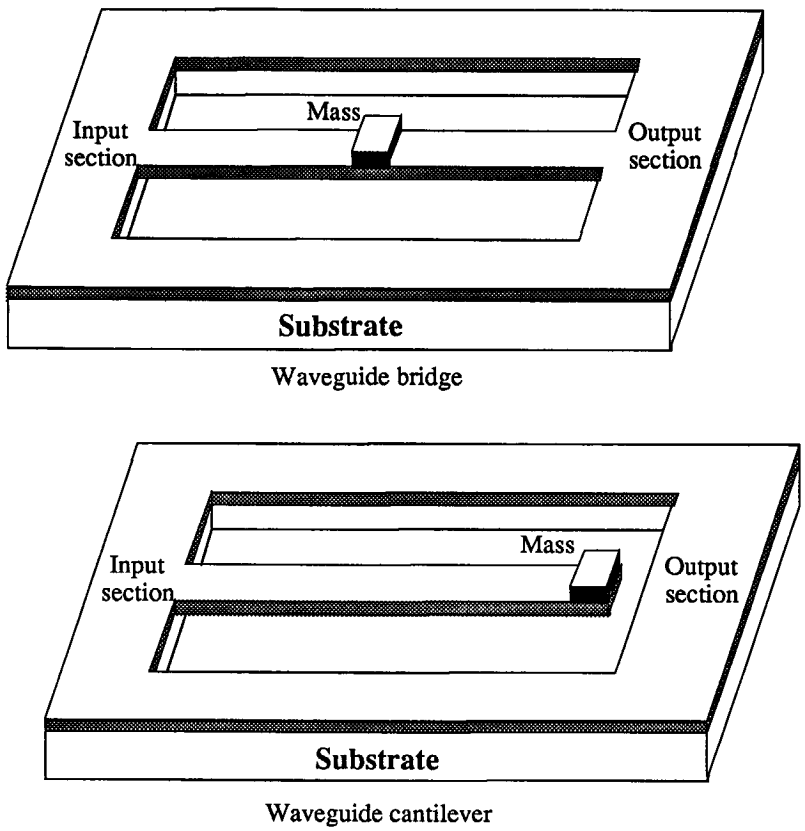

Fig. 5.11 Sensor structures for the measurement of vibration and acceleration.

5.2.2 Scanning Force Microscope and Surface Profiler

The cantilever structure may be ideal to be used as a probe for a scanning force microscope (SFM) or a surface profiler if a stylus is fabricated at its free end. Successful implementation using an all-silicon cantilever for non-optical use has already been reported [1] [2] and commercial products have been already in the market. Fig. 5.12 presents an illustration of an existing SFM.

When in operation, the sharp tip of the stylus attached to the cantilever scans across the sample surface. Due to the interaction forces (e.g. atomic, magnetic, electrostatic) between the tip and the sample, the cantilever will be either deflected or its resonance characteristics will be changed. These changes are detected and translated electronically to reveal an image of the respective surface properties such as topography or magnetic stray field.

A micro-mechanical cantilever has a high resonance frequency and therefore enables a perturbation free operation and a high scan speed. A sharp tip can be achieved to ensure high resolution imaging. Tip radii smaller than 10 nm has already been realized [1]. Most existing SFM's, like the one illustrated in Fig. 5.12, apply an optical detection scheme in which a laser beam is aimed at the tiny cantilever tip and the light reflection from the tip is detected as the sensing signal. Such a configuration can detect minute interaction forces in the order of 10^{-8} N and deflection in the order of 0.1 nm [3].

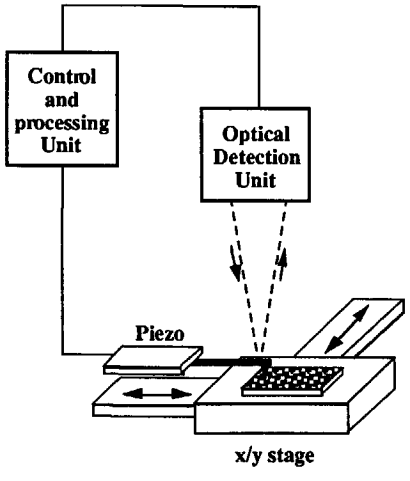

Fig. 5.12 Illustration of a scanning force microscope.

Using an optical waveguide cantilever, it is possible to arrive at a simpler and more compact SFM configuration with a higher sensitivity. Fig. 5.13 illustrates a configuration of an SFM incorporating an optical waveguide cantilever. The bulk optical detection unit, like the one in Fig. 5.12, can be replaced by a compact light source and a photodiode in the new configuration. The light source and the photodiode can be mounted or integrated on the same sensor chip.

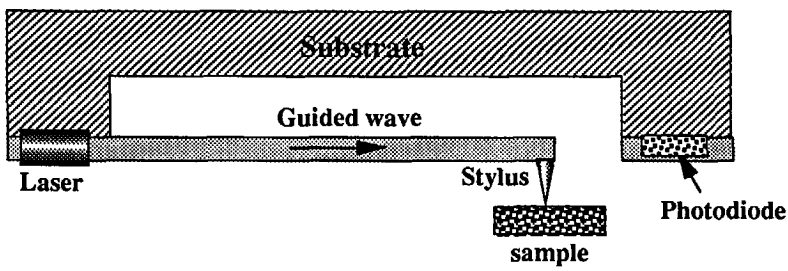

Fig. 5.13 SFM configuration using an optical waveguide cantilever structure.

5.2.3 Sensitivity Evaluation

A waveguide cantilever is very sensitive to a displacement or an interacting force at its free end. An approximate evaluation of the sensitivity is as follows. The minimum detectable displacement can be determined by considering the coupling efficiency as presented in Eq. (2.48). Let's assume that the intensity of the light source is 1 mW. The optical coupling coefficient across the cantilever's separation gap of 2.5 μm has a value of 17.3% as calculated in Fig. 2.13 for zero displacement. Under such conditions, the optical power I_0 striking the photodiode detector will be 173 μW when there is no displacement. The minimum detectable power change P_{min} of a photodiode, often noted as noise equivalent power (NEP), can usually reach the order of 10^{-14} W for a

bandwidth of 1 Hz. The photodiode that is used in our experiments has an NEP value of $4.2\times10^{-14}\ \mathrm{W}/\sqrt{\mathrm{Hz}}$. The optical power change ΔI in case of a displacement δ, according to Eq. (2.48) can be expressed as

$$\Delta I = I_0\left(1-e^{-\frac{2\delta^2}{w^2+w'^2}}\right). \tag{5.2}$$

By substituting ΔI with P_{min}, the minimum detectable displacement δ_{min} can be determined from Eq. (5.2). In this case, δ_{min} could be in the order of 10^{-2} nm theoretically. If the separation gap is taken as 1 μm, the theoretical value of the δ_{min} can be calculated as in the order of 10^{-3} nm.

We consider a cantilever with a length of 100 μm and a width of 30 μm to see what the minimum detectable external force would be. If a static force F is applied at the free end, the deflection δ at the free end due to this force satisfies (also see Eq. (2.23))

$$F = \frac{3EI}{l_c^3}\delta. \tag{5.3}$$

Here l_c is the cantilever's length; E is Young's modulus of elasticity and I is the moment of inertia. From this relation, we can estimate the minimum detectable force, by substituting δ_{min} into δ, to be in the order of 10^{-10} N for the separation gap of 2.5 μm and of 10^{-11} N for the gap of 1 μm. In these estimates, we have taken the Young's modulus of the cantilever as that of SiO_2 material which is $0.73\times10^{12}\ \mathrm{dyne}/\mathrm{cm}^2$. The moment of inertia $I = w_c t_c^3/12$, where w_c is the cantilever's width and t_c the thickness.

References

1. O. Wolter, Th. Bayer and J. Greschner, "Micromachined silicon sensors for scanning force microscopy," *J. Vac. Sci. Technol.*, vol. B9, no. 2, pp.1353 – 1357, 1991.
2. J. Brugger, R. A. Buser and N. F. de Rooij, "Silicon cantilevers and tips for scanning force microscopy," *Sensors and Actuators A*, vol. 34, pp. 193–200, 1992.
3. NANOPROBE, 7042 Aidlingen 3, Germany.
4. H. K. Wickramasinghe, "Scanning probe microscopy: current status and future trends," *J. Vac. Sci. Techn. A*, vol. 8, no. 1, pp. 363–368, Jan./Feb. 1990.
5. T. R. Albrecht, S. Akamine, M. J. Zdeblick and C. F. Quate, "Microfabrication of integrated scanning tunneling microscope," *J. Vac. Sci. Techn. A*, vol. 8, no. 1, pp. 317–318, Jan./Feb. 1990.
6. S. A. C. Gould, et al., "From atoms to integrated circuit chips, blood cells, and bacteria with the atomic force microscope," *J. Vac. Sci. Techn. A*, vol. 8, no. 1, pp. 369–373, Jan./Feb. 1990.

6

Discussion and Conclusions

Although micro-mechanical bridges and cantilevers have been applied in electronic devices, they are quite new structures in integrated optics. As stated in the first chapter of this thesis, the work presented here is one of the very early investigations on micro-mechanical structures used as optical sensor elements. The purpose of this research is to develop and evaluate the idea of using the micro-mechanical structures as optical waveguides and sensor elements. From the obtained results, it can be concluded that such bridges and cantilevers can be used as optical waveguides and can be applied as optical sensor elements.

This final chapter discusses the results as have been obtained in the present thesis. In addition, some important aspects concerning the fabrication of micro-mechanical structures and their applications to sensors as well as some future work will be indicated.

6.1 Discussion

This research is oriented to evaluate the possibility for sensor applications of micro-mechanical bridge and cantilever waveguides using optical waves as

information carriers. It is not aimed to develop actual sensor devices that can be readily used for sensor applications, although the work may serve as the first step toward this aim. Much work and time are still needed to construct practical optical sensors based on these structures.

A major part of our research was devoted to the fabrication of the micro-mechanical bridges and cantilevers. This task was complicated since the bridges and cantilevers should not only demonstrate a suitable mechanical strength, but should also satisfy the optical waveguiding requirements. To produce the bridges and cantilevers as optical waveguides, multilayer structures have been applied. In our case, these consist of a sandwich layer structure consisting of an SiO_2 buffer layer, an Al_2O_3 waveguide layer and an SiO_2 cover layer. Such a multilayer structure poses additional problems concerning the structure's mechanical properties. Difference in thermal expansion coefficients and in stress occurs among layers of different materials, and even exists among layers of the same material but prepared by different techniques. The induced stress between different layers could bend the structure or cause the structure to break during the fabrication process. Beside all these difficulties, the structure should also be able to endure a high temperature of about 750 ° during the annealing process which is needed in order to reduce the guided wave transmission loss. Using a sandwich layer structure is one way to ease those problems by balancing the thermal expansion and stress in the multilayer. Technically, it is much easier to fabricate bridges and cantilevers consisting of only a single layer of silicon (which is not really suitable for optical elements) or of some other material like SiO_2 and Si_3N_4, as is usual for electronic devices.

The other way to fabricate more successful micro-mechanical structures for optical sensors is to adopt materials with similar mechanical and thermal properties for constructing different layers. Materials closely related to the substrate material silicon seem to have advantages in this respect. Silicon dioxide might be the best choice to be used as an optical buffer layer or a cover

layer since it has optimal optical properties. An SiO_2 buffer layer can be easily obtained from the silicon substrate surface by an oxidation process. The SiO_2 cover layer works both as a protection layer for the waveguide and as a balance layer to the buffer layer. Several materials such as Si_3N_4 and SiON can be used for optical waveguide layers. Thus, sandwich structures such as SiO_2-Si_3N_4-SiO_2 and SiO_2-SiON-SiO_2 can be applied for the bridge and cantilever structures. One may also fabricate micro-mechanical structures from an Ge-doped silicon layer on a silicon substrate. The Ge-doped silicon layer can be used directly as an optical waveguide for light in the infrared wavelength region. This means monolayer micro-mechanical structures can be produced, which is favorable to obtain more uniform mechanical properties.

From the results obtained in the detection of acoustic signals, it is clear that a cantilever is more sensitive to external influences than a bridge. Since one end of the cantilever can move freely, the stress inside the cantilever is released. A bridge structure, which experiences stress, has a quite different character. The stress in a bridge will vary when the external forces change.

Our research has concentrated on the investigation of bridge and cantilever structures, but other micro-structures for integrated optical sensors are still likely to be discovered. The way to find new structures is to combine micro-structures with optical waveguides.

One important aspect concerns the fabrication techniques. There is no unique way to fabricate micro-mechanical structures. The choice of the fabrication techniques is strongly dependent on the materials used for the structures. A relatively simple way is to use isotropic etching to obtain the micro-mechanical structures, however, more complicated techniques like reactive ion etching and anisotropic etching may be needed to achieve optimal structures.

6.2 *Conclusions*

Micro-mechanical structures have been proposed as optical sensor elements. Their mechanical behavior as well as their optical properties have been analyzed. The procedures for fabricating the structures are presented as a technological base. The micro-bridges and cantilevers have been successfully produced upon silicon substrates and were applied as optical waveguides and sensor elements. Experimental results have been obtained when the structures are used as optical sensor elements for the detection of acoustic signals. The results confirmed the proposed idea of using these structures for sensor applications. Some other possible applications, which have not been experimentally investigated in this thesis, were discussed.

The micro-mechanical structures proposed in this thesis are quite new in the field of integrated optics. Only few related papers have been publicized quite recently [1] [2]. Using micro-mechanical bridges and cantilevers as optical waveguides and at the same time as optical sensor elements has been verified as an effective way to construct sensitive sensor structures.

The application of such structures lies not only in the detection of acoustic signals, but also in the measurement of vibrations and acceleration. The cantilever structure turns out as a highly sensitive structure if used for sensing forced related quantities such as in a case for scanning force microscope. As such, it is expected to have a promising future.

A theoretical method for analyzing curved waveguides has been developed for the purpose to understand the optical loss induced by the deflections of bridges or cantilevers. It is actually a general approach which differs from other methods to analyze a curved waveguide with an arbitrary cross section.

Batch fabrication is possible to produce the micro-mechanical structures and the fabrication process is compatible with conventional IC techniques. Thus, large quantities of the structures can be produced to reduce the production cost. Necessary electronic processing units can be integrated onto the same chip to ensure the reliability and compactness of possible devices. Due to miniature size of the structures, large arrays can be integrated on a small area.

References

1. H. Bezzaoui and E. Voges, "Integrated optics combined with micromechanics on silicon," Sensors and Actuators A, vol. 29, No. 3, pp.219 – 223, Dec. 1991.
2. K. E. Burcham, G. N. De Brabander and J. T. Boyd, "Micromachined silicon cantilever beam accelerometer incorporating an integrated optical waveguide," presented at *SPIE's International Symposium OE/FIBERS'92*, Boston, USA, 8 – 11 Sept., 1992.

Appendix A

Formulation for the Radiation Loss Using Coupled Mode Theory

The radiation loss of a guided mode is defined as the power coupled from the guided mode into radiation modes. The electric field and the power of the guided mode are denoted as $A_g(z)$ and $P_g(z)$, respectively. Similarly, the field of a radiation mode is labeled as $A_r(z)$. The radiation loss can then be formulated as

$$2\alpha = \frac{-dP_g(z)}{P_g(z)dz}, \quad or \quad 2\alpha = \frac{dP_r}{P_g dz}, \tag{A.1}$$

where 2α is the attenuation coefficient caused by the radiation. P_r is the total radiation power flow of all propagating radiation modes and can be expressed in the fields of these modes, i. e.

$$P_r = \sum \int_0^{n_0 k} \left(\left| A_r^+ \right|^2 + \left| A_r^- \right|^2 \right) d\rho_r . \tag{A.2}$$

The upper limit of the integral indicates that the evanescent modes do not carry power. In Eq. (A.2), power flowing in the positive z-direction has a superscript of the positive sign, while power flowing in the negative z-direction is indicated with a negative sign. The variable ρ_r has a close relation with the propagation constant β_r and the refractive index (indicated as n_0) outside of the waveguide region, i.e.

$$\rho_r = \sqrt{n_0^2 k^2 - \beta_r^2}\,. \tag{A.3}$$

According to the discussion of the sign simplification of Eq. (2.28), the two terms under the integral in Eq. (A.2) differ only in the sign of propagation constant. With the aid of Eq. (A.3), we can transform the integral to the integration variable β_r. It therefore is convenient to write Eq. (A.2) in the form

$$P_r = \sum \int_{-n_0 k}^{n_0 k} \frac{|A_r|^2}{\rho_r} |\beta_r| d\beta_r\,. \tag{A.4}$$

The field $A_r(z)$ of the radiation mode can be obtained by solving the coupled mode equations [1]:

$$\begin{aligned} \frac{dA_g}{dz} &= -j\beta_g A_g + k_{gr} A_r\,, \\ \frac{dA_r}{dz} &= -j\beta_r A_r + k_{rg} A_g\,. \end{aligned} \tag{A.5}$$

We denote the amplitudes of the fields A_g and A_r as A_{gs} and A_{rs}, respectively, such that

$$A_g = A_{gs} e^{-j\beta_g z},$$
$$A_r = A_{rs} e^{-j\beta_r z}. \tag{A.6}$$

To consider a perturbation solution of the coupled mode equations, the amplitude A_g of the guided mode is assumed to be large compared to that of the radiation mode:

$$|A_{gs}| >> |A_{rs}|. \tag{A.7}$$

This inequality implies that the amplitude A_{gs} does not vary very much, so that we can treat it as approximately constant. We can then integrate Eq. (A.5) and obtain the solution

$$A_{rs} = k_{rg} A_{gs} \frac{1}{j(\beta_r - \beta_g)} \left(e^{j(\beta_r - \beta_g)z} - 1 \right). \tag{A.8}$$

Substituting Eq. (A.8) into Eq. (A.4) with the aid of Eq. (A.6), we derive the formula for the total radiation loss as

$$P_r = \sum \int_{-n_0 k}^{n_0 k} |A_g|^2 |k_{rg}|^2 \frac{2\left(1 - \cos(\beta_r - \beta_g)z\right)}{\rho_r (\beta_r - \beta_g)^2} |\beta_r| d\beta_r. \tag{A.9}$$

The quantity $|A_g|^2$ represents the power carried by the guided mode. We thus obtain the radiation loss coefficient 2α from Eqs. (A.9) and (A.1), as has been presented in Eq. (2.40):

$$2\alpha = \sum \int_{-n_0 k}^{n_0 k} |k_{rg}|^2 \frac{2\sin(\beta_g - \beta_r)z}{\rho_r(\beta_g - \beta_r)} |\beta_r| d\beta_r . \qquad \text{(A.10)}$$

References

1. D. Marcuse, *Light Transmission Optics*. New York: Van Nostrand Reinhold Company, 1982, pp. 417–425.
2. D. Marcuse, *Theory of Dielectric Optical Waveguides*. New York: Academic Press, 1974.

Bibliography

1. Albrecht T. R., S. Akamine, M. J. Zdeblick and C. F. Quate, "Microfabrication of integrated scanning tunneling microscope," *J. Vac. Sci. Techn. A*, vol. 8, no. 1, pp. 317–318, Jan./Feb. 1990.

2. Baets R. and P. E. Lagasse, "Loss Calculation and Design of Arbitrarily Curved Integrated Optical Waveguide," *J. Opt. Soc. Am.*, vol. 73, no. 2, pp. 177–182, Feb. 1983.

3. Bassous E., "Fabrication of novel three-dimensional microstructures by the anisotropic etching of (100) and (110) silicon," *IEEE Trans. Electron Devices*, vol. ED-25, no. 10, pp. 1178–1185, October 1978.

4. Bean K. E., "Anisotropic etching of silicon," *IEEE Trans. Electron Devices*, vol. ED-25, no. 10, pp. 1185–1193, October 1978.

5. Bezzaoui H. and E. Voges, "Integrated optics combined with micromechanics on silicon," *Sensors and Actuators A*, vol. 29, no. 3, pp. 219–223, Dec. 1991.

6. Blitz J., *Elements of Acoustics*. Butterworths, London, 1964.

7. Brugger J., R. A. Buser and N. F. de Rooij, "Silicon cantilevers and tips for scanning force microscopy," *Sensors and Actuators A*, vol. 34, pp. 193–200, 1992.

8. Bulmer C. H., R. P. Moeller and W. K. Burns, "Linear Mach-Zehnder interferometers in $LiNbO_3$ for electromagnetic field sensing," in *Proc. IEE of Second European Conf. on Integrated Optics*, Florence, Italy, 1983, pp. 140–143.

9. Bulmer C. H., W. K. Burns and R. P. Moeller, "Linear interferometric waveguide modulator for electromagnetic-field detection," *Optics Lett.*, vol. 5, no. 5, pp. 176–178, 1980.

10. Burcham K. E., G. N. De Brabander and J. T. Boyd, "Micromachined silicon cantilever beam accelerometer incorporating an integrated optical waveguide," presented at *SPIE's International Symposium OE/FIBERS'92*, Boston, USA, 8 – 11 Sept., 1992.

11. Burns W. K. and G. B. Hocker, "End fire coupling between optical fibers and diffused channel waveguides," *Applied Optics*, vol. 16, pp. 2048–2050, 1977.

12. Chang D. C. and E. F. Kuester, "Radiation and Propagation of a Surface-wave Mode on a Curved Open Waveguide of Arbitrary Cross Section," *Radio Science*, vol. 11, no. 5, pp. 449–457, May 1976.

13. Csepregi L., "Micromechanics: a silicon microfabrication technology," *Microelectronic Engineering*, vol. 3, pp. 221–234, 1985.

14. Culshaw B., "Optical sensor multiplexing systems," in *Proc. Sensors and Systems'82*, Pasadena, 1982, pp. 47–57.

15. Deimel P. P., "Micromachining processes and structures in micro-optics and optoelectronics," *J. Micromech. Microeng.*, vol. 1, pp. 199–222, 1991.

16. Elliott D. J., *Integrated Circuit Fabrication Technology*. McGraw-Hill Book Company, 1982.

17. Enokihara A., M. Izutsu and T. Sueta, "Integrated-optic fluid sensor using heat transfer," *Applied Optics*, vol. 27, no. 1, pp. 109–113, Jan. 1988.

18. Fields J. N. and J. H. Cole, "Fiber microbend acoustic sensor," *Applied Optics*, vol. 19, pp. 3265–3267, 1980.

19. Gould S. A. C., et al., "From atoms to integrated circuit chips, blood cells, and bacteria with the atomic force microscope," *J. Vac. Sci. Techn. A*, vol. 8, no. 1, pp. 369–373, Jan./Feb. 1990.

20. Heiblum M. and J. H. Harris, "Analysis of Curved Optical Waveguides by Conformal Transformation," *IEEE J. Quantum Electronics*, vol. QE–11, no. 2, pp. 75–83, Feb. 1975.

21. Huang Hung-chia, *Coupled Mode Theory*. Utrecht:VNU Science Press, The Netherlands, 1984.

22. Huang Hung-chia, *Principles of Microwaves*. Beijing:Science Press, 1963.

23. Izutsu M., A. Enokihara and T. Sueta, "Optical-waveguide micro-displacement sensor," *Electronic Lett.*, vol. 18, pp. 867–868, 1982.

24. Izutsu M., A. Enokihara, N. Mekada and T. Sueta, "Optical-waveguide pressure sensor," in *Proc. IEE of Second European Conf. on Integrated Optics*, Florence, Italy, 1983, pp. 144–147.

25. Jaeger N. A. F. and L. Young, "High-voltage sensor employing an integrated optics Mach-Zehnder interferometer in conjunction with a capacitive divider," *J. Lightwave Techn.*, vol. 7, no. 2, pp. 229–235, Feb. 1989.

26. Johnson L. M., F. J. Leonberger and G. W. Pratt, Jr., "Integrated optical temperature sensor," *Appl. Phys. Lett.*, vol. 41, no. 2, pp. 134–136, July 1982.

27. Johnson M., "Optical-actuator frequency-coded pressure sensor," *Optics Lett.*, vol. 11, no. 9, pp. 587–589, Sept. 1986.

28. Joppe J. L., "Het reacief ionen etsen van een $SiO_2/Al_2O_3/SiO_2$ optisch golfgeleiderpakket op silicium," Fysisch en Elektronisch Laboratorium TNO, TNO-rapport FEL-90-B339, December, 1990.

29. Kaminsky G., "Micromachining of silicon mechanical structures," *J. Vac. Sci. Techn.*, vol. B3, no. 4, pp. 1015–1024, 1985.

30. Kaufman K. S., R. Terras and R. F. Mathis, "Curvature loss in multimode optical fibers," *J. Opt. Soc. Am.*, vol. 71, no. 12, pp. 1513–1518, Dec. 1978.

31. Kern W., "Chemical etching of silicon, germanium, gallium arsenide and gallium phosphide," *RCA Review*, vol. 39, pp. 278–308, 1978.

32. Kronig (Editor) R., *Textbook of Physics*. Pergamon Press, London, UK, 1959.

33. Lewin L., "Radiation from Curved Dielectric Slabs and Fibers," *IEEE Trans. Microwave Theory and Techn.*, vol. MTT–22, no. 7, pp. 718–727, July 1974.

34. Marcatili E. A. J., "Bends in Optical Dielectric Guides," *The Bell System Technical J.*, vol. 48, no. 7, pp. 2103–2132, September 1969.

35. Marcatili E. A. J., and S. E. Miller, "Improved Relations Describing Directional Control in Electromagnetic Wave Guidance," *The Bell System Technical J.*, vol. 48, no. 7, pp. 2161–2188, September 1969.

36. Marcuse D., "Bending Losses of the Asymmetric Slab Waveguide," *The Bell System Technical J.*, vol. 50, no. 8, pp. 2551–2563, Oct. 1971.

37. Marcuse D., *Light Transmission Optics*. New York:Van Nostrand Reinhold Company, 1982.

38. Marcuse D., *Theory of Dielectric Optical Waveguides*. New York:Academic Press, 1974.

39. McGraw-Hill, *Dictionary of Scientific and Technical Terms*. McGraw-Hill, 1984.

40. Miyagi M. and S. Nishida, "Bending losses of dielectric rectangular waveguides for integrated optics," *J. Opt. Soc. Am.*, vol. 68, no. 3, pp. 316–319, March 1978.

41. Morse P. M. and K. U. Ingard, *Theoretical Acoustics*. Princeton University Press, Princeton, New Jersey, USA, 1986.

42. NANOPROBE, 7042 Aidlingen 3, Germany.

43. Nathanson H. C. and R. A. Wickstrom, "A resonant-gate silicon surface transistor with high-Q bandpass properties," *Appl. Phys. Lett.*, vol. 7, p. 84, 1965.

44. Nathanson H. C., W. E. Neweil, R. A. Wickstrom and J. R. Davis, Jr., "The resonant gate transistor," *IEEE Trans. Electron Devices*, vol. ED-14, p. 117, 1967.

45. Nellen Ph. M., K. Tiefenthaler and W. Lukosz, "Input grating couplers as biochemical sensors," *Sensors and Actuators*, vol. 15, pp. 285–295, 1988.

46. Neumann E. and H. Rudolph, "Radiation from Bends in Dielectric Rod Transmission Lines," *IEEE Trans. Microwave Theory and Techn.*, vol. MTT–23, no. 1, pp. 142–149, Jan. 1975.

47. Nishihara H., M. Haruna and T. Suhara, *Optical Integrated Circuits*. McGraw-Hill Book Company, 1989.

48. Ohkawa M., M. Izutsu and T. Sueta, "Integrated optical pressure sensor on silicon substrate," *Applied Optics*, vol. 28, no. 23, pp. 5153–5157, Dec. 1989.

49. Pennings E. C. M., *Bends in Optical Ridge Waveguides*. Ph.D. Thesis of Delft University of Technology, 1990, ISBN 90-9003413-7.

50. Petersen K. E., "Dynamic micromechanics on silicon: techniques and devices," *IEEE Trans. Electron Devices*, vol. ED-25, pp. 1241–1250, 1978.

51. Petersen K. E., "Silicon as a mechanical material," *Proc. IEEE*, vol. 70, no. 5, pp. 420–457, May 1982.

52. Rediker R. H., T. A. Lind and F. J. Leonberger, "Integrated optics wave front measurement sensor" *Appl. Phys. Lett.*, vol. 42, no. 8, pp. 647–649, April 1983.

53. Seidel H. and L. Csepregi, "Three-dimensional structuring of silicon for sensor applications," *Sensors and Actuators*, vol. 4, pp. 455–463, 1983.

54. Smit M. K., A. Acket and C. J. van der Laan, "Al_2O_3 Films for Integrated Optics," Thin Solid Films, vol. 138, pp. 171–181, 1986.

55. SPIE Conference 1793 – Integrated Optics and Microstructures, *SPIE's International Symposium OE/FIBERS'92*, Boston, USA, 8 – 11 Sept., 1992.

56. Spohn P. K. and M. Seifert, "Interaction of aqueous solutions with grating couplers used as integrated optical sensors and their pH behavior," *Sensors and Actuators*, vol. 15, pp. 309–324, 1988.

57. Stephens R. W. B. and A. E. Bate, *Acoustics and Vibrational Physics*. Edward Arnold (Publishers) Ltd., London, UK, 1966.

58. Takato N. and A. Sugita, "Silica-based single-mode waveguides and their applications to integrated-optical devices," in *Materials Research Society Symposium Proc.*, vol. 172, *Optical Fiber Materials and Processing*, J. W. Fleming et al, Ed., Pittsburgh:Materials Research Society, 1990, pp. 253–264.

59. Tamir (Editor) T., *Integrated Optics*. New York:Springer-Verlag, 1979.

60. Thomson W. T., *Theory of Vibration with Applications*. Prentice-Hall, Inc., Englewood Cliffs, New Jersey, USA, 1972.

61. Tiefenthaler K. and W. Lukosz, "Integrated optical switches and gas sensors," *Optics Lett.*, vol. 9, pp. 137–139, 1984.

62. Ura S., T. Suhara and H. Nishihara, "Integrated-optic interferometer position sensor," *J. Lightwave Techn.*, vol. 7, no. 2, pp. 270–273, Feb. 1989.

63. Wickramasinghe H. K., "Scanning probe microscopy: current status and future trends," *J. Vac. Sci. Techn. A*, vol. 8, no. 1, pp. 363–368, Jan./Feb. 1990.

64. Wolter O., Th. Bayer and J. Greschner, "Micromachined silicon sensors for scanning force microscopy," *J. Vac. Sci. Technol.*, vol. B9, no. 2, pp.1353 – 1357, 1991.

65. Wu S. and H. J. Frankena, "An integrated optical interferometer and a coupled-waveguide humidity sensor," in Sensors and Actuators, A. Driessen, Ed., Kluwer Technical Books, 1990, pp. 75–78.

66. Wu S. and H. J. Frankena, "Integrated optical interferometer with a stacked waveguide structure," *Applied Optics*, vol. 28, no. 20, pp. 4424–4428, Oct. 1989.

67. Wu S. and H. J. Frankena, "Integrated optical sensors using micromechanical bridges and cantilevers," presented at *SPIE's International Symposium OE/FIBERS'92*, Boston, USA, 8 – 11 Sept., 1992.

68. Wu S. and H. J. Frankena, "Micromechanical structures as integrated optical sensor elements," in *Integrated Photonics Research*, OSA Technical Digest Series, vol. 10, pp.158 – 159, 1992.

69. Wu S., "Theoretical analysis of curved waveguides with arbitrary cross section," in Lightwave Technology and Communications, A. Altintas and G. Saplakoglu, Ed., Meteksan, 1992, pp. 183–189.

Summary

This thesis reports an investigation on micro-mechanical structures (bridges and cantilevers) and their application as integrated optical sensor elements. The work presented here is one of the early investigations on this subject.

Since bridges and cantilevers are mechanically unstable structures which vibrate or deflect due to external influences, especially force-related disturbances, they can be utilized as sensor elements. The development of such structures for sensor applications is the result of a combination of integrated optics and micro-mechanics. Integrated optics lays down the operational principles and uses guided waves as the information carriers of sensor signals, while micro-mechanics provides micro-structures as transducing interfaces to external influences and governs the mechanical behavior of the structures.

The micro-bridges and cantilevers are fabricated upon silicon substrates and are used as optical waveguides. The waveguides have a sandwiched layer structure of an SiO_2 buffer, an Al_2O_3 waveguide and an SiO_2 cover.

Theoretical analysis on the mechanical (both dynamic and static) behavior of the bridges and cantilevers, on the optical loss induced by waveguide bending during vibrations or acceleration, and on the optical coupling in the cantilever structures has been carried out to understand the operational principles of these optical sensor elements. The theory of optical bending loss is

essentially a general theory for a curved waveguide with an arbitrary cross-section. An estimate shows that the cantilever structures are very sensitive for detecting force related quantities; the theoretically minimum detectable displacement lies in the order of 10^{-2} nm and the minimum detectable force is in the order of 10^{-10} N.

Micro-fabrication technology for producing three-dimensional micro-structures has been summarized briefly with the emphasis on the logical scheme for the fabrication process. Details of the fabrication processes for the micro-bridges and cantilevers for integrated optical sensors have been described. Etching techniques like isotropic, anisotropic and reactive ion etching (RIE) have been applied for the fabrication of the bridges and cantilevers. Numerous bridges and cantilevers of different dimensions have fabricated. These include structures with lengths of 500 μm, 200 μm, 100 μm, 50 μm and 25 μm, while for each length four different widths of 30 μm, 20 μm, 10 μm and 5 μm occur. For cantilever-shaped waveguides, the separation distances between a cantilever's free end and the output section have been chosen as 2.5 μm, 10 μm and 25 μm. The structures have a thickness of about 2.5 μm and occur about 10 μm above the silicon substrate surface with an air gap in between.

To verify experimentally the operation of such bridges and cantilevers, waveguiding through such micro-structures has been investigated. The application of such structures as optical sensor elements is evaluated and confirmed by the experiment results of acoustic signal detection. Some other possible applications, such as for the measurement of vibrations or acceleration, and for scanning force microscopy or surface profiling, are also proposed and discussed briefly.

The results obtained from both theoretical and experimental investigation have confirmed that micro-mechanical structures like ours are effective optical sensor elements.

Samenvatting

Dit proefschrift omvat het verslag van een studie over micro-mechanische structuren (bruggen en hefbomen) en hun toepassing als sensorelement in geïntegreerde optische schakelingen. Het hierin weergegeven werk is een van de eerste onderzoeken op dit gebied.

Bruggen en hefbomen zijn mechanisch onstabiele structuren, die onder invloed van uitwendige invloeden, en wel in het bijzonder door verstoringen die met krachten te maken hebben, trillen of verbuigen; daardoor kunnen zij gebruikt worden als sensorelementen. De ontwikkeling van zulke structuren voor toepassing in sensoren betekent een samengaan van geïntegreerde optica en micromechanica. Daarbij bepaalt de geïntegreerde optica de principes van de werking, die gebruik maakt van geleide golven als informatiedragers, terwijl de micromechanica structuren aanlevert die kunnen dienen als transducenten naar de uitwendige invloeden en het mechanische gedrag van de sensor beheerst.

De zeer kleine bruggen en hefbomen worden vervaardigd op substraten van silicium en dienen als optische golfgeleiders. Zij hebben een gelaagde structuur bestaande uit een buffer van SiO_2, een golfgeleider van Al_2O_3 en een deklaag van SiO_2.

Ten einde de werking van deze sensorelementen te doorzien, is theoretisch onderzoek uitgevoerd naar het mechanische gedrag (statisch zowel als

dynamisch) van de bruggen en hefbomen, naar de optische verliezen door het buigen van de golfgeleiders door het buigen tijdens trillingen of versnellingen en naar de optische koppeling in de hefboom configuraties. De theorie met betrekking tot de optische verliezen ten gevolge van het buigen is in wezen een algemene theorie van een gebogen golfgeleider met willekeurige doorsnede. Een schatting laat zien dat de hefbomen zeer gevoelig zijn voor het detecteren van grootheden die met krachten verband houden; de theoretisch minimaal te detecteren verplaatsing ligt in de orde van 10^{-2} nm en de minimaal te detecteren kracht ligt rond 10^{-10} N.

De technologie voor microfabricage, noodzakelijk om de driedimensionale microstructuren te produceren, wordt kort samengevat met de nadruk op het fabricageschema. Details van dit proces voor zover het betrekking heeft op bruggen en hefbomen als optische golfgeleiders worden beschreven. Dit omvat etstechnieken zoals isotroop, anisotroop en reactief ionen (RIE) etsen. Vele bruggen en hefbomen van verschillende afmetingen zijn werkelijk geproduceerd. Zo zijn structuren met lengten van 500μm, 200μm, 100μm, 50μm en 25μm gemaakt, terwijl voor elke lengte de breedten 30μm, 20μm, 10μm en 5μm voorkomen. Voor de hefbomen zijn afstanden tussen het vrije einde en het uitkoppel-gedeelte van de sensor gekozen van 2,5μm, 10μm en 25μm. De structuren zijn ongeveer 2,5μm dik en hangen ongeveer 10μm boven het siliciumsubstraat, met lucht daartussen.

Om de werking van zulke bruggen en hefbomen experimenteel na te gaan, is de golfgeleiding er doorheen bestudeerd. De mogelijkheden voor toepassen van zulke structuren als optische sensorelementen is hieruit nagegaan en naderhand aangetoond uit de resultaten voor akoestische detectie. Enkele andere toepassingen zijn voorgesteld en kort besproken, zoals voor het meten van trillingen of versnellingen, en in scanning microscopen of bij de profielmeting aan oppervlakken.

De theoretisch en experimenteel bereikte resultaten hebben bevestigd dat microstructuren zoals hier voorgesteld inderdaad goed werkende optische sensorelementen zijn.

微机械结构光学传感元件

本论文主要研究微机械结构(桥型和悬臂型)及其作为集成光学传感元件方面的应用。本文所述内容是这一领域较早的研究成果之一。

桥型及悬臂型结构在机械性能上属于不稳定结构，在外界影响下，尤其在外力作用下，会产生弯曲和振动，正因为如此，它们可用作传感器元件。微机械结构的光学传感器应用，是集成光学和微机械力学相互催化及结合的成果。一方面，集成光学决定了元件的传感原理并利用光导波作为传感信号的载波，另一方面，微机械力学决定了结构的机械性能并提供微结构作为元件和外界的传感界面。

本文所提出的微型桥及微型悬臂可以制备在硅基片上，其本身又可作为光波导。这类波导由二氧化硅缓冲层，氧化铝波导层以及二氧化硅覆盖层重叠组成夹心结构。

为更好地明了这类传感元件的机理，论文从理论上分析了桥及悬臂的动态及静态性能，由波导弯曲和振动所引起的光损耗，以及悬臂结构中导波的耦合过程。由此而提出的弯曲波导一般理论可用来分析任意截面的弯曲波导。粗略

的估计显示，悬臂结构对外力作用非常敏感，最小可测位移的理论值可达百分之一纳米，最小可探测力为十的负十次方牛顿o

本文概述了制备三维微型结构的微处理技术，并强调制备过程的逻辑概念o 论文对微型桥及悬臂的制备过程有详细的论述，在制备过程中采用了均匀，非均匀，及离子反应蚀刻技术o 已制备的各种微型桥及悬臂的尺寸包括长度为500，200，100，50 和 25 微米，每个长度对应有四个不同宽度，分别为 30，20，10 和 5 微米o 对于微型悬臂，从悬臂的自由端到输出段的距离又可分为 2.5，10 和 25 微米，所有这些结构的厚度约只有2.5微米，并悬于基片表面上10微米处o

作为实验验证，本文对激光通过微型桥及悬臂结构时的传输过程作了详细观测o 这些结构也被用来作传感器对声波信号作了探测，实验结果充分肯定了结构的传感器应用o 本文还讨论了一些其它可能的应用，如振动和加速度的测量，扫描微力探测器及表面轮廓测量等o

理论及实验均充分证实了本文所述之微机械结构可以用作高效的传感器o

Index

Acoustic signal detection 77
Acoustic signal response
  bridge 81
  cantilever 83
ADVANTEST TR 9402 Digital
    Spectrum Analyzer 79
Annealing 62
Attenuation 27
Audio-frequency spectrum 78
Beams 18
  deflection 19
  flexural rigidity 19
  transverse vibration 18
Bending moment 24
Boundary conditions 19
Bridge 10
Cantilever 10
Characteristic equation 20, 21
Coupled mode equations 33, 102
  perturbation solution 103
Coupling coefficient 28, 33, 35, 40
Coupling efficiency 37
Curved waveguides 26
Deflection 12
Etch rate 50
Etching 49
  anisotropic etching 50
  dry etching 50
  isotropic etching 50
  wet etching 50
Etching process 49
Etching undercut 62
Experimental setup 78
Exposure mask 57
Exposure process 59
Fabrication process 58, 65
Forced vibration 21
Free vibration 20

Frequency response
bridge 83
cantilever 83
measuring setup 81
Gaussian approximation 39
Gaussian beam 39
Hewlett Parkard 8904A Multi-function Synthesizer 79
HF buffered etching 59
Hybrid coupler 7
Inhomogeneous stress 37
Integrated optical sensor 3
Lithography 47
Maxwell's equations 28
Measurement of acceleration 87
Measurement of vibrations 87
Mechanical behavior 17
dynamic behavior 18
static behavior 24
Micro-bend sensor 4
Micro-bridge 17
Micro-cantilever 17
Micro-fabrication 9
Micro-machining 9, 49
Micro-mechanical structures 10
bridge 10
cantilever 10
operational principles 11
Micro-mechanics 9, 10
Micro-processing 49
Micro-structures 9
Minimum allowable radius 26
Minimum detectable displacement 92
Minimum detectable force 92
Mode conversion 27
Moment of inertia 19
Natural frequency 19
Noise equivalent power (NEP) 79
Optical fiber sensor 3
Optical IC's 45
Optical interferometer 4
Mach-Zehnder interferometer 7
Michelson interferometer 7
Optical sensor 2
intensity sensor 4
phase sensor 4
polarization sensor 4
spectral sensor 5
Patterning methods 47
Potassium hydroxide (KOH) 67
Power loss 35
Propagation constant 33
Propagation constant changes 33
Radiation loss 26, 35, 101
Reactive ion etching (RIE) 65
Reference microphone 79
RIE process 65
Rippled patterns 63

Sandwiched waveguide
structure 56
Scanning force microscope 89
Sensitivities 37
Sensor 2
classification 2
definition 2
operational principle 2
Sensor response 86
Silicon etching 59
Silicon planar PIN photodiode 79
Singular point 36
SiO_2 waveguide 59
Soft-baking 59
Sony 1120 Integrated Amplifier 79
Spin coating 59
Sputtering process 60, 62
Stress 96
Surface profiler 89
Thermal oxidation 58
Thin film deposition 46
Thin film growth 46
Three-dimensional structures 45
Transducing mechanisms 5
Tibration 12
Vifa type M-110 speaker 79
Waveguide layer structure
Al_2O_3 waveguide 56
SiO_2 buffer 56
SiO_2 cover 56
Young's modulus 19

Biography

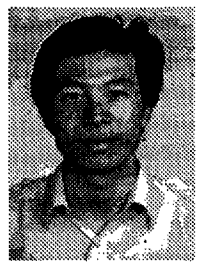

Shaodong Wu was born on October 17, 1962 in Zhejiang Province, China. He graduated from Sandu Primary School in 1975 and Sandu High School in 1979, both in Zhuji, Zhejiang Province. From 1979 to 1983, he was a student at the Department of Applied Physics of Xian University of Electronic Technology (formerly known as Northwest Telecommunication Engineering Institute). He received the Bachelor degree in Engineering in the field of laser technology in July 1983. In the same year, after a nation-wide contest among university graduates and post-graduates, he was selected by the Chinese Education Ministry for further study in foreign countries. From September 1983 to July 1984, he followed an intensive English language program organized by the Chinese Education Ministry at Shanghai Institute for Foreign Languages in Shanghai.

He was involved in a research project on developing TEA CO_2 laser systems and did some theoretical research on optical four-wave mixing before he came to the Netherlands in July 1985. He finished his master thesis on integrated optical interferometers at the Department of Applied Physics of Delft University of Technology and received the Master degree in May 1987.

Since December 1988, he has been working towards the Ph.D. degree at the Department of Applied Physics of the Delft University of Technology. During this Ph.D. period, he has published seven papers in journals and conferences.

He is currently holding memberships of the SPIE–The International Society for Optical Engineering, the Optical Society of America, the European Optical Society and the Netherlands' Physical Society.